The proliferation of rodent astrocytes – implications for a modulatory role of dopamine and aquaporin 4

Dissertation

zur Erlangung des Grades eines Doktors
der Naturwissenschaften

der Mathematisch-Naturwissenschaftlichen Fakultät
und
der Medizinischen Fakultät
der Eberhard-Karls-Universität Tübingen

vorgelegt
von

Britta Wachter
aus Buchheim, Deutschland

Juli 2011

Tag der mündlichen Prüfung:	07.10.2011
Dekan der Math.-Nat. Fakultät:	Prof. Dr. W. Rosenstiel
Dekan der Medizinischen Fakultät:	Prof. Dr. I. B. Autenrieth
1. Berichterstatter:	PD Dr. E. Küppers
2. Berichterstatter:	Prof. Dr. H. Wolburg
Prüfungskommission:	PD Dr. E. Küppers
	Prof. Dr. H. Wolburg
	Prof. Dr. S. Grissmer
	Prof. Dr. H.-J. Wagner

Ich erkläre, dass ich die zur Promotion eingereichte Arbeit mit dem Titel: *„The proliferation of rodent astrocytes – implications for a modulatory role of dopamine and aquaporin 4.“* selbstständig verfasst, nur die angegebenen Quellen und Hilfsmittel benutzt und wörtlich oder inhaltlich übernommene Stellen als solche gekennzeichnet habe. Ich versichere an Eides statt, dass diese Angaben wahr sind und dass ich nichts verschwiegen habe. Mir ist bekannt, dass die falsche Abgabe einer Versicherung an Eides statt mit Freiheitsstrafe bis zu drei Jahren oder mit Geldstrafe bestraft wird.

Tübingen, den 14.12.2011 B. Wachtler

Datum Unterschrift

"Ein Gelehrter in seinem Laboratorium ist nicht nur ein Techniker; er steht auch vor den Naturgesetzen wie ein Kind vor der Märchenwelt."

(Marie Curie, 1867-1934)

Für meine Familie

Summary

Astrocytes of the striatum express both dopamine receptors and transporters, which indicates that dopamine plays a functional role in striatal astrocytes. Dopamine is known to modulate proliferation of precursor cells during development and also in the adult brain. However, it is unknown whether dopamine affects proliferation of astrocytes.

In this study we investigated a putative role of dopamine on the proliferation of striatal astrocytes *in vitro* and *in vivo*. Using striatal mouse astrocyte cultures we found that dopamine decreased proliferation of astrocytes and the expression of the water channel AQP4, more precisely the isoform M23, both on the mRNA and protein levels. We hypothesized that the decreased expression of the water channel is linked to the observed decrease in proliferation. We confirmed this hypothesis in studies where we knocked-down AQP4 by siRNA in striatal mouse astrocytes cultures and in human pancreatic cancer cell lines (BxPC3 and PANC1) that express AQP4. We observed a decreased proliferation following the knock-down of AQP4, thus clearly demonstrating a role of AQP4 in proliferation.

Under physiological conditions, the striatum represents a target area of dopaminergic projections arising in the midbrain. We hypothesized that dopamine might keep AQP4 expression at a low level and hence prevent proliferation of astrocytes in the striatum *in vivo*. Consequentially, *in vivo* depletion of dopamine should result in an increased expression of AQP4 and an increase of proliferation of astrocytes. To investigate this hypothesis we intraventricularily injected 6-hydroxydopamine, a catecholaminergic neurotoxin that destroys dopaminergic neurons. Under these conditions AQP4 mRNA expression, specifically the AQP4 M23 isoform, was increased in the striatum, and we observed that proliferation was significantly increased in the striatum and the lateral cortex, both regions that were affected by the loss of dopamine.

Even though we confirmed our hypothesis that depletion of dopamine *in vivo* would result in an increase of proliferation, the nature and origin of these proliferating cells remained unclear. Therefore, in a follow-up study we aimed to determine the phenotype and origin of the proliferating cells in the dopamine-depleted striatum in the rat *in vivo* Using immunohistochemistry, we showed that the proliferating cells in the striatum and the lateral cortex in the 6-OHDA lesion model stained positive for the astrocyte marker GFAP and the progenitor marker nestin. The proliferating $GFAP^+$ cells did not originate from subventricular zone derived progenitor cells that migrated into the striatum and the lateral cortex. Moreover, we demonstrated that only a minor fraction (~5 %) of the proliferating $GFAP^+$ cells in the striatum might be derived from NG2 glia. Therefore, we assumed that the proliferating $GFAP^+$ cells may originate from resident mature astrocytes that de-differentiated. In accordance with this hypothesis, the proliferating $GFAP^+$ cells not only expressed the progenitor marker nestin, but also the intermediate filament vimentin and the transcription factor Pax6, which are all expressed in radial glia cells, indicating that some astrocytes regain a more immature phenotype.

Besides the observation of presumably de-differentiation of mature resident astrocytes following dopamine-depletion by 6-OHDA lesion, we observed an increase of tyrosine hydroxylase immunoreactive cells in the lateral cortex. These cells co-expressed c-Fos and calretinin thus resembling the molecular phenotype of cortical interneurons.

Abbreviations

6-OHDA	6-hydroxy dopamine
ABC	avidin-biotin peroxidase complex
Abdb	antibody dilution buffer
AQP	auqaporin
ATP	adenosine trisphosphate
BCA	bicinchoninic acid
BBB	blood brain barrier
bFGF	basic fibroblast growth factor
cAMP	cyclic adenosine monophosphate
CHIP	channel forming integral protein
CNS	central nervous system
DA	dopamine
DAB	diaminobenzidin
DAPI	4',6-diamidino-2-phenylindole
Dcx	doublecortin
DNA	deoxyribonucleic acid
L-DOPA	3,4,-dihydroxy-L-phenylalanine
E	embryonal day
FACS	fluorescent-activated cell sorting
GABA	γ-amino butyric acid
Gad	glutamic acid decarboxylase
GAPDH	glyceraldehyde-3-phosphate dehydrogenase
GFAP	glial fibrillary acidic protein
GLT1	glutamate transporter 1
HEK	human embryonic kidney
HPLC	high-performance liquid chromatography
HPRT	hypoxanthine phophorilbosyl-treansferase
Iba-1	ionized calcium binding adaptor molecule 1
IC_{50}	half maximal inhibitory concentration
IF	intermediate filament
ip	intraperitoneal
L-DOPA	L-3,4-dihydroxyphenylalanine
LSM	laser scanning microscope
MAO	monoamine oxidase
MAP-	microtubule associated protein-2
MFB	medial forebrain bundle
MM	master mix
MPTP	1-methyl-4-phenyl-1,2,3,6-tetrahydropyridine
mRNA	messenger ribonucleic acid
NMDA	N-methyl-D-aspartic acid
OAP	orthogonal array of particles
OD	optical density
P	postnatal day
PBS	phosphate buffered saline
pCREB	phosphorylated cAMP response element-binding
PD	Parkinson’s disease
PKC	protein kinase C
Roi	region of interest
RT-PCR	reverse transcriptase polymerase chain reaction
siRNA	small interfering ribonucleic acid
SN	substantia nigra
SVZ	subventricular zone
TEA	tetra-ethyl-ammonium
TH	tyrosine hydroxylase
VTA	ventral tegmental are

1. Introduction

1.1 Astrocytes

The mammalian central nervous system (CNS) is composed of neuronal and non-neuronal cell populations. The non-neuronal cell population involves glia cells, which are ubiquitously distributed throughout the brain. Glia cells outnumber neurons and were thought for a long time merely to function as a structural scaffold for neurons and to provide them with an appropriate environment [3,4]. This is also reflected in the name ´glia´ being derived from the greek word *gliok*, which means glue or slime [3]. However, over the last years it has become evident that glia cells play a key role in the healthy and pathological CNS. Glia cells are subdivided into astrocytes, oligodendrocytes and the just recently added NG2 cells [5]. In the following we will focus on astrocytes.

Astrocyte morphology

Astrocytes are characterized by several long processes that radiate from the cell body [3]. Early studies of astrocytes divided them into protoplasmic and fibrous astrocytes based on differences in the anatomical location and morphology [6]. Protoplasmic astrocytes (Fig. 1) are situated in gray matter and exhibit several major processes that ramify extensively. Fibrous astrocytes are situated in white matter and exhibit several long, thick, and less branched processes [6]. Both types contact blood vessels with the endfeet of their processes and are in contact with neurons [7]. Later on the astrocyte family was extended by several specialized types of astrocytes such as Müller glia in the retina, Bergmann glia in the cerebellum, pituicytes in the posterior pituitary, tanycytes located in certain areas of the third ventricle and the stem-cell like radial glia during development [7]. These specialized types of astrocytes exhibit a radial morphology [8].

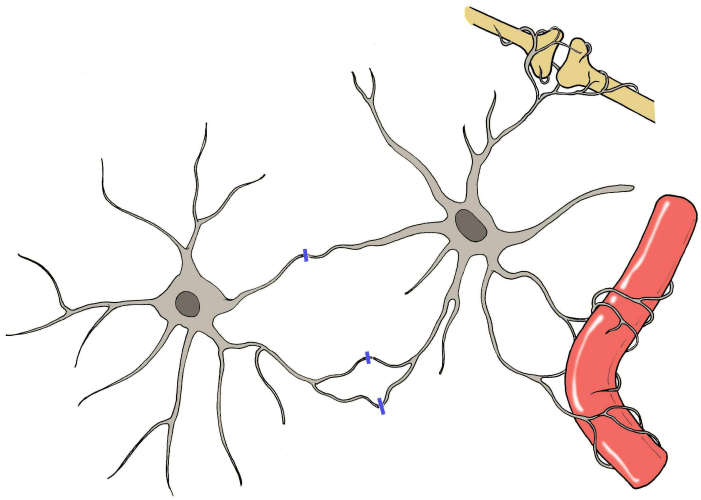

Figure 1 Schematic presentation of protoplasmic astrocytes and their outstanding position, which allows neuro-vascular coupling and connection to the astrocytic network. Astrocytes are in contact with each other in the periphery of their micro-domains via gap junctions (blue lines). They enwrap synapses with their endfeet, which are equipped with several transporters and channels that allow a rapid clearance of ions and neurotransmitters following neuronal activity. Furthermore, due to their contact with vasculature, astrocytes can for example take up glucose from the blood.

Anatomical organization

Astrocytes are uniformly distributed in the entire CNS. Protoplasmic astrocytes in the rodent cortex and hippocampus were recently described to span three-dimensional micro-domains with their extensively branched processes, respectively [3,4]. While the cell bodies and the major processes of adjacent astrocytes have no contact, the astrocyte processes in the periphery of the micro-domains are in direct contact with each other (Fig. 1). This way astrocytes demarcate the

gray matter into functional domains, whose significance however is still unknown. Within its micro-domain a single astrocyte can enwrap more than 100 000 synapses and may be in contact with several hundred dendrites from distinct neurons [7]. Micro-vessels are often located along the border of the astrocytic micro-domains, which allows several adjacent astrocytes to enwrap them with their end-feet [3]. A similar micro-domain system of fibrous astrocytes is likely to occur, but has not yet been detected [7].

Astrocyte physiology

The unique positioning of astrocytes, which allows them to contact neurons on one side and the vasculature on the other side (Fig. 1), indicates that astrocytes exert important roles in the CNS [4]. The expression of a wide range of receptors for several neurotransmitters, hormones, cytokines and peptides allows them to sense their environment and respond to several extracellular stimuli from distinct cell types around them [9,10]. Astrocytes are equipped with a plethora of transporters and channels [3] allowing them to actively control their environment. Functionally astrocytes are involved in several essential and complex functions in the physiological CNS, which include maintenance of the extracellular environment (ion and pH homeostasis), metabolic support for surrounding neurons, regulation of synaptogenesis, active control of synaptic functions and neurotransmission, neurovascular coupling, and maintenance of the blood brain barrier (BBB) integrity [3,4,7,9,11,12,13]. The contribution of astrocytes to the neural network activity is becoming increasingly recognized. A lot of research has been conducted, which revealed the regulatory input of astrocytes at the synapse, which is now acknowledged in the model of the tripartite synapse (for a review see [14]. Astrocytes also communicate with each other via gap junctions (Fig. 1) [3,15]. Gap junctions allow the transfer of small molecules (< 1000 Da) such as second messengers, energy molecules, or metabolites between neighbouring cells thereby connecting astrocytes within a wide communication network [15].

An intriguing discovery in the last years was the existence of astrocyte-like stem and progenitor cells during development and in the neurogenic niches of the adult brain in addition to the above described parenchymal astrocytes. Therefore, a specific subset of astrocyte-like cells may also contribute to neurogenesis [2,16].

Heterogeneity of Astrocytes

The accumulating number of astrocytic functions in the physiological CNS resulted in a growing field of astrocyte research [7]. It was shown that astrocytes not only increased in number during evolution but also in diversity. In the adult mammalian CNS astrocytes are very heterogeneous, concerning their morphology, molecular equipment and function [4]. Studying astrocytes hence requires a reliable marker. All astrocytes have in common the expression of the astrocyte-specific intermediate filament (IF) glial fibrillary acidic protein (GFAP) during at least one point in their life span [17]. GFAP is usually the most prominent component of the mature IF network in astrocytes. However, depending on the subpopulation the level of GFAP varies [4,17,18]. Other commonly used astrocyte markers are the calcium-binding protein S100β [4], the glutamine synthetase and the recently suggested aldehyde dehydrogenase 1 family member L1 [7].

Differences between astrocytes are found to be regional, implying adaptation of astrocytes to functionally distinct neuronal networks, but also local distinctions are found [4]. The exact mechanisms behind astrocyte heterogeneity have not yet been determined. Phenotypic plasticity denotes that astrocyte heterogeneity may be the result of a flexible plasticity of one astrocyte type responding to environmental cues [4,17], whereas astrocytes in distinct regions of the CNS may also originate from distinct progenitors. Some authors suggest a combination of both to be responsible for astrocyte heterogeneity [4].

1.2 Intermediate filaments of astrocytes

Astrocytes express four IF proteins, namely GFAP, vimentin, nestin and synemin [19]. IFs form together with microtubules and microfilaments the cytoskeleton in most eukaryotic cells. With a diameter of ~10 nm, they are intermediate in size compared to microtubules (25 nm) and microfilaments (6-8 nm) [20]. While microtubules are composed of tubulins and microfilaments of actin, IFs consist of different members of the IF protein family [21] that are expressed in a tissue-, cell-, developmental- and differentiation-specific pattern. The mammalian IF protein family consists of ~ 70 members [22] that are divided into six different subdivisions (Tab. 1) based on sequential, structural and biochemical similarities [1,23]. Although IF proteins exhibit a low sequence homology, they all share a common tripartite structure (Fig. 2) [22]. Since IF proteins can be stretched to a multiple of their own length without breaking they play a major role during mechanical stress and strain [24]. In general, the dynamic IF network plays an important role in mechanical stabilization [21,22], cell shape and motility [22].

Table 1 Classification of intermediate filament proteins

Type	Members	Localization
I	acidic keratins	epithelia, hair
II	basic keratins	epithelia, hair
III	vimentin	mesenchymal
	desmin	muscle
	GFAP	astrocytes
	peripherin	neurons
	syncoilin	muscle
IV	neurofilaments	neurons
	α-internexin	neurons
V	nuclear lamins	ubiquitous
VI	nestin	neuroepithelia, diverse
	synemin	muscle, diverse

1.2.1 GFAP

GFAP is the main IF protein in mature astrocytes. GFAP expression is highly regulated and induced in response to brain injury or neurodegeneration and its expression increases with age even under physiological conditions [19]. The type III IF protein (Tab. 1) [19] was discovered in 1971 by Eng and co-workers in the brains of patients with multiple sclerosis [25]. Further studies in the mature mammalian CNS revealed GFAP immunoreactivity exclusively in astrocyte processes [25] and hence GFAP was suggested to be astrocyte specific. However, it was later shown that the GFAP content in astrocytes can vary from highly expressed down to a non-detectable level under physiological conditions [4,17,18].

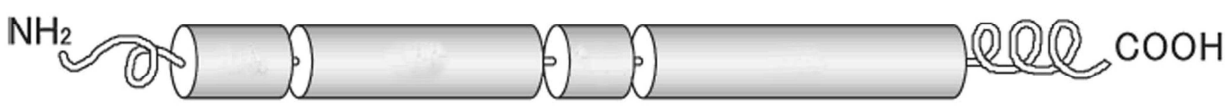

Figure 2 Schematic structural model of an intermediate filament protein. A highly conserved central α-helical rod domain, divided into four coiled segments linked by short non-helical regions is flanked by variable IF protein-specific non-helical end domains. The N-terminus is seen as the head and the C-terminus as the tail. Figure adapted from [1]

$GFAP^+$ cells are also found in the two neurogenic niches in the adult brain, the subventricular zone (SVZ) and the dentate gyrus in the hippocampus [2]. This discovery raised the discussion about a putative stem/progenitor cell potential of astrocytes [2,8,16,19]. In the last few years eight different isoforms of GFAP have been discovered and increasing evidence points to an

astrocyte subtype-specific expression of the isoforms, which warrants a re-evaluation of already acquired data that only took into account one isoform of GFAP [19].

GFAP on transcriptional and translational level
GFAP gene expression is highly regulated by the *GFAP* promoter, however the exact regulation of *GFAP* transcriptional activity is still unclear [19]. Several modulators of *GFAP* expression are described including hormones and several growth factors [26]. In addition, epigenetic mechanisms like phosphorylation and DNA methylation are shown to influence *GFAP* transcription [19]. The mature GFAP mRNA yields a size of about 3 kb [25]. Alternative splicing results in eight splice variants, GFAP α, β, γ, δ/ε, κ, Δ135, Δexon6, and Δ164. All forms have been found in the rodent and with the exception of GFAPβ also in the human CNS. GFAPα is the most common and known isoform. Of the other isoforms, GFAPδ has received the most attention since it is expressed in the proliferating SVZ astrocytes that are suspected to be neural stem cells [19].

GFAP in intermediate filaments and its function
IF proteins exist either in a non-filamentous form or are incorporated into IFs of distinct lengths [22,27]. GFAP or at least GFAPα is the only astrocyte IF protein that is capable to form homopolymeric filaments, although these exhibit an abnormal organization [19,22,27,28]. Usually GFAP co-assembles with vimentin to form IFs [28]. The structure and properties of GFAP filaments are regulated by the GFAP protein concentration, post-translational modifications and through GFAP interacting proteins. Like the other type III IF proteins, GFAP is involved in the structural maintenance of the cytoskeleton, providing mechanical support and strength for the cell. GFAP expression changes throughout development and aging of the CNS [19], as well as in response to brain insults [29], indicating distinct functions over time and under pathological conditions. Several GFAP knock-out mouse lines were generated in the past years and quite surprisingly when the phenotype of the first GFAP $^{-/-}$ mouse was presented in 1995 the overall appearance was indistinguishable from wild-type mice, although they lacked IFs [30,31]. Later studies however showed that GFAP $^{-/-}$ mice did differ from wild-types especially in the "challenged" CNS and that GFAP and vimentin apparently exert overlapping functions, which were perturbed in a GFAP/vimentin double knock-out mouse [29]. In summary, a functional involvement of GFAP was revealed in astrocyte motility and migration, vesicle trafficking, induction of the BBB, neuron-glia interactions and proliferation (for a review see [19]).

1.2.2 Nestin

In 1985, Hockfiel and McKay presented the antibody Rat.401, which binds mainly in the proliferative area of the neural tube and was thereafter suggested to be a neural stem cell marker [32]. Further research indicated that Rat.401 binds to an IF protein, which is mainly expressed in neuroepithelial stem cells and the gene was named *nestin*. Although the *nestin* sequence exhibited a region similar (16-29 %) to the conserved α-helical rod domain of already known IF proteins it exhibited otherwise an extremely short N-terminal domain (11 amino acid residues) and an extremely long C-terminal domain not known from any other IF protein. Furthermore, the location of the three introns in the *nestin* gene were distinct to those of other types of IF proteins. Lehndahl *et al.,* suggested it to be a new class, the VI class of IF proteins [33] (Tab. 1). The n*estin* gene is conserved in rodents and humans and results in a protein with more than 1600 amino acid residues and a molecular weight of 198 kDa [34].

Expression of Nestin
Over the years it become clear that nestin is not only expressed in neuroepithelial stem cells [33,35]. During development, nestin is expressed in radial glia [32,36] and basically all precursor cells of neurons and astrocytes [34]. In the adult CNS, nestin expression remains in the proliferating niches such as the SVZ [36,37] and the dentate gyrus of the hippocampus [34]. It is also found in ependymal cells lining the ventricle [37,38], in endothelial cells [37,38,39,40], in perivascular cells [37,40] and in a variety of primary CNS tumours [39]. The *nestin* gene can be re-induced in astrocytes in the adult CNS in case of brain injury [40,41] and astrocytes *in vitro* are shown to express nestin [40,42]. Additionally, nestin^{+} cells were detected outside the CNS in e.g. developing skeletal muscle [33], bone marrow mesenchymal stem cells [43], in the adult retina, striated muscle, cardiac muscle, teeth, liver, pancreas, kidneys, testicles and adrenals [34], indicating that nestin is more than just a neural stem cell marker.

Regulation and functional aspects of Nestin
Nestin requires type III or IV IF proteins to form IFs *in vitro* [44] and *in vivo* [34]. While nestin does not co-assemble with GFAP it forms heteropolymeric filaments with vimentin [28]. *In vitro* studies revealed that IFs are only formed as long as the amount of nestin in the heterooligomere does not exceed 25 % [44]. Low phosphorylation of nestin facilitates IF assembly, while a high level of phosphorylation results in disassembly [34]. The functional involvement of nestin in the IF network was recently challenged with the creation of a knock-out mouse [45]. Mice lacking nestin exhibit embryonic lethality. Nestin$^{-/-}$ embryos (E8.5) showed less neural stem cells in the neuroepithelium of the developing tube and enhanced apoptosis *in vivo*, while other organ systems seemed not to be affected besides of a smaller size. Surprisingly, embryonic nestin$^{-/-}$ cell cultures revealed that a lack of nestin had no impact on the integrity of the cytoskeleton and proliferation, migration, attachment and differentiation seem not to be altered. However, nestin$^{-/-}$ cells exhibit a drastically decreased potential for self-renewal and increased apoptosis *in vitro* [45]. Other studies imply that the unusual long C-terminal tail that contains several highly charged peptide repeats may protrude from the IF core and function as a spacer between IF and other cytoskeletal components. This would indicate the involvement of nestin in the regulation of a dynamic supra-molecular organization within the cell [44]. Recent data also point out an involvement of nestin as a scaffold for several intracellular signalling molecules [46,47]. In summary, it is not completely clear yet which function(s) nestin exerts when it is expressed but it may be that nestin is involved in IF-independent tasks.

1.3 Developmental aspects of astrocytes

Considering the evolution of the CNS, it stands out that the number of astrocytes expands in higher mammals compared to neurons. This increase of astrocytes with evolution is suggested to be connected with the increasing network complexity in the CNS in higher mammals. The more complex and sophisticated a neuronal network gets, the more local control and modulation is needed [3]. Furthermore, while in lower organisms, as for example in *Drosophila,* neurons and astrocytes are generated simultaneously during development, a subsequent generation of neurons and glia cells is observed in the developing vertebrate CNS. This subsequent order allows first for the establishment of a neural circuitry followed by a matched positioning of glia cells [48]. In the rodent CNS the first neurons appear on embryonic day 9-10 (E9-E10) [49] and the generation of new neurons lasts until E18, followed by the generation of astrocytes, which peaks in the neonatal period. Oligodendrocytes are the last cells to occur postnatally [48].

Radial glia and the switch from neurogenesis to astrogenesis

During early development neuroepithelial stem cells transform into radial glia. Studies in the last decade revealed radial glia as the stem and progenitor cells during development that give rise to ependymal cells, neurons, astrocytes or distinct intermediate progenitor cells that generate neurons, oligodendrocytes or astrocytes, respectively [2]. Radial glia express several markers like glutamate-aspartate transporter, brain lipid binding protein, glutamine synthetase, S100β, tenascin-C, vimentin, nestin and in some species, but not in rodents, GFAP. Many of these markers are known to be expressed in mature astrocytes [50]. The potential of radial glia cells to produce a distinct cell type underlies a complex spatially and temporarily regulated mechanism, which is still not fully understood. Morphogenic gradients of e.g. bone morphogenetic proteins or sonic hedgehog provide the cells with spatial information and sections the developing CNS in specific progenitor domains [49]. Radial glia and neuroepithelial cells must interpret these gradients and via distinct set-ups of transcription factors produce the appropriate cell type [2]. The switch from neurogenesis to gliogenesis in the precursors is a complex interplay of environmental cues, transcription factors and intrinsic developmental programs. During neurogenesis, gliogenesis is repressed by a complex interaction of intrinsic mechanisms and environmental cues [48].

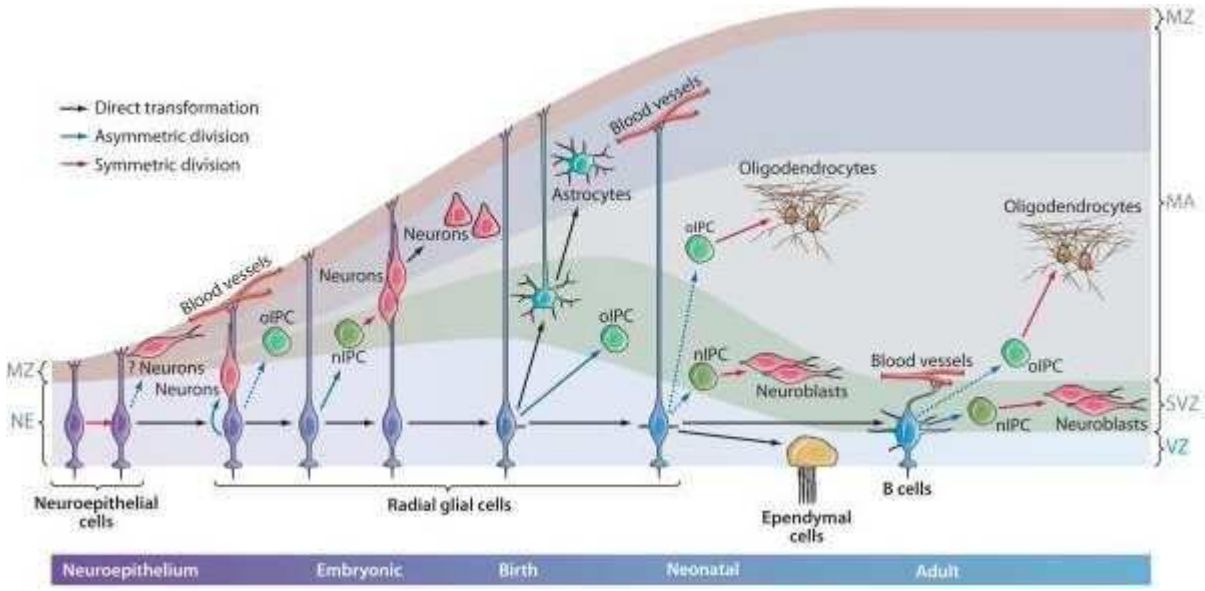

Figure 3 Development in the forebrain. During early development neuroepithelial cells, with the potential to self-renew, are located along the ventricular zone (VZ). They are capable of generating few neurons but are mostly transformed into radial glia cells at the beginning of neurogenesis (E9-E10 in rodents). Radial glia cells are located like neurepithelial cells along the ventricles, exhibit an apical-basal polarity and undergo kinetic nuclear migration. They are in contact with the pial surface and act therefore as a scaffold for neuronal migration to the outer cortical layers. Radial glia give rise to ependymal cells, neurons or distinct intermediate progenitor cells (IPC) that give rise to neurons (nIPC), oligodendrocytes (oIPC) or astrocytes, respectively. At the end of development, radial glia transform directly into astrocytes. MZ, marginal zone; MA, mantle; NE, neuroepithlium; SVZ, subventricular zone. Figure taken from [2]. Reproduced with permission from Annual Reviews Inc.

Once a cell has entered the path of becoming an astrocyte, the astrocyte precursor migrates to its final position and begins its terminal differentiation [49]. Some progenitor cell types endure in the adult CNS in distinct germinal areas such as the SVZ and the dentate gyrus of the hippocampus, where continuous neurogenesis occurs and also new glia cells can be produced [2].

Developmentally regulated expression of type III and VI IF proteins in astrocytes
The constitutive IF protein reflects the differentiation state during development, maturation and in disease [24]. During development of the rodent CNS nestin and vimentin are both expressed very early in neuroepithelial stem cells and in radial glia [50]. It seems that the transition from an undifferentiated proliferating state to a post-mitotic differentiated cell type during development is accompanied by the loss of the IF nestin and its replacement by a lineage typical IF protein such as GFAP in astrocytes and α-internexin or neurofilaments in neurons [33,51]. Immunohistochemical studies showed that in the rat cortex nestin protein disappears between P14 – P18, while simultaneously mature astrocytes increased [36]. Vimentin, the major IF protein in the neonatal brain is progressively replaced by GFAP and in the mature brain declines in most astrocytes to an undetectable level [52] although Bergman glia and astrocytes in the hippocampus and corpus callosum constantly co-express vimentin and GFAP in the adult CNS [19].

1.4 Reactive astrocytes

Astrocytes in the adult CNS are described to become rapidly activated in case of basically any insult to the brain [7,53]. This phenomenon is conserved among several species and termed reactive gliosis [53]. In 2010 Sofroniew presented the temporary definition of reactive gliosis:
"(1) Reactive astrogliosis is a spectrum of potential molecular, cellular and functional changes in astrocytes that occur in response to all forms and severities of CNS injury and disease including subtle perturbations, (2) the changes undergone by reactive astrocytes vary with severity of the insult along a gradated continuum of progressive alterations in molecular expression, progressive cellular hypertrophy, and in severe cases, proliferation and scar formation, (3) the changes of reactive astrogliosis are regulated in a context-specific manner by inter- and intracellular signalling molecules, (4) the changes undergone during reactive astrogliosis have the potential to alter astrocyte activities both through gain and loss of functions that can impact both beneficially and detrimentally on surrounding neural and non-neural cells" [7].
Reactive gliosis occurs in e.g. viral infections, oedema, trauma, stroke, epilepsy, inflammatory disorders, brain tumours and neurodegenerative diseases [7,53]. Following activation, astrocytes upregulate the expression of a plethora of molecules including adhesion molecules, calcium binding proteins, cytokines, growth factors, cytoskeletal components, early response genes, eicosanoids, enzymes, receptors and transporters. Many of these molecules are either not detected at all or are found to be expressed at lower levels in quiescent astrocytes [53], indicating that reactive astrocytes might acquire additional new functions in the disturbed CNS. Classical hallmarks of reactive gliosis are the upregulation of GFAP expression [7,53], cellular hypertrophy of cell body and processes, proliferation and glia scar formation, although proliferation and scar formation are now recognized to occur only in severe reactive gliosis [7].

Glia scar formation
In the case of severe tissue damage and/or infection, astrocytes migrate to the damaged area and in concert with other cells such as microglia or NG2 glia demarcate the injured area from the surrounding healthy brain tissue. This glia scar is protective in a way that it encloses inflammatory cells and infectious agents to the damaged area and allows a rapid healing. On the other hand, it prevents axonal and cellular migration and hence neuroregeneration [7].

Upregulation of GFAP and other IF proteins
Upregulation of the IF protein GFAP is a classical hallmark of reactive gliosis. It can occur in many astrocytes that do not normally express GFAP at detectable levels under physiological conditions [7]. Furthermore, an upregulation of the IF proteins nestin and vimentin, which are

abundantly expressed in immature astrocytes, is observed in reactive astrocytes. The functional role of IF protein upregulation is not yet fully understood. Studies in GFAP knock-out mice revealed that GFAP is not required for astrocytes to become activated. Only in cases of GFAP/vimentin double knock-outs, which result in no IF formation at all, changes in reactive gliosis were observed [29]. Reactive astrocytes in GFAP$^{-/-}$/vimentin$^{-/-}$ mice exhibited less hypertrophic cell processes, a slower migration and a loose and less organized glia scar [29], which allowed neurite outgrowth and remarkable synaptic regeneration following hemisection of the spinal cord [54].

Proliferation
In cases of severe reactive gliosis astrocytes have been shown to proliferate [7]. It is known that following brain injury microglia are activated [8] and rapidly start proliferating [55]. Furthermore, NG2 glia, a ubiquitously distributed cell population with the potential to proliferate under physiological conditions, mainly generating oligodendrocytes (2009_Nishiyama, 2009_Wang), quickly upregulate proliferation following brain injury [56]. However, parenchymal astrocytes are usually seen as quiescent, post-mitotic, differentiated cells that do not proliferate [7]. Since terminal differentiation is assumed to involve exit of the cell cycle [57] it is suggested that proliferating astrocytes following brain injury made a step backwards towards a less differentiated state. The group of Magdalena Götz in Munich showed that following stab wound lesion, cortical de-differentiated, proliferating astrocytes give rise to neurospheres in culture [58]. These neurospheres exhibit self-renewal and multipotency indicating stem cell potential of cortical de-differentiated astrocytes following injury, at least *in vitro*. These results highlight resident astrocytes as a promising cell source for brain repair following injury [58].

Regulation of reactive gliosis and their functional outcome
Several inter- and intracellular signalling molecules have been identified in case of reactive gliosis and it was shown that the activation of astrocytes is highly context-specific. Trigger molecules that activate astrocytes can be released by all cell types in the CNS in response to all forms of CNS insult and activate distinct intracellular signalling cascades (for a review see [7]). Reactive gliosis can be both beneficial and detrimental. Glia scar formation is a good example of the Janus face of reactive gliosis, where on one hand axonal regeneration is inhibited but on the other hand the spread of inflammation and infection to the healthy tissue is prevented [7].

1.5 Aquaporins

Astrocytes are the main cell population in the adult CNS that express the water channel aquaporin 4 [59], which constitutes the main pathway for osmotically driven water transport into and out of the brain [60].
Water constitutes the largest part of the cell and a well working water homeostasis is important. The plasma membrane of a cell functions as a natural barrier to water flow. However, the phospholipid bilayer of the plasma membrane is slightly permeable to water and allows diffusion of water molecules through the membrane [61,62]. In 1957, scientists hypothesized that water pores or channels in plasma membranes may exist allowing a more efficient and quick water flow through membranes, as it was observed in red blood cells [63] and later in distinct mammalian epithelia and in plant tissue [61]. It took more than 30 years until the first water channel termed CHIP (channel forming integral protein), later aquaporin 1, was discovered by Peter Agre and his co-workers in the late 1980s. For the discovery of the water channel Agre was awarded the Nobel Prize in Chemistry in 2002.

Properties of aquaporins

As of today 13 water channels, so called aquaporins (AQPs), have been identified in mammals [64] and many more in other vertebrates, invertebrates, plants, fungi, archea and eubacteria [65]. AQPs are small (monomer size ~ 30 kDa), hydrophobic, mostly constitutively expressed intrinsic membrane proteins [64]. Typically AQPs are located in the plasma membrane [64], however recent studies reported the location of some AQPs in the membranes of intracellular organelles [66]. AQPs assemble as tetramers in the membrane with each monomer representing a distinct water channel [64]. Water transport occurs bidirectional following an osmotic gradient [67] and compared to mere membrane diffusion, channel-mediated water flow exhibits a 5-50 times higher permeability rate [64]. Some AQPs not only transport water but also small molecules and other solutes [64]. Based on these permeability characteristics the AQP-family was subdivided into two main groups namely aquaporins facilitating only water transport (AQP0, AQP1, AQP2, AQP4, AQP5) and aquaglyceroporins (AQP3, AQP7, AQP9, AQP10) transporting water, glycerol and other solutes such as e.g. urea [68]. In addition an unorthodox AQP subgroup was recently assigned comprising uncharacteristic AQPs (AQP11, AQP12) whose function is not clear yet and AQPs permeable for ions (AQP6, AQP8) [68].

Structure of aquaporins

Despite the subdivision into the two main groups, namely aquaporin and aquaglyceroporins according to permeability characteristics [63], and an amino acid sequence identity ranging from 19 to 52 % [69], it is assumed that these AQPs share a common molecular structure [63]. The first structure identified on atomic level was for AQP1. Every water channel consists of four monomers arranged as tetramers (Fig. 4) and dissimilar to ion channels, each monomer subunit contains its own (water) pore [67]. Each AQP protein exhibits six transmembrane spanning α-helices, three extracellular loops, two short intracellular loops, an intracellular amino- and carboxy-terminus [64]. Soon after the discovery of APQ1 it was noticed that water transport through AQP1 did not permit passage of protons or other ions together with the water molecules, thus protecting the transmembrane proton gradient [61]. This indicated a uniquely selective mechanism for water permeation through AQPs and led to the prediction of the 'hourglass model' for AQP structure (Fig. 4) [67] consisting of an extracellular vestibule and an intracellular vestibule connected by a 20 Å trim span. In solution, water molecules form hydrogen bonds with other water molecules, allowing protons to move freely between the molecules thus protons could easily permeate together with a water molecule. To prevent the passage of protons several mechanisms are embedded in the vestibule: size restriction, electrostatic repulsion and water dipole reorientation (Fig. 4) [67]. The rate of water transport through AQPs is relatively quick with 2-4 x 10^9 water molecules per second in one monomer [61].

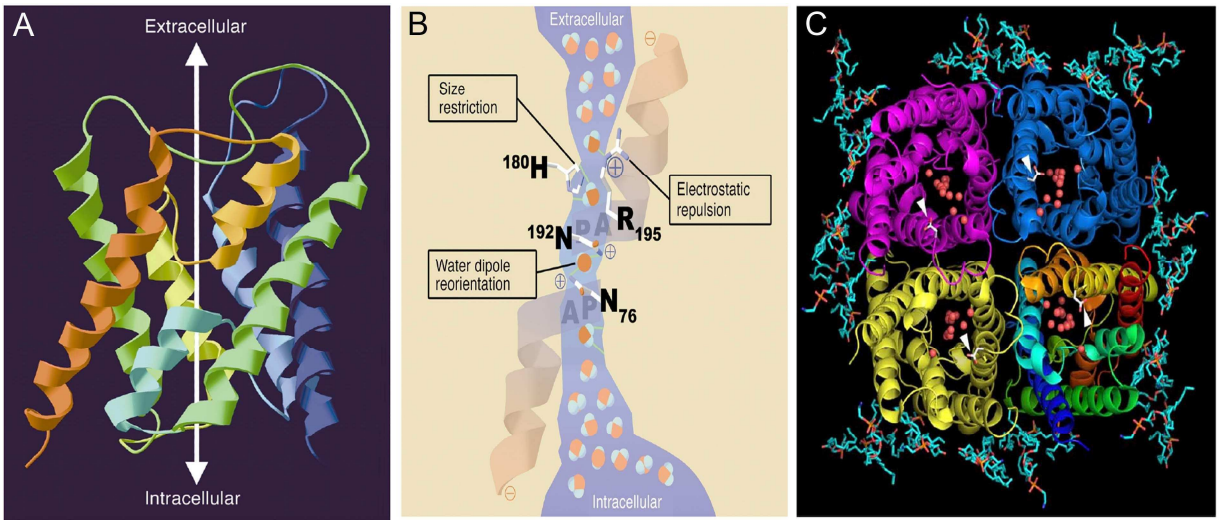

Figure 4 Aquaporin structure **A** Ribbon diagram displaying the side view of an AQP monomer. **B** Schematic overview of the AQP architecture. **C** Ribbon diagram displaying an AQP tetramer viewed from the cytoplasmic side. Figures taken from [65] (**A, B**) and [70] (**B**). Reproduced with permission from the American society for clinical investigation and from Elsevier.

Aquaporins in physiological conditions
High water flow across the membrane is required in many specialized tissues in the mammalian body including organs such as the kidney, lung, vascular system, eye, skin, exocrine glands and the brain [71,72]. For an efficient water flow in these tissues it is shown that several thousands AQPs per μm^2 of cell membrane are present in a cell [64]. Many more functions of AQPs in physiological processes are known now, such as in glandular fluid secretion, urinary concentration mechanism, cell migration, neural signal transduction, skin moisturization and fat metabolism [72].

Aquaporins in the brain
Regulation of water homeostasis is crucial in many organs and tissues. In the brain it is especially important as only a limited volume fits underneath the protective skull and a volume dilation in case of impaired water homeostasis can be fatal [71]. AQPs are of crucial importance in facilitating water flow into and out of the brain [72], and producing cerebrospinal fluid thereby controlling the intracranial pressure [71]. Six AQPs have been reported to be expressed on mRNA level in the CNS, namely AQP1, AQP3, AQP4, AQP5, AQP8 and AQP9 [63]. However, only AQP1, AQP4 and AQP9 are detected on protein level [68]. AQP1 is exclusively detected on the apical membrane of epithelial cells in the choroid plexus, where it is involved in cerebrospinal fluid production [61]. The aquaglyceroporin AQP9 is expressed in ependymal cells, in glucose-sensitive neurons and faintly on astrocytic processes and cell bodies [63]. It is suggested to play a major role in brain energy metabolism using its ability to transport lactate across astrocyte membranes [73]. AQP4 is the most abundantly expressed water channel found in the CNS, localized extensively on astrocytes and seems to be the major route for water into and out of the brain [63]

1.5.1 Aquaporin 4

In 1994 Peter Agre and colleagues reported a water-channel termed AQP4 that is abundantly expressed in mature rat brain but also found in kidney, eye, intestine, lung [74] and skeletal muscle [75]. AQP4 is structurally similar to the other AQPs and belongs to the group of AQPs that only transport water. Unlike other AQPs, AQP4 lacks the cysteines, reported in mercury inhibition of AQPs and studies confirmed that osmotic water permeability is not blocked by $HgCl_2$ [74].

AQP4 distribution
In the CNS AQP4 is highly expressed at the borders between the brain parenchyma and the main fluid compartments [74,76]. On the cellular level, AQP4 is predominantly expressed in glia cells and a subpopulation of ependymal cells [59]. Although in some in situ hybridization experiments AQP4 mRNA expression seemed to be localized in neurons [74,77], it is the general assumption that AQP4 expression is strictly non-neuronal [59,78,79]. A faint expression of AQP4 was also shown in endothelial cell [78] and in adult progenitor/stem cells [80]. Some sporadic reports of AQP4 expression in oligodendroytes [80] or reactive microglia [81] exist.
In astrocytes, AQP4 exhibits a highly polarized expression *in vivo*. AQP4 is expressed predominantly in end feet whose membranes facing pial or perivascular basal laminae [59,82]. This polarization is assumed to depend on the dystrophin complex or more specific on α-synthropin, a member of the dystrophin complex. The dystrophin complex forms a crucial link

between the cytoskeleton of a cell and the surrounding extra-cellular matrix [83]. Mice lacking α-syntrophin exhibit a misallocation of AQP4 in astrocyte endfeet, especially in membranes facing pial basal laminae. However, only a 50 % loss of AQP4 expression in membranes facing perivascular basal laminae is observed indicating the existence of further anchoring proteins [83].

AQP4 isoforms

AQP4 has several isoforms [59,74,84,85,86] that differ in their intracellular N-terminus. In the first study about AQP4 in rat, Agre and colleagues reported two isoforms on AQP4, whose transcriptional initiation site were identified at methionine 1 or methionine 23, therefore the isoforms were termed AQP4 M1 and M23, respectively [74]. The C-terminus of AQP4 M1 is 22 amino acids longer than in M23, yielding a polypeptide with ~32 kDa, while the shorter M23 yields a polypeptide with ~30 kDa [74]. Indications of additional AQP4 isoforms followed [84] and three isoforms are now described in the mouse brain, termed M1, M23 and M23x [85] and just recently six isoforms were reported in the rat brain [86]. The AQP4 isoforms detected in the rat brain were termed AQP4a-f, where AQP4a corresponds to M1 and AQP4c corresponds to M23. Only three isoforms (AQP4a (M1), AQP4c (M23) and AQP4e (z)) were identified as functional water channels expressed in the plasma membrane [86]. Most literature so far dealt only with the isoforms M1 and M23. The AQP4 isoforms were originally suggested to be derived by alternative splicing [75]. In addition, Frigeri and colleagues recently suggested that the isoform M23 may also be derived from a “leaky scanning” mechanism on translational level [87]. The characteristic formation of AQP tetramers in the membrane was shown for AQP4 to comprise both the M1 and the M23 isoform, resulting in the formation of heterotetramers [84].

AQP4 and OAPs

Soon after the discovery and localization of AQP4 it was shown that AQP4 constitutes structures that have been observed for a while in freeze-fracture analysis [75] and were termed orthogonal arrays of particles (OAPs) [13]. AQP4 heterotetramers consisting of M1 and M23 arrange to these higher order complexes, consisting of four - several hundreds heterotetramers [13]. The size of the OAP is suggested to be determined by the ratio of the isoforms [13]. Transfection of Chinese hamster ovary cells with M23 only, results in large lattices in the membrane, while transfection with M1 only, yields no or merely tiny arrays. Transfection with both AQP4 isoforms results in the formation of OAPs similar to those observed in astrocytes *in vivo* [88]. *In vivo* OAPs are found primarily in astrocyte endfeet and less in parenchymal membranes. The functional significance of OAPs is still undetermined [13], though it is speculated that OAP formation may enhance the water permeability [89].

AQP4 function and regulation in the CNS

Water transport across membranes is critically involved in CNS homeostasis under physiological conditions [59]. AQP4 is localized in the same membrane areas such as e.g. the cholinergic muscarinic receptors [90], the potassium channel Kir4.1 [91] or the Na^{2+}/K^{+} ATPase [92], indicating that AQP4 plays a role in several important astrocytic housekeeping functions such as potassium siphoning, where AQP4 may provide a passage for concomitant water flux [76,84,90]. Water flux mediated by the astrocyte endfeet enwrapping vasculature or synapses may also regulate the perivascular volume or the extrasynaptic space, respectively [90]. More functions of AQP4 were detected with the help of AQP4 knock-out mice [72], revealing an important role of AQP4 in brain oedema formation and resolution [82] as well as an involvement in cell migration [60,68]. Water flux through AQP4 is not only regulated by a concentration gradient across the membrane, but also by the channel permeability and the abundance of APQ4 in the cell membrane [68]. Regulation of AQP4 is subject of both dynamical short-term regulation such as

e.g. phosphorylation and dephosphorylation or protein-protein interactions but also long-term regulation based on changes in AQP4 expression on mRNA or protein level (for a review see [68]).

1.6 Dopamine

The dopamine (DA) system in the CNS controls locomotion and is involved in goal oriented behaviour (attention and reward), cognition, emotion and neuroendocrine secretion [93,94]. Disorders of the DA system are shown in several diseases such as for example Parkinson's disease (PD), Huntington's disease or schizophrenia [94].

Dopamine synthesis pathway

The neurotransmitter DA belongs together with norepinephrine and epinephrine to the catecholamine family. All three catecholamines, are successively synthesized from L-tyrosine (Fig. 5).

Figure 5 Catecholamine synthesis pathway. The enzyme tyrosine hydroxylase (TH) converts L-tyrosine to 3,4,-dihydroxy-L-phenylalanine (L-DOPA) which is further decarboxylated to dopamine by DOPA decarboxylase (DDC). Addition of a hydroxyl group to dopamine by dopamine β-hyroxylase (DBH) leads to the formation of norephinephrine, which can further be converted to epinephrine via N-methylation by phenylethanolamine N-methyltransferase (PNMT).

Tyrosine hydroxylase (TH), the enzyme for the first step in the synthesis of catecholamines is found in all cells producing catecholamines, while all other enzymes involved in the catecholamine synthesis exhibit a less frequent distribution [95].

Dopamine receptors and signalling pathways

DA receptors belong to the superfamily of G-protein coupled receptors. Five subtypes of DA receptors are known, which are referred to as D_1-like receptors (D_1 and D_5) and D_2-like receptors (D_2, D_3 and D_4) based on sequence homology, differences in their signalling transduction and in their drug specificity [95,96]. Each DA receptor family has a distinct localization pattern in the brain and induces a distinct intracellular signalling cascade, so DA can result in distinct effects depending on the cell type involved and the expressed DA receptor(s) [96,97,98]. Like other neurotransmitter receptors, DA receptors are endocytosed and recycled following stimulation [96,98]. DA receptors are also found on astrocyte membranes in diverse brain regions [10,99,100,101,102,103].

The dopaminergic system

In the peripheral nervous system DA serves mainly as a substrate for norepinephrine and epinephrine [94]. In the CNS DA regulates the proper function of the basal nuclei and their associated projections.

Dopaminergic neurons of the midbrain are located in the substantia nigra (SN) and the ventral tegmental area (VTA) [94] and project into the forebrain via three major pathways: the nigrostriatal pathway, the mesolimbic pathway and the mesocortical pathway [94,97] (Fig. 6). The striatum is the largest structure of the basal nuclei and located between the lateral ventricles and the cortical area. It receives its dopaminergic input via the nigrostriatal pathway from

dopaminergic neurons located in the SN pars compacta [94]. Cell death of these dopaminergic neurons and subsequent loss of DA in the striatum is involved in PD [104].
Contrary to classical neurotransmitters, DA acts not directly on ion channels, but as mentioned before via signal transduction cascades. Therefore, DA acts not simply as an excitatory or inhibitory neurotransmitter, but rather modulates the response of a cell to another neurotransmitter depending on the DA receptor and the state of the cell at the time of the stimulation [105]. The involvement of DA in movement, attention, motivation, and mood are described in the adult mammal [98]. However, DA is also present during early development (~ E13 in the mouse) where it exerts a regulatory effect in e.g. maturation of GABAergic neurons [106,107] an in proliferation of progenitors [108,109]. Although astrocytes are shown to express DA receptors [99,100,101,102,103] and the DA transporter (DAT) [110], little is known about an effect of DA on astrocytes.

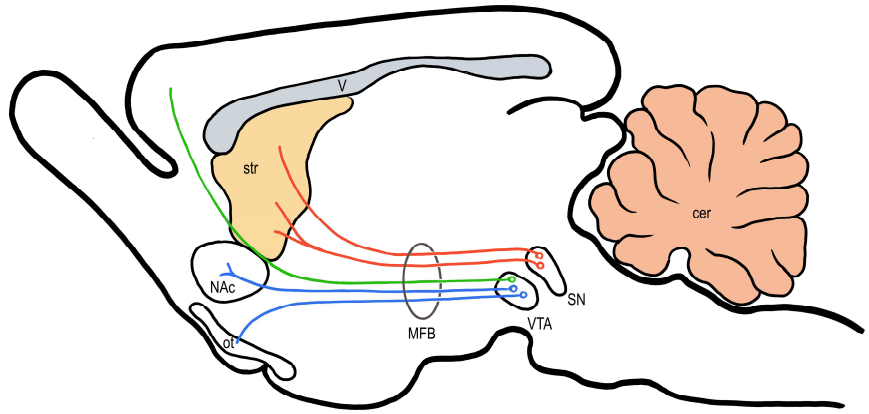

Figure 6 Schematic overview of the midbrain dopaminergic projections in the rodent brain. Nigral dopaminergic neurons are located in the substantia nigra (SN) pars compacta and project via the nigrostriatal pathway (red line) to the dorsal striatum (str). The dopaminergic neurons of the ventral tegmental area (VTA) project via the mesolimbic pathway (blue line) to the ventral striatum including nucleus accumbens (NAc) and part of the olfactory tubercle (ot)). Dopaminergic neurons form the VTA also project via the mesocortical pathway (green line) to the prefrontal cortex.

Dopamine and 6-hydroxydopamine cytotoxicity
Increased concentrations of DA, either intracellular or extracellular, under pathological conditions (e.g. ischemia or hypoxia) are toxic for neuronal and non-neuronal cells [111]. Cytotoxicity of DA is linked to oxidative metabolism (Fig. 7). Auto-oxidation or enzyme catalyzed oxidation of DA produces reactive oxygen species (ROS) and quinones that impair cellular components such as lipids, proteins and DNA and can induce apoptosis [93,111,112,113]. Several mechanisms such as amine oxidation, deamination by monoamine oxidase (MAO) and/or mitochondrial inhibition are suggested in DA cytotoxicity (Fig. 7) [111]. 6-hydroxy dopamine (6-OHDA) is a structural analogue to DA with the difference of an additional hydroxyl group at the benzene ring on position six [104,114]. 6-OHDA is highly toxic for catecholaminergic neurons [104,115]. Natural production of 6-OHDA is rare, but synthetically synthesized 6-OHDA is commonly used in research to mimic PD pathogenesis. 6-OHDA is preferentially taken up like ordinary DA into both dopaminergic and adrenergic neurons via amine transporters located on the outer membrane [104,114]. Once inside a neuron, 6-OHDA exhibits a neurotoxicity, which involves oxidative stress, although the exact mechanism is not yet fully understood (Fig. 7). 6-OHDA accumulates in the cytosol and induces cell death independent of its uptake into synaptic vesicles [104].

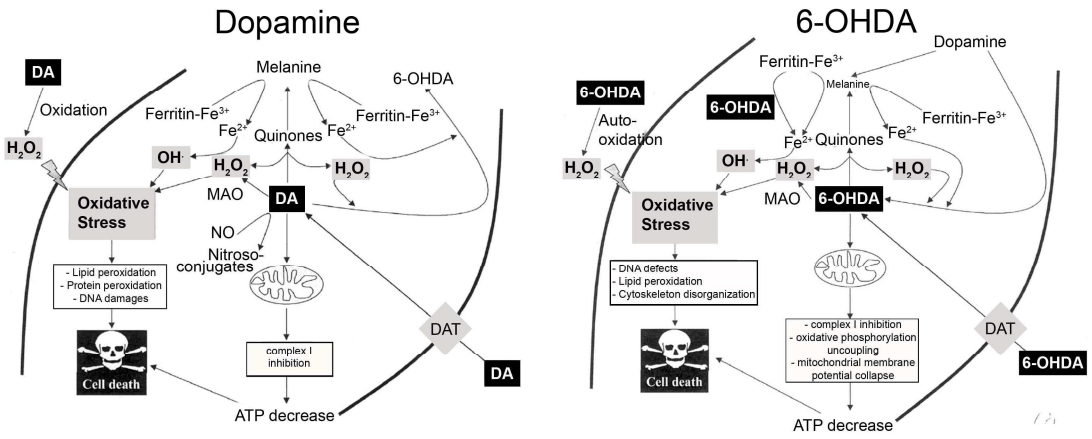

Figure 7 Cytotoxic involvement of dopamine and 6-OHDA. The described mechanism underlying neurotoxicity of DA and 6-OHDA involves oxidative stress. Auto-oxidation leads to the formation of cytotoxic reactive oxygen species. Oxidation forms quinones, which can be converted to hydroxyl radicals ($OH^{\cdot}$) through interaction with H_2O_2. Further, inhibition of the mitochondrial respiratory complex I as wells as induction of apoptosis due to activation of cytoplasmic caspases may occur. 6-OHDA is not only a respiratory toxin but also causes DNA damage and acts as a clastogen. Figure taken from [111]. Reproduced with permission from Elsevier

2. Aim

The aim(s) of the presented PhD thesis was to investigate the following questions:

Does dopamine exert an effect on the proliferation of astrocytes and on the expression of the water channel aquaporin 4 in astrocytes?

Does aquaporin 4 play a modulatory role in astrocyte proliferation?

Which cell type in the striatal astrocyte cultures is susceptible for dopamine-induced decrease in proliferation?

What is the phenotype and origin of the proliferating cells in the dopamine-depleted striatum in the rat model?

3. Results

3.1 Dopamine induced changes in proliferation of astrocytes *in vitro*

Striatal mouse astrocyte cultures were treated with 100 µM DA for 72h. Quantification of DAPI stained cell nuclei revealed a decrease of ~20 % in cell number in DA-treated cultures in comparison to untreated control cultures (Fig. 8A). To examine if the observed decrease in cell number was due to reduced proliferation, we estimated proliferation in untreated and DA-treated cultures seeded at different densities. The proliferation assay clearly demonstrated a cell density dependent effect of DA on cell proliferation (Fig. 8B). Cells seeded at a density of 10 000 cells/well were reduced in proliferation following DA treatment of ~15 %, while cells seeded at a lower density (1250 cells/well) were reduced of ~65 % .

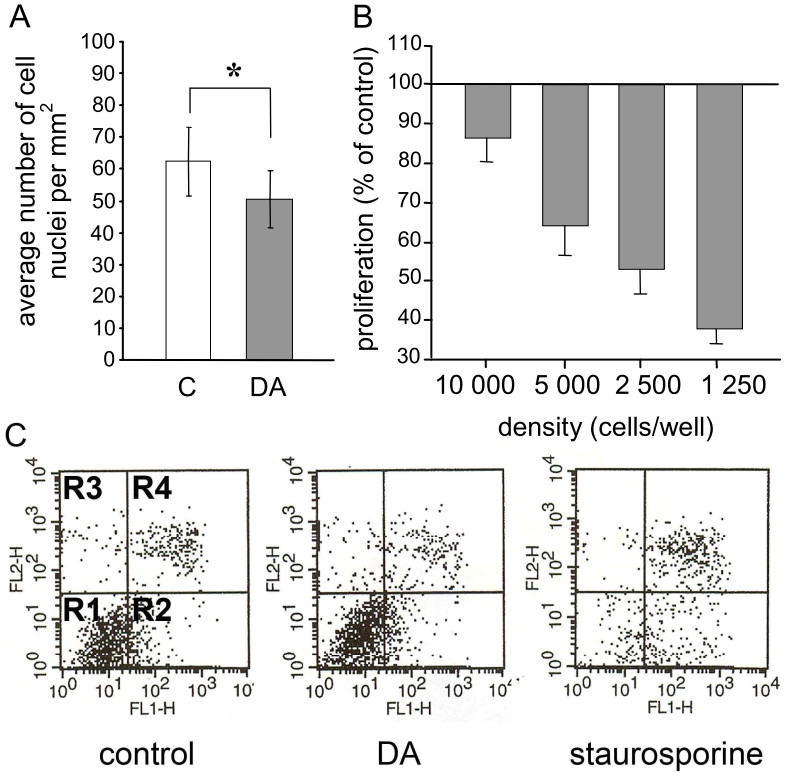

Figure 8 Dopamine (DA) induced effects in mouse striatal astrocytes *in vitro* following treatment with 100 µM DA for 72h. **A** Cell nuclei stained with DAPI were counted in untreated (C) (n=6) and DA-treated (n=6) cell cultures, initially seeded at a density of 5000 cells/well. Data are mean +/- SEM; Student´s t-test for paired data, * p = 0.009. **B** Cells were seeded at different densities and proliferation was assayed (n=3-6) following DA-treatment. Bars represent the percentage of reduction in proliferation of DA-treated cultures compared to control cultures. Data are mean - SEM. **C** Cell death was assayed (n=3) and apoptotic cells are indicated by a shift from polygonal gate R1 to R2, while necrotic cells are defined in polyconal gate R3. Treatment with 300 nM staurosporine for 24h was used as a positive control.

To investigate if the DA treatment increased apoptotic cell death, apoptosis was assayed in DA-treated cell cultures and compared to untreated cultures and cultures stimulated for 24h with 300 nM of the apoptosis-inducing agent staurosporine [116]. DA treatment did not increase apoptosis since a similar amount of apoptotic cells was observed in both DA-treated and in untreated astrocyte cultures (Fig. 8C).

3.2 Dopamine induced changes in AQP4 expression *in vitro*

DA is described to decrease the water permeability of AQP4 in kidney cells [117]. In the CNS, astrocytes are the main cell type known to express the water channel AQP4 [59]. It is not known whether DA has an effect on the expression of AQP4.

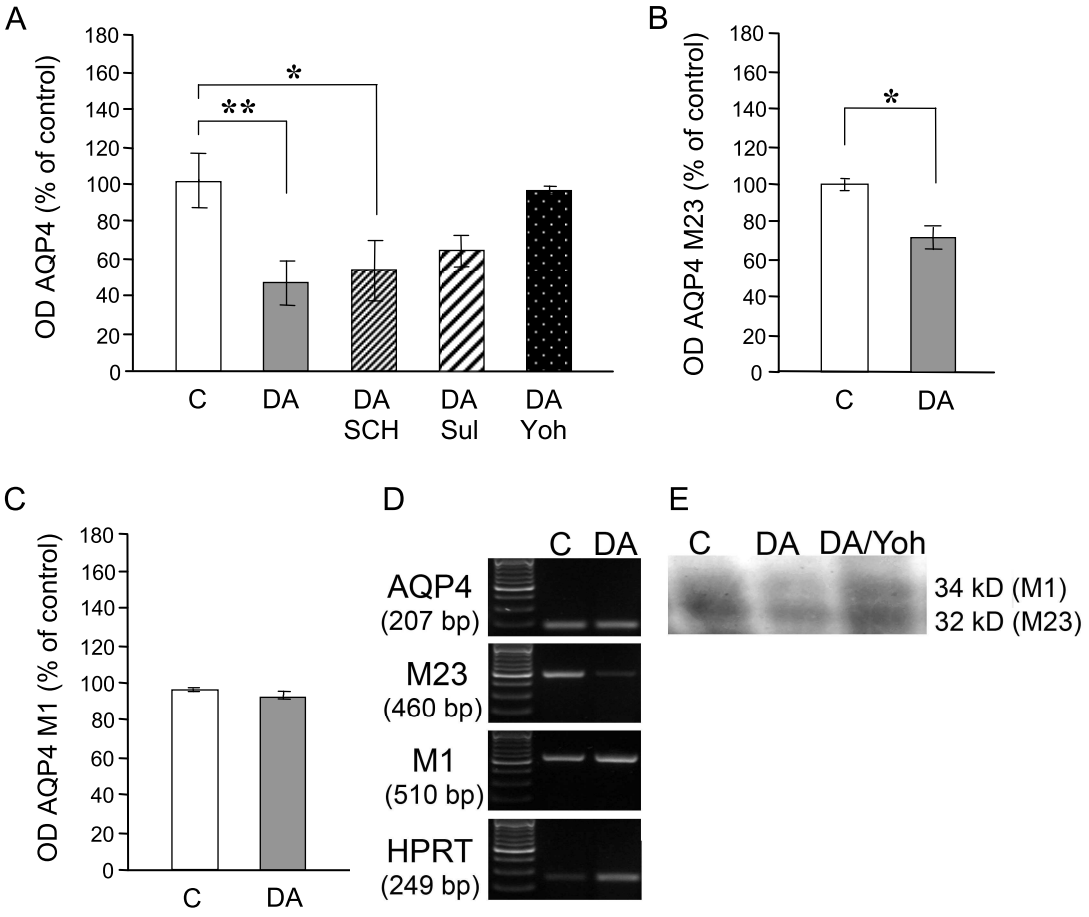

Figure 9 Dopamine (DA) treatment influenced the expression of aquaporin 4 (AQP4) in mouse striatal astrocytes *in vitro*. **A** Relative quantification of AQP4 mRNA expression in untreated cultures (C) and following treatment with 100 µM DA for 72h alone or in combination with 1 µM of a receptor antagonist (SCH, SCH 23390; Sul, sulpiride; Yoh, yohimbine). HPRT was used as internal reference. Data (n=10) are mean +/- SEM; Student´s t-test for unpaired data, ** p = 0.003, * p = 0.016. OD, optical density. **B-C** Relative quantification of AQP4 M23 (**B**) (n=3) and M1 (**C**) (n=3) mRNA following DA treatment. Data are mean +/- SEM; Student´s t-test for unpaired data, * p = 0.003. **D** Representative agarose gels of RT-PCR products. **E** Representative AQP4 Western Blot of untreated and treated cell cultures.

Analysis of AQP4 mRNA expression revealed a significant decrease of ~50 % in DA-treated striatal mouse astrocyte cultures compared to untreated cultures (Fig. 9A,D). To determine the DA receptor family that mediated this effect, we simultaneously treated striatal astrocyte cultures with 100 µM DA and 1 µM of either the D_1 – like receptor antagonist SCH 23390 or the D_2 – like receptor antagonist sulpiride. Neither of these antagonists abolished the DA-induced decrease in AQP4 mRNA expression (Fig. 9A). DA is also reported to act via noradrenergic receptors [101,118,119,120]. Indeed, co-treatment with 1 µM of the α_2 – adrenergic receptor antagonist yohimbine abolished the DA effect (Fig. 9A).

AQP4 has two major isoforms termed M1 and M23 [74]. RT-PCR was performed with primers specific to the sequence of *AQP4 M1* and *AQP4 M23*, respectively. The relative expression of AQP4 M23 mRNA significantly decreased of ~30 % in DA-treated astrocyte cultures compared to untreated cultures (Fig. 9B,D), while AQP4 M1 mRNA expression did not change following DA treatment (Fig. 9C,D). Expression analysis of the AQP4 protein level confirmed the

significant decrease of AQP4 M23 in DA-treated cultures (n=3, Student's t-test for unpaired data: C vs. DA p = 0.04) (Fig. 9E).

3.3 AQP4 knock-down or pharmacologically blocking decreased cell proliferation *in vitro*

To see if DA exerts its inhibitory effect on the proliferation of striatal mouse astrocytes *in vitro* via regulation of AQP4 expression, we investigated cell proliferation following AQP4 knock-down with siRNA or pharmacologically blocking of the water channel with tetra-ethyl-ammonium chloride (TEA). Astrocyte cultures were transfected with 1 nM, 5 nM and 10 nM AQP4 siRNA [121] for 48h and the AQP4 knock-down was examined. Both AQP4 mRNA (Fig. 10A) and protein (Fig. 10B-D) levels were reduced by ~85 %.

Cell proliferation was induced in astrocyte cultures by 10 µg/ml basic fibroblast growth factor (bFGF). bFGF treatment for 72h increased cell proliferation of ~130 % compared to untreated cell cultures (Fig. 10E). This proliferation enhancing effect of bFGF was prevented by either simultaneous transfection with 5 nM AQP4 siRNA (Fig. 10E) or by concurrent pharmacological blocking of AQP4 using 10 µM TEA [122] (Fig. 10E). Transfection of astrocyte cultures with 1 nM or 5 nM AQP4 siRNA for 72h also significantly reduced basal proliferation of ~40-60 % in comparison to untreated control cultures (Fig. 10F). Treatment with 10 µM TEA or simultaneous treatment with 100 µM DA and transfection with 5 nM AQP4 siRNA for 72h led to a similar decrease in basal proliferation (Fig. 10F).

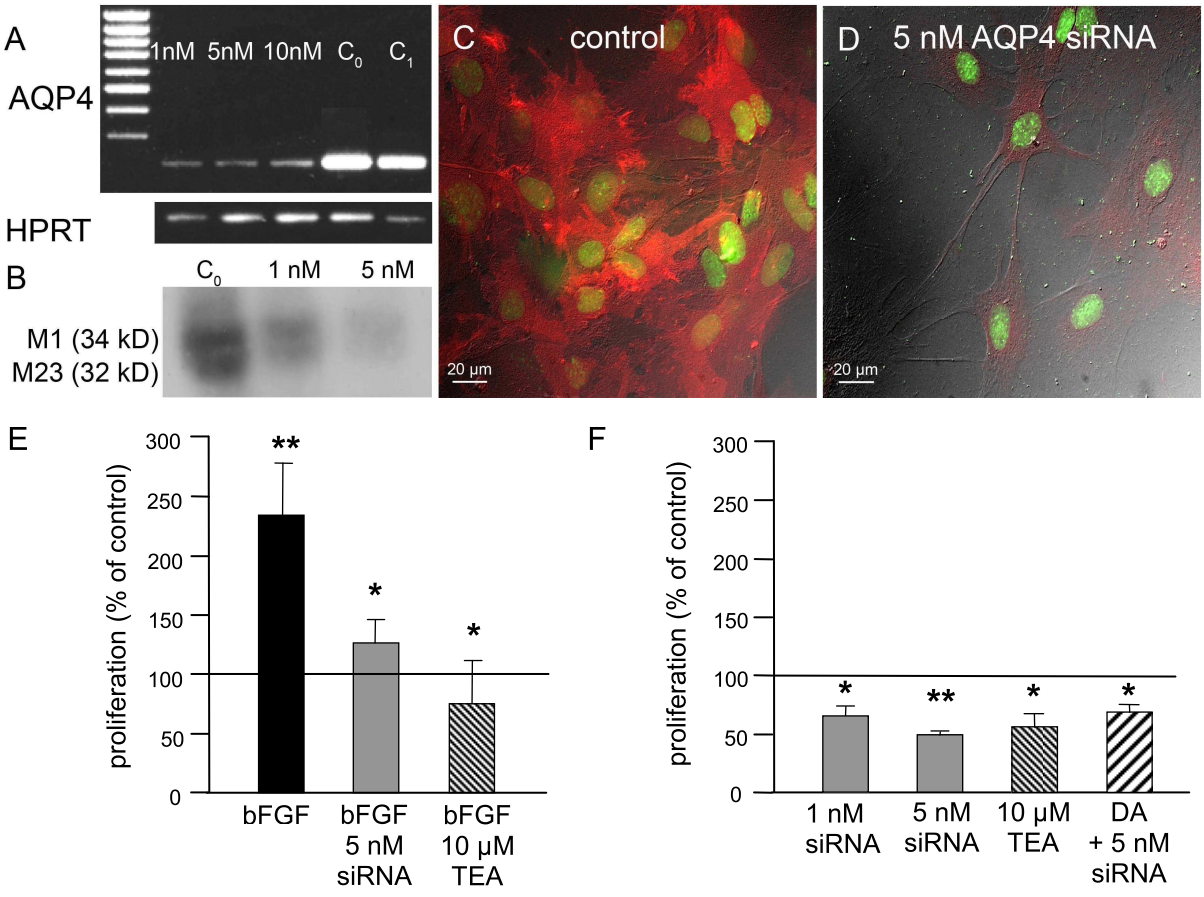

Figure 10 Effect of aquaporin 4 (AQP4) knock-down by siRNA or blocking with tetra-ethyl-ammonium chloride (TEA) on proliferation in mouse striatal astrocytes *in vitro*. **A** Representative agarose gel of AQP4 mRNA expression in cultures transfected with AQP4 siRNA (1 nM, 5 nM and 10 nM), untreated cultures (C_0) and cultures treated with transfectant only (C_1) for 48h. HPRT was used as reference gene. **B** Representative Western Blot of AQP4 protein in siRNA treated cell cultures. **C-D** Immunocytochemical staining of AQP4 after 48h of treatment. Cell nuclei are depicted in green. **E-F** Proliferation was assayed (n=3-6) following treatment for 72h in cell cultures seeded at an initial density of 10 000 cells/well. Cells were treated with either 10 µg/ml basic fibroblast growth

factor (bFGF) alone or in combination with 5 nM AQP4 siRNA or 10 µM TEA (**E**) and with different concentrations of AQP4 siRNA, TEA and a combination of 100 µM DA and 5 nM AQP4 siRNA (**F**). Data are mean + SEM; Mann-Whitney Rank-sum test or Student´s t-test for unpaired data, * p = < 0.05, ** p = < 0.01.

3.4 AQP4 knock-down decreased proliferation in BxPC3 and PANC1 cell cultures

To clarify if the modulatory effect of AQP4 on cell proliferation is specific for striatal mouse astrocytes *in vitro* or represents a general feature of AQP4 expressing cells, we investigated the human pancreatic cancer cell lines BxPC3, PANC1 and MIA PaCa-2 for a role of AQP4 in cell proliferation. As a control for AQP4 expression we used human embryonic kidney (HEK) cells stably transfected with AQP4.

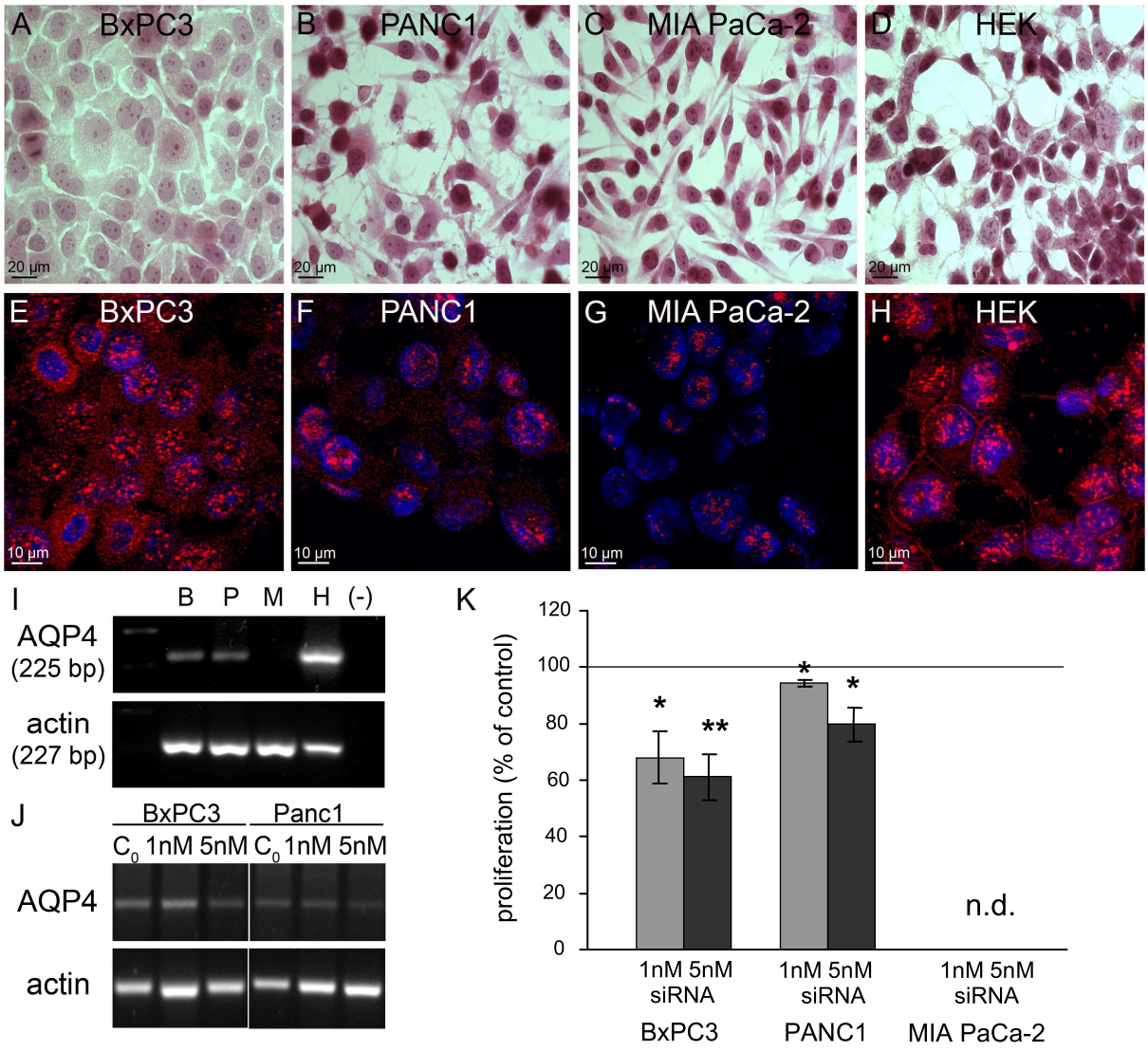

Figure 11 Aquaporin 4 (AQP4) expression and proliferation in the human pancreatic cancer cell lines BxPC3 (B), PANC1 (P), MIA PaCa-2 (M) at 3d *in vitro*. **A-D** Hematoxylin and Eosin (HE) staining. Human embryo kidney cells (HEK) stably transfected with AQP4 were used as positive controls in the experiments. **E-H** AQP4 immunocytochemistry. Cell nuclei are depicted in blue. **I** Representative agarose gel of AQP4 mRNA expression. (H) positive control, (-) negative control for PCR. Actin was used as internal reference gene. **J** Representative agarose gel of AQP4 mRNA expression in untreated cultures (C_0) and in cultures transfected with AQP4 siRNA (1 nM and 5 nM) for 72h. **K** Proliferation was assayed in BxPC3 cell cultures (n=5) and PANC1 cell cultures (n=4) seeded at a density of 600 cells/well and transfected with different concentrations of AQP4 siRNA for 72h. Data are mean +/- SEM; Student´s t-test for paired data, * p = < 0.05, ** p = < 0.01. (n.d., not done)

HEK cells displayed a multipolar morphology with long processes (Fig. 11D) when examined at 3d *in vitro*. BxPC3 cells exhibited a flat and polygonal morphology and grew in patches (Fig. 11A). PANC1 cells exhibited a fibroblast-like morphology with processes (Fig. 11B) and MIA PaCa-2 cells were fusiform, bipolar cells with a large nucleus/cytoplasm ratio (Fig. 11C). Immunostaining for AQP4 (Fig. 11E-H) revealed in HEK cells a diffuse, punctual scattered staining with some distinct membrane associated staining especially in regions where cells were in contact with each other (Fig. 11H). BxPC3 cells showed comparable AQP4 staining (Fig. 11E), although no defined AQP4 staining between adjacent cells was observed. AQP4 immunoreactivity in PANC1 cells was only weakly observed (Fig. 11F), while in MIA PaCa-2 cells hardly any AQP4 immunoreactivity was detected besides some punctual scattering (Fig. 11G). AQP4 mRNA was clearly expressed in BxPC3 and PANC1 cells, although at a lower level than in HEK cells (Fig. 11I). No expression of AQP4 mRNA was detected in MIA PaCa-2 cells (Fig. 11I).
BxPC3 and PANC1 cells were transfected with 1 nM or 5 nM AQP4 siRNA for 72h and the AQP4 knock-down was examined. AQP4 mRNA expression in BxPC3 cells was reduced by ~15 % and ~45 % for 1 nM and 5 nM AQP4 siRNA, respectively and in PANC1 cells by ~8 % and ~18 %, respectively (Fig. 11J). Since in preliminary experiments no effect of AQP4 siRNA was observed in MIA PaCa-2 cell cultures, this cell line was not further investigated. Proliferation was assayed following AQP4 siRNA transfection for 72h. Proliferation decreased in BxPC3 cells transfected with 1 nM and 5 nM AQP4 siRNA by ~32 % and ~39 %, respectively (Fig. 11K) and in PANC1 cells by ~6 % and ~20 %, respectively (Fig. 11K). Pharmacological blocking with 10 µM TEA for 72h did not change proliferation in the human pancreatic cancer cells (data not shown).

3.5 Which are the target cells for the dopamine effect in the striatal astrocyte cultures?
Astrocytes are a very heterogeneous cell population [4] and not all cells in our striatal astrocyte cultures may be susceptible to DA treatment. Moreover, treatment with DA might change the molecular phenotype of some cells in that sense that there may be a shift in the proportional expression of AQP4 with respect to GFAP or nestin expression. Therefore we determined the number of $AQP4^+$, $GFAP^+$, and $nestin^+$ cells alone and with respect to each other.
After 3d *in vitro* untreated striatal mouse astrocytes were ~70-80 % confluent. Cells were mostly flat with distinct cell shapes (Fig. 12A). Immunostaining with the neuronal marker MAP-2 or the NG2 glia and oligodendrocyte precursor marker NG2 were predominantly negative (data not shown), indicating purity of the astrocyte cultures. Staining with the microglia marker Iba-1 revealed a marginal presence of microglia in the cultures (data not shown).
Immunocytochemistry with the astrocyte marker GFAP [19] revealed cells with distinct morphologies (Fig. 12B). Most $GFAP^+$ cells resembled the phenotype of so called protoplasmic astrocytes (Fig. 12D), although occasionally fibrous $GFAP^+$ astrocytes were detected (< 2 %) (Fig. 12E). GFAP immunoreactivity exhibited the dense IF fibre network in the cytoplasm (Fig. 12D). The intensity of the GFAP immunoreactivity differed between cells and ranged from highly $GFAP^+$ to virtually undetectable levels (Fig. 12B). Immuno-positive cells were counted and expressed as percentage of the total number of cells that were counted. In untreated astrocyte cultures 52.1 % (+/- 3.8 %) of all cells expressed GFAP (Fig. 12H).
Astrocytes *in vitro* are known to express the progenitor marker nestin [40,42]. Immunostaining of the IF protein nestin exhibited a similar staining pattern as GFAP, exhibiting the dense IF network in the cytoplasm (Fig. 12F). In the untreated striatal astrocyte cultures 80.3 % (+/- 2.8 %) of all cells expressed nestin (Fig. 12H).

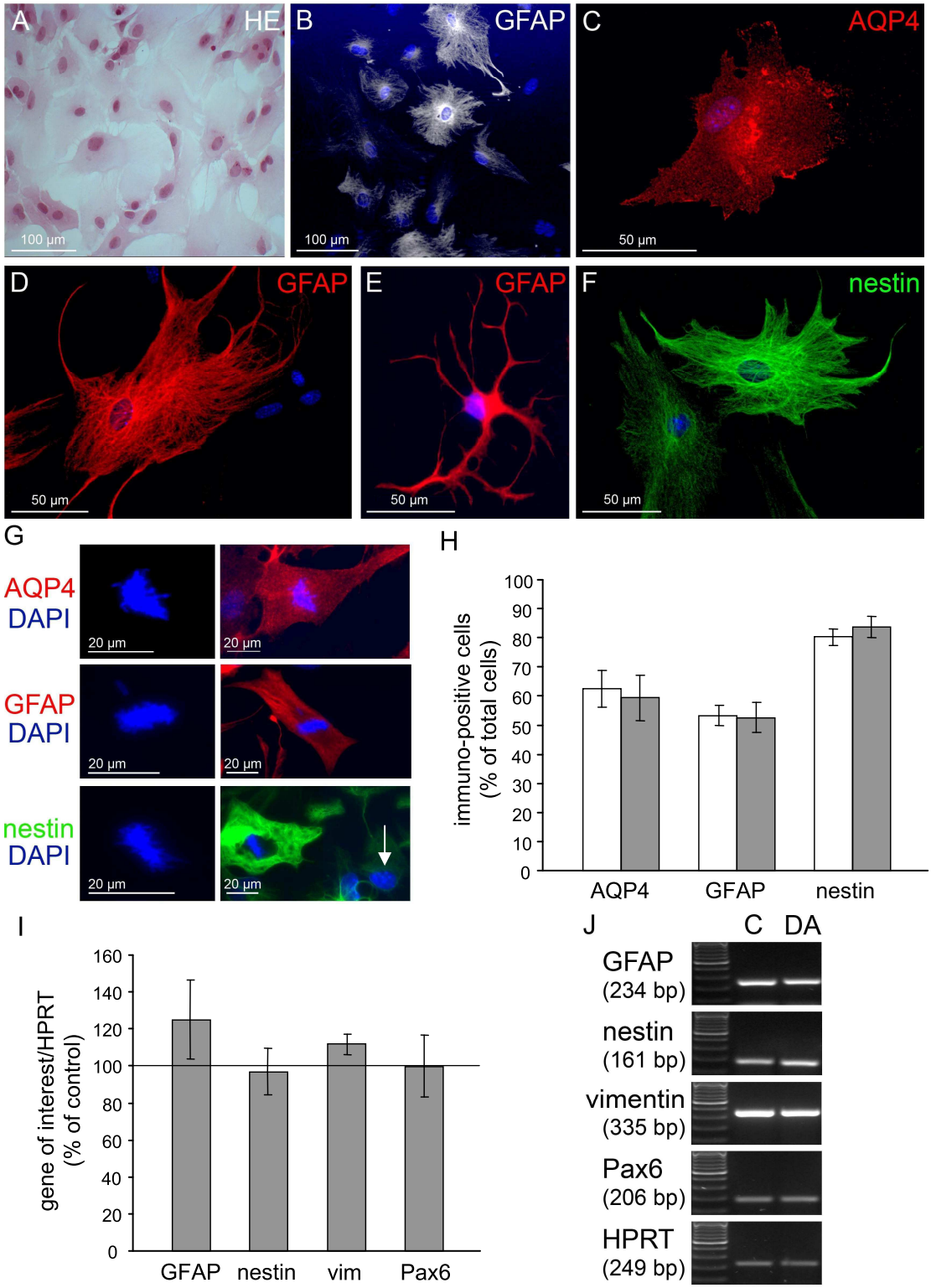

Figure 12 Expression of aquaporin 4 (AQP4), glial fibrillary acidic protein (GFAP), nestin, vimentin and Pax6 in striatal mouse astrocytes at 3d *in vitro*. **A** Hematoxylin and Eosin (HE) staining. **B** Immunocytochemistry of GFAP in an untreated cell culture. **C-F** Representative immunoreactive cells for AQP4 (**C**), GFAP (**D, E**) and nestin (**F**) in untreated cultures. **G** Untreated cells stained by immunocytochemistry caught during mitosis. Cell nuclei are depicted in blue (**B-G**). The white arrow indicates a quiescent cell nuclei. **H** Quantification of immunoreactive cells in untreated cell cultures (white bars) (n=3-7) and in cell cultures treated with 100 µM DA for 72h (grey bars) (n=3-7). Cells were seeded at an initial density of 5000 cells/well. Data are mean +/- SEM. **I** Relative quantification of GFAP (n=4-7), nestin (n=4-6), vimentin (n=4-7) and Pax6 (n=4-7) mRNA expression in cells seeded at an initial density of 20 000 cells/well. Cell cultures were treated with 100 µM DA (grey bars) for 72h and compared to untreated control cultures. HPRT was used as internal reference gene. Data are mean +/- SEM. **J** Representative agarose gels with RT-PCR samples from untreated (C) and DA-treated cells.

Immunoreactivity for AQP4 revealed a diffuse staining with occasional membrane associated AQP4 staining (Fig. 12C). 66.4 % (+/- 6.3 %) of all cells in the mouse striatal astrocyte cultures expressed AQP4 (Fig. 12H). Occasionally mitotic figures were observed (Fig. 12G) and the dividing astrocytes stained positive for AQP4, GFAP and nestin (Fig. 12G). Therefore we examined if the observed DA-induced decrease in proliferation of striatal astrocytes affected in particular the population of $AQP4^+$, $GFAP^+$ or $nestin^+$ cells. However, DA treatment did not change the numbers of $AQP4^+$, $GFAP^+$ or $nestin^+$ cells, respectively (Fig. 12H).
Furthermore, on molecular level we detected no change in the mRNA expression of GFAP, nestin, vimentin and Pax6 following DA treatment (Fig. 12I-J).

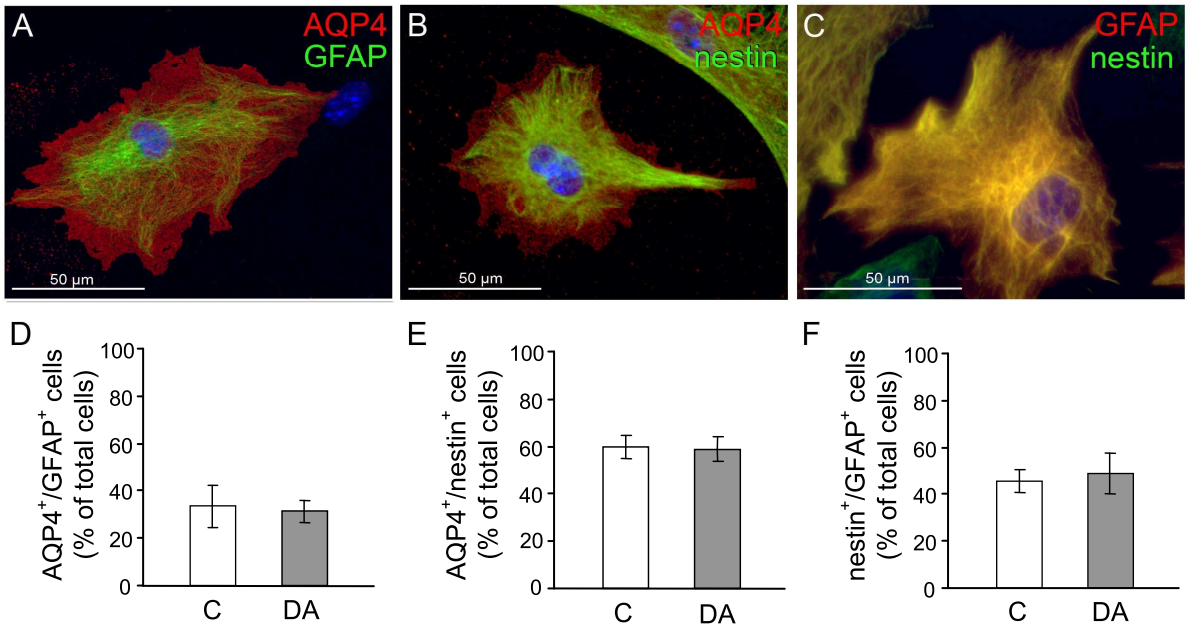

Figure 13 Double immunocytochemistry of mouse striatal astrocytes at 3d *in vitro*. **A-C** Representative double-stainings. Cell nuclei are depicted in blue **D-F** Quantitative analysis of the number of double-positive cells in untreated cultures (C) (n=3-4) and cultures treated with 100 µM dopamine (DA) (n=3) for 72h. Data are mean +/- SEM.

Double-immunocytochemistry revealed co-expression of AQP4 and GFAP (Fig. 13A), AQP4 and nestin (Fig. 13B) and GFAP and nestin (Fig. 13C). Quantification revealed that in untreated striatal astrocyte cultures 33.6 % (+/- 9.0 %) of all cells were $AQP4^+/GFAP^+$ (Fig. 13D), 59.9 % (+/- 4.9 %) of all cells were $AQP4^+/nestin^+$ (Fig. 16E) and 45.7 % (+/- 9.9 %) were $GFAP^+/nestin^+$ (Fig. 13F). DA treatment did not change the number of $AQP4^+/GFAP^+$ (Fig. 16D), $AQP4^+/nestin^+$ (Fig. 16E) and $GFAP^+/nestin^+$ cells (Fig. 13F).

3.6 Dopamine depletion in a toxin-induced Parkinson's model in the rat

In mouse striatal astrocyte cultures we showed that DA treatment decreased AQP4 mRNA expresion (Fig. 9A), AQP4 protein expression (Fig. 9E) and cell proliferation (Fig. 8B). Subsequent experiments indicated that AQP4 expression and proliferation may be linked and we revealed a modulatory role of AQP4 on proliferation *in vitro* (Fig. 10E-F). To see, if DA exerts an effect on proliferation and/or AQP4 expression *in vivo* we examined these parameters in the DA-depleted striatum *in vivo*.
6-OHDA is a catecholamine selective neurotoxin, which destroys dopaminergic neurons and thus leads to DA depletion in e.g. the striatum [111]. Adult rats were bilaterally injected into the lateral ventricles (Fig. 14A) with either a relatively mild dosage of 6-OHDA (105 µg in ascorbic acid solution) [115] or only ascorbic acid solution (sham animals). The animals were investigated at 1d, 4d, 7d and 24d post-lesion. To confirm that the 6-OHDA lesions were

successful, TH expression in the striatum was investigated by means of immunohistochemistry, Western Blotting and RT-PCR.

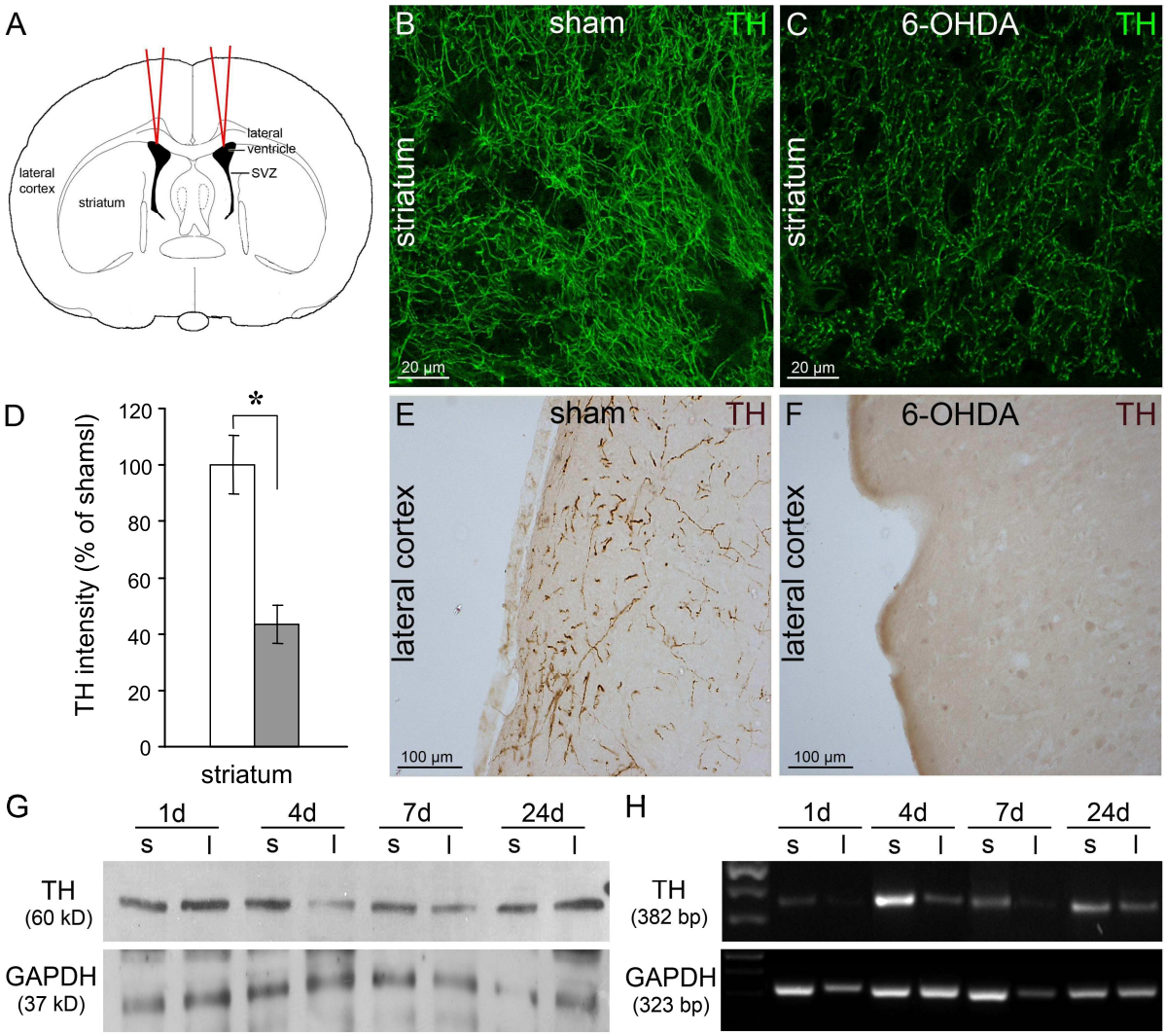

Figure 14 Decreased tyrosine hydroxylase (TH) expression in 6-OHDA lesioned rats. **A** Schematic overview of the investigated coronal sections. The red lines indicate the needle puncture. **B-C** TH^+ fibers in the striatum 4d post-lesion. **D** Quantification of the intensity of the TH immunoreactivity in the striatum at 4d post-lesion in sham (white bars) (n=5) and 6-OHDA lesioned rats (grey bars) (n=3). Data are mean +/- SEM; Student´s t-test for unpaired data, * p = 0.008. **E-F** TH immunoreactivity (DAB) in the lateral cortex 4d post-lesion. **G** Representative Western Blot for the striatum at several days after the lesion. GAPDH was used as a internal reference. (s, sham ; l, 6-OHDA-lesion). **H** Representative agarose gel for RT-PCR samples from the striatum.

Immunohistochemistry of TH, the rate-limiting enzyme in DA synthesis [95], revealed the dense TH^+ fibre network of dopaminergic afferents in the striatum of sham animals (Fig. 14B). Four days post-lesion 6-OHDA lesioned animals exhibited a highly diminished TH^+ dopaminergic fibre network and sprouted fibres in the striatum (Fig. 14C). Intensity measurements of the TH immunoreactivity showed a significant decrease in TH intensity (Fig. 14D) on average of ~57 % in 6-OHDA lesioned animals. Animals with a decrease of less than 10 % were not taken into the experiment. Additionally, at 4 days post-lesion the marginal TH^+ fibre network in the lateral cortex (Fig. 14E) was also drastically reduced in 6-OHDA lesioned animals (Fig. 14F). Western Blotting confirmed the decrease in TH protein expression in the striatum (Fig. 14G). The relative TH protein expression decreased in 6-OHDA lesioned rats on average of ~50 % on the first day post-lesion and remained decreased at all other time-points examined (4d, 7d and 24d post-

lesion) (Fig. 14G). TH mRNA expression decreased for more than 60 % in all 6-OHDA lesioned animals at the first day post-lesion and stayed decreased within the first week of the lesion. 24d post-lesion TH mRNA expression in 6-OHDA lesioned rats was lowered by ~33 % (Fig. 14H).

3.7 Proliferating cell in the striatum and the lateral cortex of 6-OHDA lesioned rats

The proliferation marker Ki-67 labels cells in all active phases of the cell cycle (G_1, S, G_2, M) [123]. Proliferating Ki-67$^+$ cells were clearly visible in the SVZ in both sham and 6-OHDA lesioned animals (Fig. 15A) at 4d post-lesion. Ubiquitously distributed Ki-67$^+$ cells were observed in the striatum (Fig. 15D) and the lateral cortex (Fig. 15F) of 6-OHDA lesioned rats, while basically no Ki-67$^+$ cells were observed in these areas in sham animals (Fig. 15C,E). Quantification of proliferating cells confirmed a significant increase in the number of Ki-67$^+$ cells following 6-OHDA lesions in the striatum by a factor of ~14 and in the lateral cortex by a factor of ~ 18 (Fig. 15B). No change was observed in the SVZ (Fig. 15B).

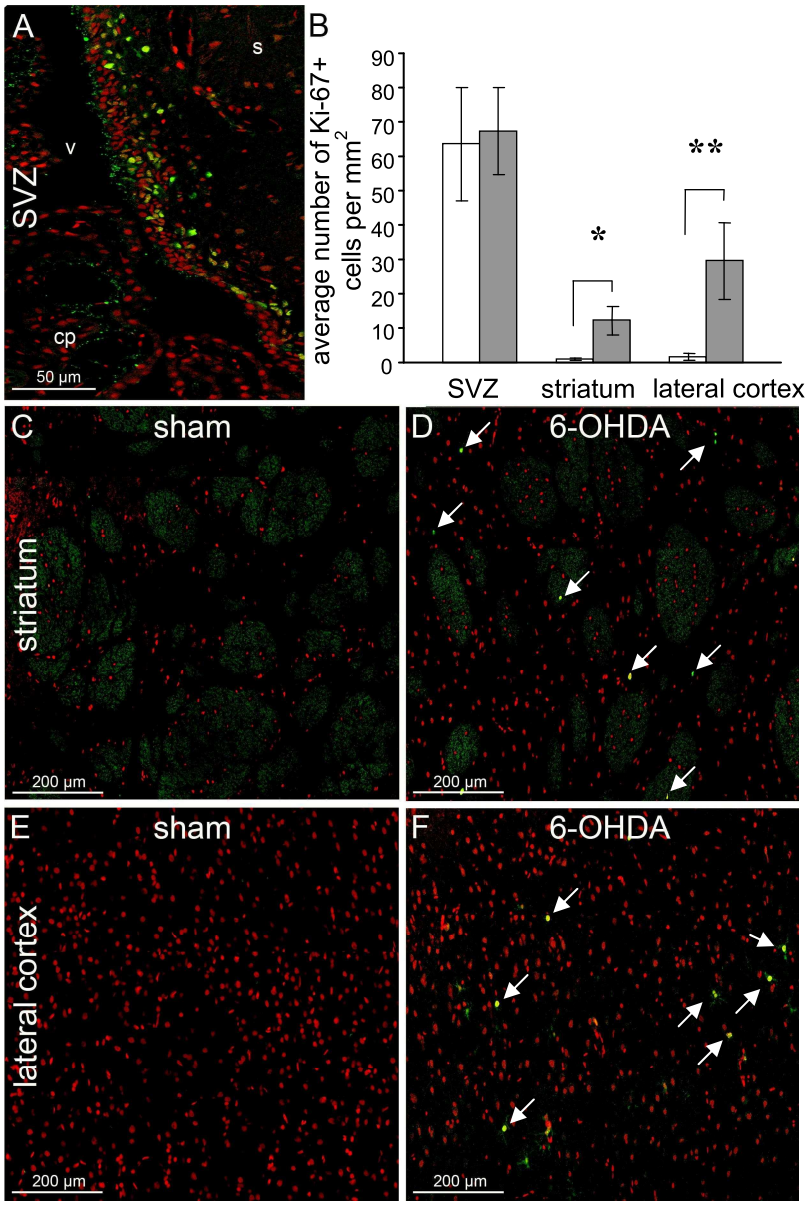

Figure 15 Increased expression of the proliferation marker Ki-67 in 6-OHDA lesioned rats at 4d post-lesion. **A** Ki-67$^+$ cells were observed in the subventricular zone (SVZ) in both sham and 6-OHA lesioned animals. Cell nuclei are depicted in red (V, ventricle; cp, choroid plexus; s, striatum). **B** Quantitative analysis of Ki-67$^+$ cells in sham animals (white bars) (n=3) and 6-OHDA lesioned animals (grey bars) (n=3). Data are mean +/- SEM; Mann-

Whitney Rank-sum test ** p = <0.01, Student´s t-test for unpaired data * p = 0.015. **C-F** Immunohistochemical staining of Ki-67. White arrows indicate Ki-67^{+} cells. Cell nuclei are depicted in red.

3.8 Expression of AQP4 in the dopamine-depleted striatum

The expression of AQP4 was investigated by means of immunohistochemistry, Western Blotting and RT-PCR. AQP4 immunoreactivity in the striatum exhibited a diffuse staining in the gray matter and a clear labelling along blood vessels (Fig. 16A-B). Intensity measurement of the AQP4 immunoreactivity at 4d post-lesion revealed no significant change in 6-OHDA lesioned rats in comparison to sham animals (Fig. 16C).

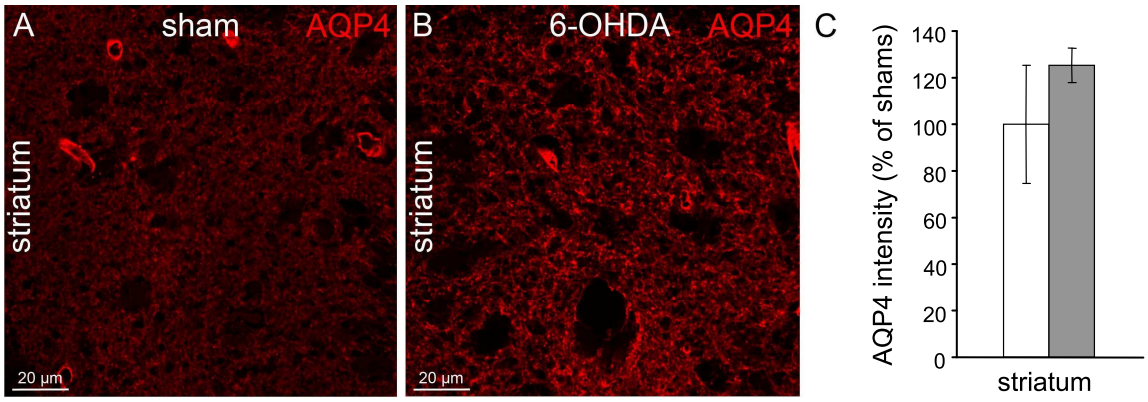

Figure 16 Aquaporin 4 (AQP4) immunoreactivity in the striatum of sham and 6-OHDA lesioned rats at 4d post-lesion **A-B** AQP4 immunohistochemistry. **C** Intensity measurement of the AQP4 immunoreactivity in the striatum in sham (white bars) (n=3) and 6-OHDA lesioned rats (grey bars) (n=3). Data are mean +/- SEM.

AQP4 mRNA expression was investigated by means of RT-PCR in the striatum at 1d, 4d, 7d and 24d post-lesion in sham and 6-OHDA lesioned animals (Fig. 17A). The obtained data were normalized to the AQP4 mRNA expression at 24d post-lesion in sham rats. It was assumed that the mRNA expression in sham animals 24d after the lesion was not affected by any surgery-related changes and therefore represents a valuable reference.
AQP4 mRNA in the striatum at the first day after the surgery was drastically increased in sham animals (~3.3 fold) and 6-OHDA lesioned animals (~1.9 fold) in comparison to sham 24d post-lesion (Fig. 17A). In sham animals it declined thereafter, while it remained significantly increased in 6-OHDA lesioned rats 4d (~1.6 fold) (Fig. 17A,E) and 24d (~ 1.4 fold) post-lesion (Fig. 17A). We also examined mRNA expression of the AQP4 isoforms M23, M1 and z [86] in the striatum following the 6-OHDA lesion. At 4d post-lesion, AQP4 M23 mRNA expression was significantly increased (~2.1 fold) in 6-OHDA lesioned rats in comparison to sham 24d post-lesion (Fig. 17B,E), while AQP4 M1 mRNA expression was not changed (Fig. 17C,E). AQP4 z mRNA expression at 4d post-lesion in 6-OHDA lesioned animals was similar to M23 mRNA expression significantly increased (~2.6 fold) (Fig. 17D,E). There was no increased mRNA expression of M23, M1 or z at any of the other observed time points (data not shown).
Investigation of AQP4 protein expression by means of Western Blotting revealed bands that correspond to the major AQP4 isoforms M23 (32 kD) and M1 (34 kD) [86] (Fig. 17F). Contrary to the observed mRNA expressions the relative expression of AQP4 M23 protein in the striatum was not significantly changed at 4d post-lesion (Fig. 17G), while M1 protein expression was significantly decreased by ~53 % in comparison to sham 24d post-lesion (Fig. 17H).

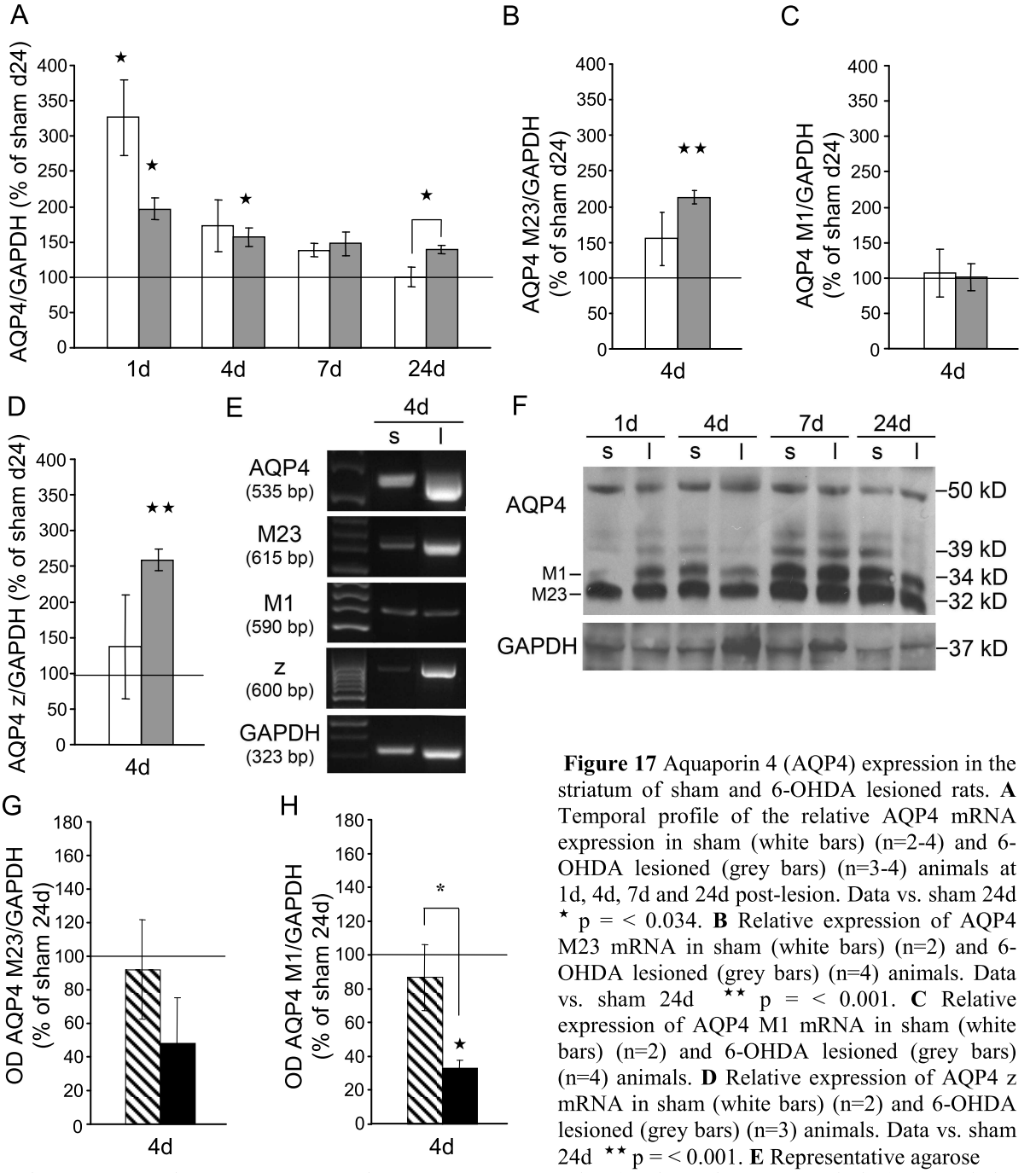

Figure 17 Aquaporin 4 (AQP4) expression in the striatum of sham and 6-OHDA lesioned rats. **A** Temporal profile of the relative AQP4 mRNA expression in sham (white bars) (n=2-4) and 6-OHDA lesioned (grey bars) (n=3-4) animals at 1d, 4d, 7d and 24d post-lesion. Data vs. sham 24d ★ p = < 0.034. **B** Relative expression of AQP4 M23 mRNA in sham (white bars) (n=2) and 6-OHDA lesioned (grey bars) (n=4) animals. Data vs. sham 24d ★★ p = < 0.001. **C** Relative expression of AQP4 M1 mRNA in sham (white bars) (n=2) and 6-OHDA lesioned (grey bars) (n=4) animals. **D** Relative expression of AQP4 z mRNA in sham (white bars) (n=2) and 6-OHDA lesioned (grey bars) (n=3) animals. Data vs. sham 24d ★★ p = < 0.001. **E** Representative agarose gels of RT-PCR products. **F** Representative AQP4 Western Blot (s, sham; l, 6-OHDA lesion). **G** Relative expression of AQP4 M23 protein in 6-OHDA lesioned rats (blackbars) (n =4) and sham animals (black and white bars) (n=3). **H** Relative expression of AQP4 M1 protein in 6-OHDA lesioned rats (black bars) (n =4) and sham animals (black and white bars) (n=3). Sham vs. 6-OHDA * p = 0.007, data vs. 24d sham ★ p = 0.005.
All data (**A-D, G-H**) are normalized to the average expression in the respective sham animals 24d post-lesion. GAPDH was used as internal reference gene. Data are mean +/- SEM. Statistics: Student´s t-test for unpaired data.

3.9 Increased expression of GFAP and nestin following 6-OHDA lesion

In our *in vitro* studies we showed that DA negatively regulated the proliferation of striatal mouse astrocytes (Fig. 8B). In the DA-depleted CNS in the adult rat *in vivo* we showed that the loss of DA increased proliferation in the striatum and the lateral cortex (Fig. 15B). To investigate if the loss of DA following 6-OHDA lesion affects astrocytes we examined the striatum and the lateral cortex for the astrocyte marker GFAP.

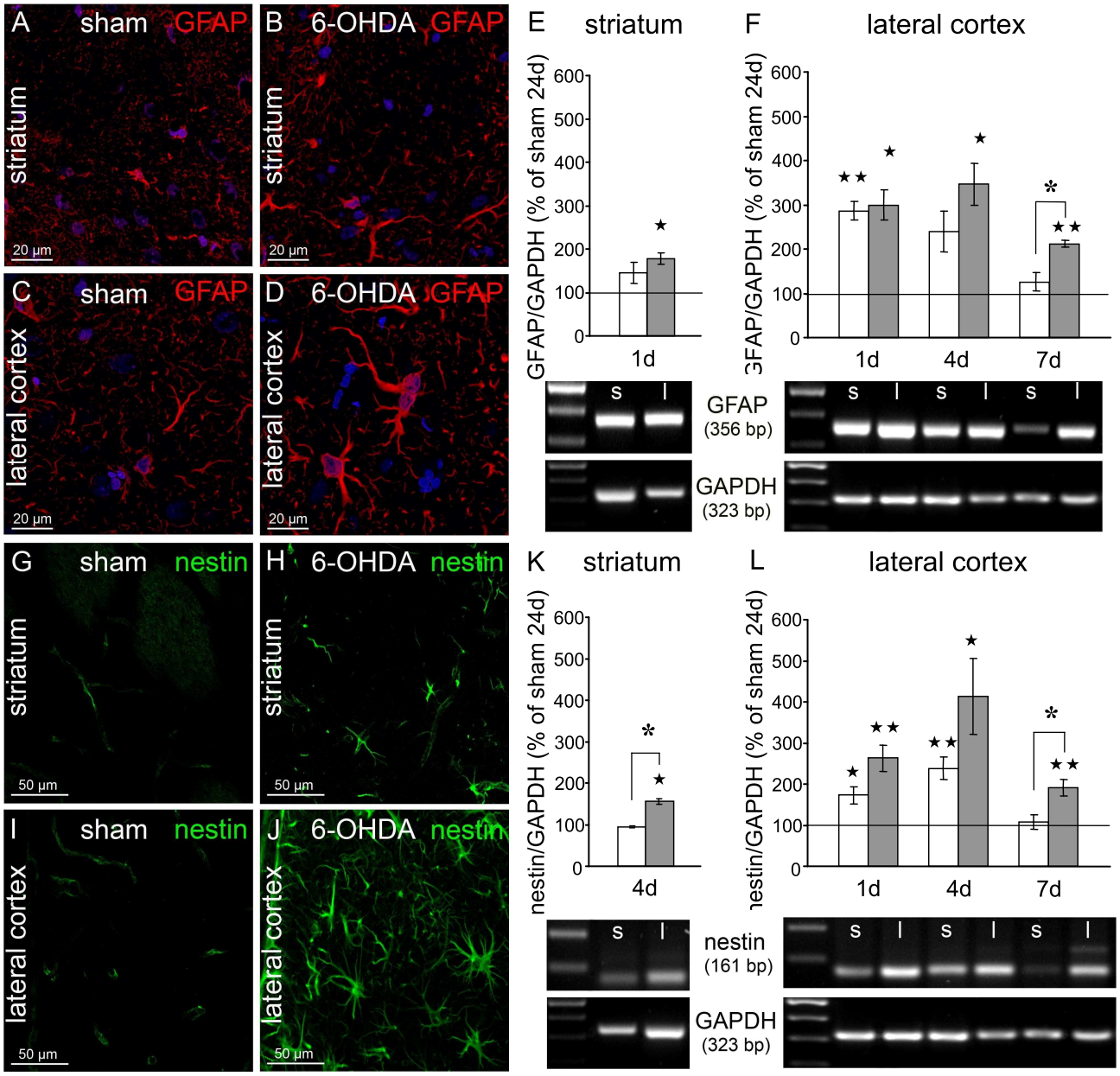

Figure 18 Upregulation of glial fibrillary acidic protein (GFAP) and nestin following 6-OHDA lesion in the striatum and the lateral cortex. **A-D** GFAP immunoreactivity 4 days post-lesion. Cell nuclei are depicted in blue. **E-F** Relative quantification of GFAP mRNA expression. Data from both sham-operated (white bars) (n=2-4) and 6-OHDA lesioned animals (grey bars) (n=3-4) were normalized to the average GFAP mRNA expression in sham animals 24d post-lesion. GAPDH was used as internal reference. Data are mean +/- SEM; Student´s t-test for unpaired data: data vs. sham 24d ★★ $p = \leq 0.001$, ★ $p = < 0.01$, sham vs. 6-OHDA * $p = 0.006$. The agarose gels demonstrate representative samples for the respective day and treatment (s, sham; l, 6-OHDA lesion). **G-J** Immunohistochemistry of nestin 4d post-lesion. **K-L** Relative quantification of nestin mRNA expression. Data analysis as described for GFAP mRNA quantification. Data vs. sham 24d ★★ $p = \leq 0.01$, ★ $p = < 0.04$, sham vs. 6-OHDA * $p = < 0.04$. **M** Quantification of stellated nestin$^+$ cells in sham-operated (white bars) (n=3) and 6-OHDA lesioned animals (grey bars) (n=3) 4d post-lesion. Data are mean +/- SEM; Mann-Whitney Rank-sum test * $p = < 0.01$.

Immunohistochemistry indicated an increased intensity of the GFAP immunoreactivity at 4d post-lesion in the striatum (Fig. 18B) and the lateral cortex (Fig. 18D) in 6-OHDA lesioned rats in comparison to sham animals (Fig. 18A,C). On the molecular level, relative quantification of GFAP mRNA expression demonstrated a significant increase (~1.8 fold) of GFAP mRNA at the first day post-lesion in the striatum of 6-OHDA lesioned rats in comparison to sham animals 24d post-lesion (Fig. 18E), while no changes occurred at 4d and 7d post-lesion (data now shown). In the lateral cortex of 6-OHDA lesioned rats GFAP mRNA was increased in both sham (~2.8 fold) and 6-OHDA lesioned (~3 fold) animals at the first day after the surgery (Fig. 18F). In 6-OHDA lesioned animals GFAP mRNA expression peaked (~ 3.5 fold) at 4d post-lesion and was still significantly increased (~2.1 fold) at one week post-lesion in comparison to sham 24d post-lesion (Fig. 18F).

Upregulation of GFAP as well as cell proliferation are described in reactive gliosis [7]. We additionally observed in 6-OHDA lesioned rats GFAP$^+$ cells that resembled morphologically reactive astrocytes exhibiting cellular hypertrophy (Fig. 18D). Since reactive astrocytes are known to re-induce the progenitor marker nestin [40,41], we investigated nestin expression in the striatum and the lateral cortex. In sham rats, nestin immunoreactivity in the striatum (Fig. 18G) and the lateral cortex (Fig. 18I) was restricted to blood vessels, while a striking appearance of stellated nestin$^+$ cells in both areas was observed in 6-OHA lesioned rats at 4d post-lesion (Fig. 18H, J). Quantification of these stellated nestin$^+$ cells revealed a significant increase by a factor of 15 in the striatum and a factor of 35 in the lateral cortex (Fig. 18M).

On the molecular level we showed a significantly increased expression (~1.6 fold) of nestin mRNA in the striatum of 6-OHDA lesioned rats at 4d post-lesion in comparison to sham animals 24d post-lesion (Fig. 18K). No changes of nestin mRNA expression were observed at 1d or 7d post-lesion (data not shown). In the lateral cortex a vast increase of nestin mRNA expression was observed in both sham and 6-OHDA lesioned animals at 1d (sham: ~1.7 fold; 6-OHDA: ~2.6 fold) and 4d post-lesion (sham: ~2.4 fold; 6-OHDA: ~4.1 fold) (Fig. 18L). Nestin mRNA expression remained elevated (~1.9 fold) in 6-OHDA lesioned animals until one week post-lesion (Fig. 18L).

3.10 6-OHDA lesions resulted in an up-regulation of vimentin

A third IF protein known to be up-regulated in reactive astrocytes is vimentin [52].

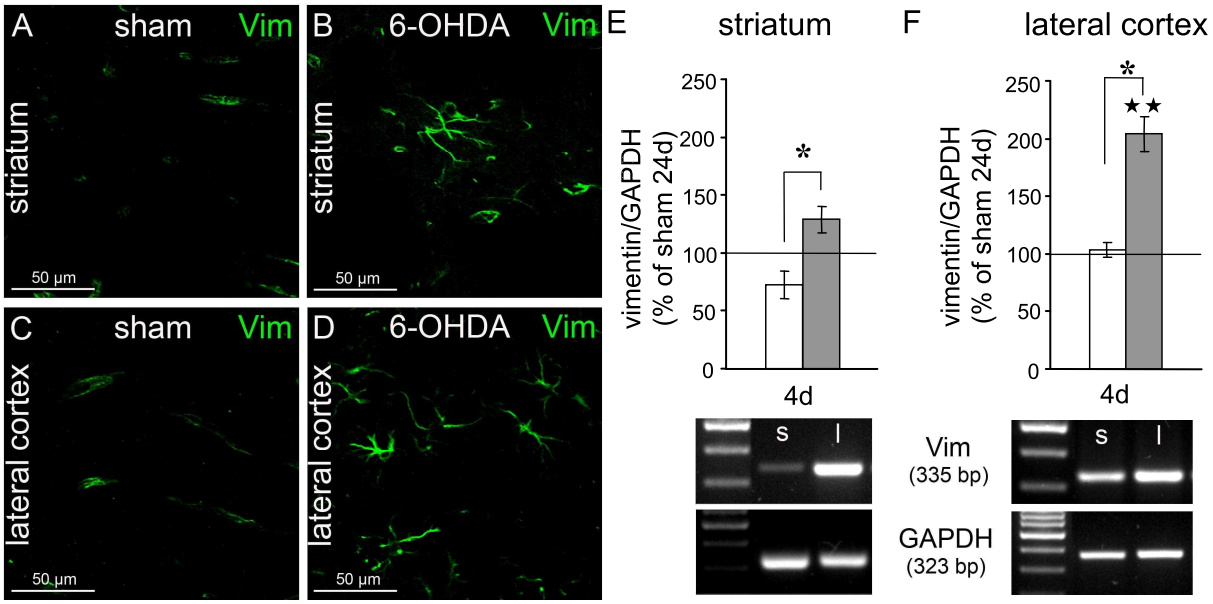

Figure 19 Increased vimentin expression 6-OHDA lesioned animals at 4d post-lesion in the striatum and the lateral cortex. **A-D** Immunostaining of vimentin at 4d post-lesion. **E-F** Relative quantification of vimentin mRNA expression in the striatum (**E**) and the lateral cortex (**F**). Data of both sham-operated (white bars) (n=2) and 6-

OHDA lesioned animals (grey bars) (n=4) were normalized to the average vimentin mRNA expression in sham animals 24d post-lesion. GAPDH was used as an internal reference. Data are mean +/- SEM; Student´s t-test for unpaired data: data vs. sham 24d ** p = < 0.01, sham vs. 6-OHDA * p = 0.04. The agarose gels demonstrate representative samples (s, sham; l, 6-OHDA lesion).

Vimentin immunoreactivity was detected along few blood vessels under all conditions at 4d post-lesion (Fig. 19A-D). Stellated vimentin$^+$ cells were detected in representative sections of the striatum (Fig. 19B) and the lateral cortex (Fig. 19D) in 6-OHDA lesioned animals and vimentin mRNA expression in 6-OHDA lesioned animals at 4d post-lesion was significantly increased both in the striatum (~1.3 fold) (Fig. 19E) and in the lateral cortex (~2 fold) (Fig. 19F) in comparison to either sham animals 24d post-lesion and/or the respective sham value at 4d post-lesion. No changes in the vimentin mRNA expression was detected at 1d or 7d post-lesion (data not shown).

3.11 Proliferating Ki-67$^+$ cells co-express GFAP and nestin

To fully confirm an astrocytic phenotype of the proliferating cells in the striatum and the lateral cortex following a 6-OHDA lesion we performed double immunohistochemistry of the proliferation marker Ki-67 and GFAP or nestin at 4d post-lesion.

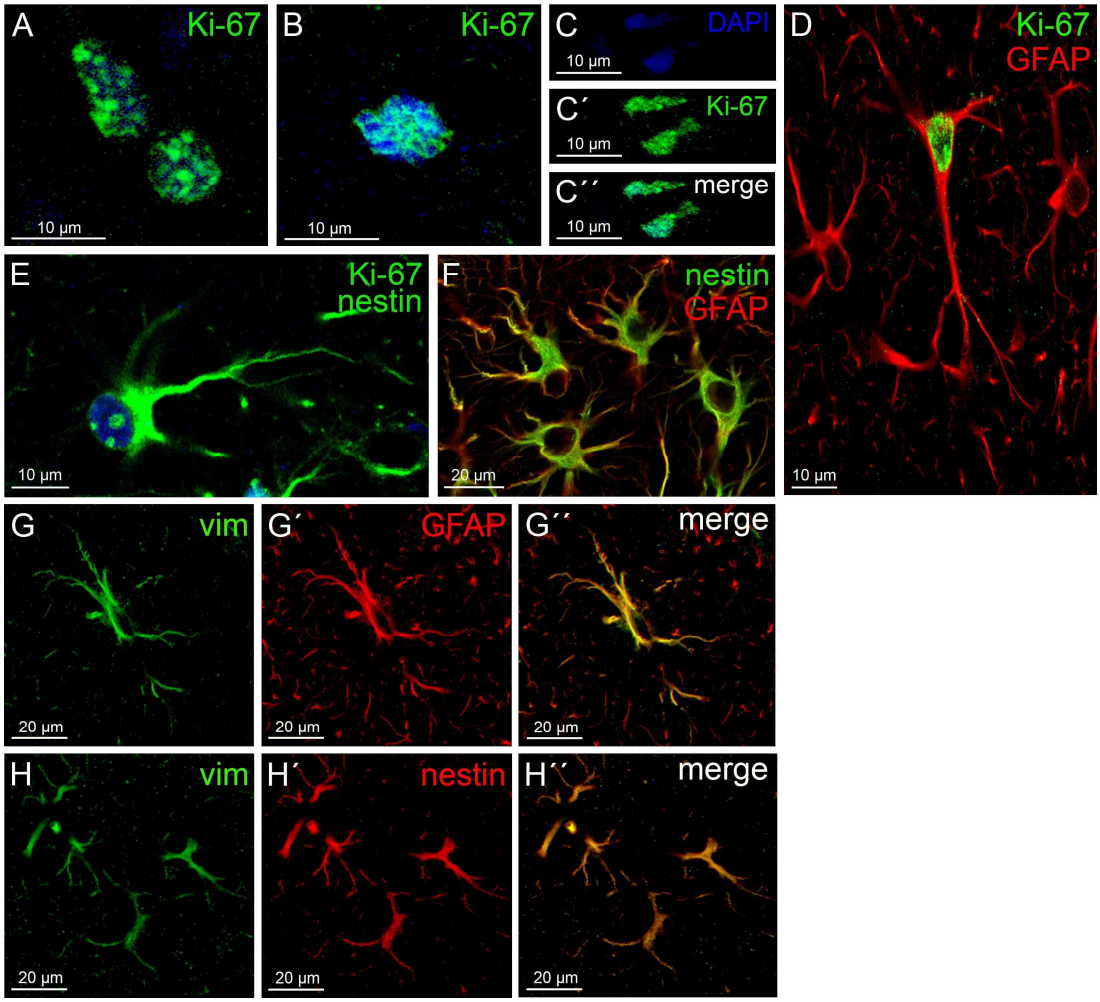

Figure 20 Determination of the phenotype of the proliferating Ki-67$^+$ cells observed 4d days after the 6-OHDA lesion in the striatum and the lateral cortex. **A-C** Ki-67$^+$ cells. **D-F** Double immunohistochemistry of Ki-67 and glial fibrillary acidic protein (GFAP) (**D**), Ki-67 and nestin (**E**), nestin and GFAP (**F**), vimentin and GFAP (**G**) and vimentin and nestin (**H**).

Ki-67 staining was restricted to the nucleus and was seen both in cells during interphase (Fig. 20A) [123] and in cells undergoing mitosis (Fig. 20B-C). Ki-67$^+$ cells often appeared in pairs (Fig. 20A). Co-immunostaining with the astrocyte marker GFAP clearly double labeled Ki-67$^+$/GFAP$^+$ cells (Fig. 20D). Quantification of the Ki-67$^+$/GFAP$^+$ cells demonstrated that 85.71 % (+/- 7.35 %) of all examined Ki-67$^+$ cells in the striatum were GFAP$^+$ and 78.06 % (+/- 1.87 %) of all Ki-67$^+$ cells in the lateral cortex were GFAP$^+$ (n=3 animals, data are mean +/- SEM). Double immunostaining of nestin with Ki-67 clearly revealed double positive cells (Fig. 20E). Furthermore double immunostaining of nestin and GFAP (Fig. 20F) revealed that in the striatum 98.89 % (+/- 1.11%) of all nestin$^+$ cells co-expressed GFAP and 95.60 % (+/- 2.51 %) of all nestin$^+$ cells in the lateral cortex co-expressed GFAP (n=3 animals, data are mean +/- SEM). In addition we demonstrated that both GFAP$^+$ (Fig. 20G) and nestin$^+$ (Fig. 20H) cells co-stained with vimentin.

3.12 What is the origin of the proliferating GFAP$^+$ cells?

After we have determined an astrocytic phenotype of the Ki-67$^+$ cells we were interested in the site of origin of these proliferating GFAP$^+$ cells that appeared in the striatum and the lateral cortex at 4d after a 6-OHDA-lesion.

3.12.1 Are migrating SVZ-progenitor cells a source of the proliferating cells?

Progenitor cells have been described to migrate from their site of origin, the SVZ, into adjacent injured brain tissue [124,125]. To determine whether progenitor cells were the source of the proliferating GFAP$^+$ cells we performed double staining with the migration marker doublecortin (Dcx), which is known to be expressed in progenitor cells [125]. Dcx immunoreactivity was detected both in sham and 6-OHDA lesioned rats in cells in the SVZ, some of them co-expressing Ki-67 (Fig. 21A). Dcx$^+$ cells were observed in the tissue destroyed by the needle puncture at the dorsal lateral ventricle (Fig. 21B, 14A). However, no Dcx$^+$ cells were detected in the striatum (data not shown) or in the lateral cortex (Fig. 21C).

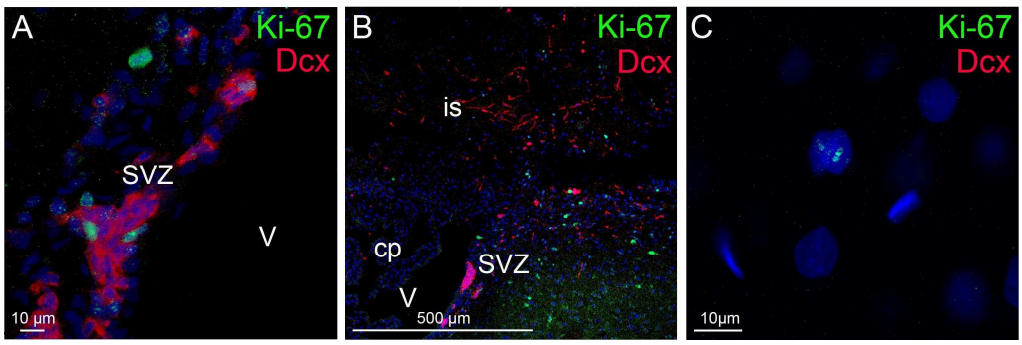

Figure 21 Investigation of migrating progenitor cells at 4d post-lesion. **A** Imunostaining for Ki-67 and the migration marker doublecortin (Dcx) in the SVZ in a sham animal. **B** Double immunohistochemistry for Dcx and Ki-67 in the destroyed tissue at the ventricular injection site. **C** Dcx and Ki-67 double staining in the lateral cortex of a 6-OHDA lesioned animals. Cell nuclei are depicted in blue (cp, choroid plexus; is, injection site; np, needle puncture; SVZ, subventricular zone; V, ventricle).

3.12.2 Do NG2 glia contribute to the proliferating cell population?

NG2 glia have the potential to proliferate in the adult CNS under physiological conditions and to a greater extend following brain injury [5]. Immunohistochemistry of NG2 and Ki-67 revealed proliferating NG2 cells in the striatum of 6-OHDA lesioned rats (Fig. 22A) but not in the lateral cortex (Fig. 22B). Quantification of the total number of NG2$^+$ cells (Fig. 22C) confirmed an increase of NG2$^+$ cells in the striatum of 6-OHDA lesioned animals of about 6 % (Fig. 22C) in comparison to sham animals, while the amount of NG2$^+$ cells remained unchanged in the lateral cortex (Fig. 22C). Quantification of the Ki-67$^+$/NG2$^+$ cells revealed that with respect to the total

fraction of Ki-67$^+$ cells, the NG2$^+$ cells counted only for 5 % (+/- 3.8 %) (n=3, data are mean +/- SEM).

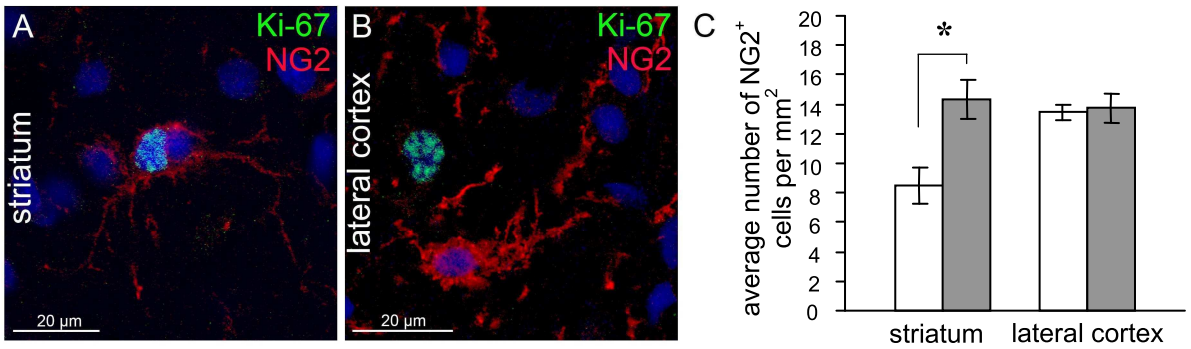

Figure 22 NG2$^+$ cells at 4d post-lesion. **A-B** Double immunohistochemistry of NG2 and Ki-67 in a 6-OHDA lesioned rat. Cell nuclei are depicted in blue. **C** Quantitative analysis of NG2$^+$ cells in sham (white bars) (n=3) and 6-OHDA lesioned rats (grey bars) (n=3). Data are mean +/- SEM; Student´s t-test for unpaired data, * p = 0.034.

3.12.3 Are the proliferating cells derived from resident de-differentiated astrocytes?

We were then interested if the proliferating GFAP$^+$, nestin$^+$ and presumably vimentin$^+$ cells were astrocytes from begin with.

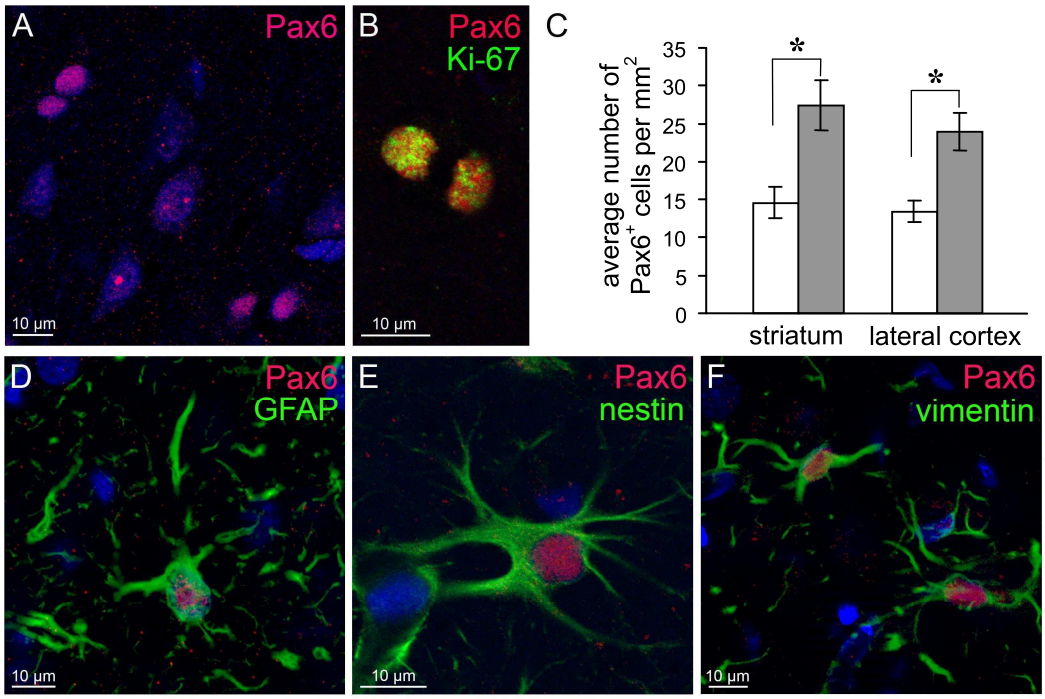

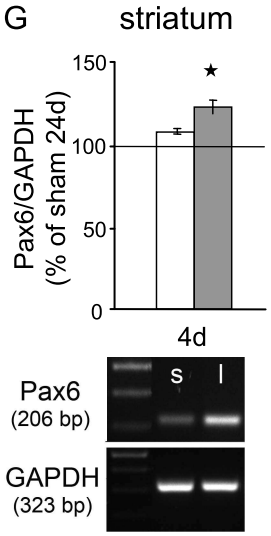

Figure 23 Expression of the transcription factor Pax6 at 4d post-lesion. **A** Pax6 immunoreactivity in the lateral cortex of a sham animal. Cell nuclei are depicted in blue **B** Double immunostaining for Pax6 and Ki-67 in the lateral cortex. **C** Quantitative analysis of Pax6$^+$ cells in sham (white bars) (n=3) and 6-OHDA lesioned rats (grey bars) (n=3). Data are mean +/- SEM; Striatum, Mann-Whitney rank sum test, * p = 0.001, lateral cortex, Student´s t-test for unpaired data, * p = 0.009. **D-F** Double immuno histochemistry in the lateral cortex of a 6-OHDA lesioned rat. Cell nuclei are depicted in blue. **G** Relative quantification of Pax6 mRNA expression. Data from both sham (white bars) (n=2) and 6-OHDA lesioned animals (grey bars) (n=4) were normalized to the average Pax6 mRNA expression in sham animals 24d post-lesion. GAPDH was used as internal reference. Data are mean +/- SEM; Student´s t-test for unpaired data: data vs. sham 24d ⋆ p = 0.047. The agarose gels demonstrate representative samples (s, sham; l, 6-OHDA lesion).

A subpopulation of mature, resident astrocytes in the rodent cortex have been described to de-differentiate in response to a stab wound lesion [58]. De-differentiated astrocytes may express makers usually found in glial progenitors, such as nestin and vimentin [50]. The transcription factor Pax6 is known to be expressed in neurogenic radial glia during development [2] and was recently shown in diverse astrocyte subpopulations in the adult brain [126,127,128]. *In vitro* studies suggested that de-differentiated astrocytes upregulate Pax6 [129,130]. We detected Pax6 immunoreactivity both in the striatum and the lateral cortex in sham and 6-OHDA lesioned rats at 4d post-lesion. Pax6 staining was localized to the cell nucleus (Fig. 23A), although several cells seemed to exhibited a faint Pax6 staining in their somata (Fig. 23A). For our investigations we only considered nuclear Pax6 expression.

3.13 Do microglia contribute to the proliferating cell population?

Microglia belong to the CNS immunsystem and become activated after brain insults. Activated microglia are known to proliferate [55]. We examined sections of the striatum and the lateral cortex 4d post-lesion by means of immunohistochemistry using the microglia marker Iba-1 to investigate if microglia contribute to the proliferating cell population following 6-OHDA lesion. At the injection site of the needle in the dorsal cortex (Fig. 25A), immunoreactivity of Iba-1 (Fig. 24A) was clearly visible and Ki-67^{+}/Iba-1^{+} cells were detected in both sham (Fig. 24A, insert) and 6-OHDA lesioned animals (data not shown). However, we detected neither in the lateral cortex (Fig. 24B) nor in the striatum (data not shown) Ki-67^{+}/Iba-1^{+} cells.

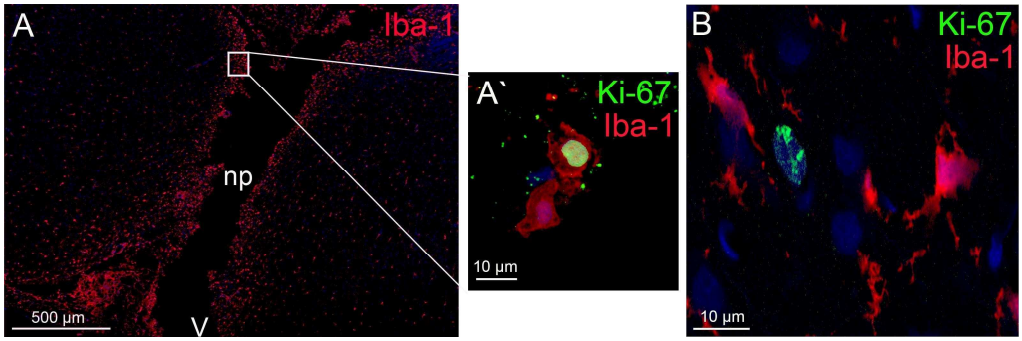

Figure 24 Investigation of microglia at 4d post-lesion. **A** Immunostaining for the microglia marker Iba-1 at the injection site in a sham animal. The insert shows a Ki-67^{+}/Iba-1^{+} cell. **B** Double immuno-staining for Ki-67 and Iba-1 in the lateral cortex of a 6-OHDA lesioned rat. Cell nuclei are depicted in blue (np, needle puncture; V, ventricle).

3.14 TH$^+$ cells increased in the lateral cortex following 6-OHDA lesion

Besides indications for astrocyte de-differentiation following the 6-OHDA lesion, we also observed an increased appearance of weakly stained TH$^+$ somata in the lateral cortex at 4d post-lesion (Fig. 25A,B,D). Quantification of the TH$^+$ cells confirmed an 18 fold increase in the lateral cortex of 6-OHDA lesioned animals (Fig. 25C). The TH$^+$ cells were estimated to occur mainly in layer III-IV (Fig. 25D) and exhibited a non-pyramidal morphology (Fig. 25D, insert). Often one thick and long process ascended towards layer V-VI (Fig. 25D, insert).

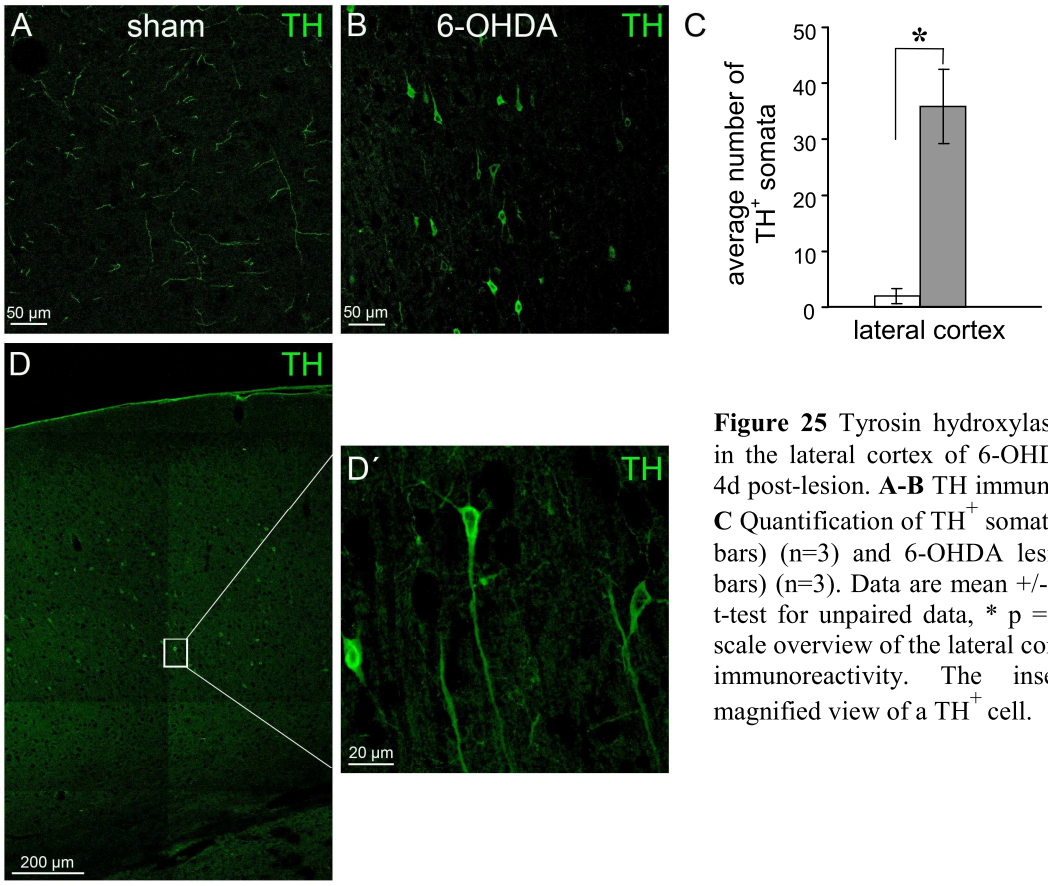

Figure 25 Tyrosin hydroxylase (TH)$^+$ somata in the lateral cortex of 6-OHDA lesioned rats 4d post-lesion. **A-B** TH immunohistochemistry. **C** Quantification of TH$^+$ somata in sham (white bars) (n=3) and 6-OHDA lesioned rats (grey bars) (n=3). Data are mean +/- SEM. Student´s t-test for unpaired data, * p = 0.007. **D** Large scale overview of the lateral cortex showing TH immunoreactivity. The insert showed a magnified view of a TH$^+$ cell.

Double immunostaining with TH and either GFAP or nestin did not show co-expression of TH with any of these markers (data not shown) nor did staining with the neuronal marker MAP-2 (Fig. 26A) reveal a clear co-expression of TH and MAP-2. Other studies that revealed TH$^+$ cell somata in the cortex stated that they are TH$^+$ interneurons [131,132,133,134,135] expressing the inhibitory neurotransmitter GABA and/or its synthesizing enzyme glutamic acid decarboxylase 67 (Gad67) [131,132,134,135].

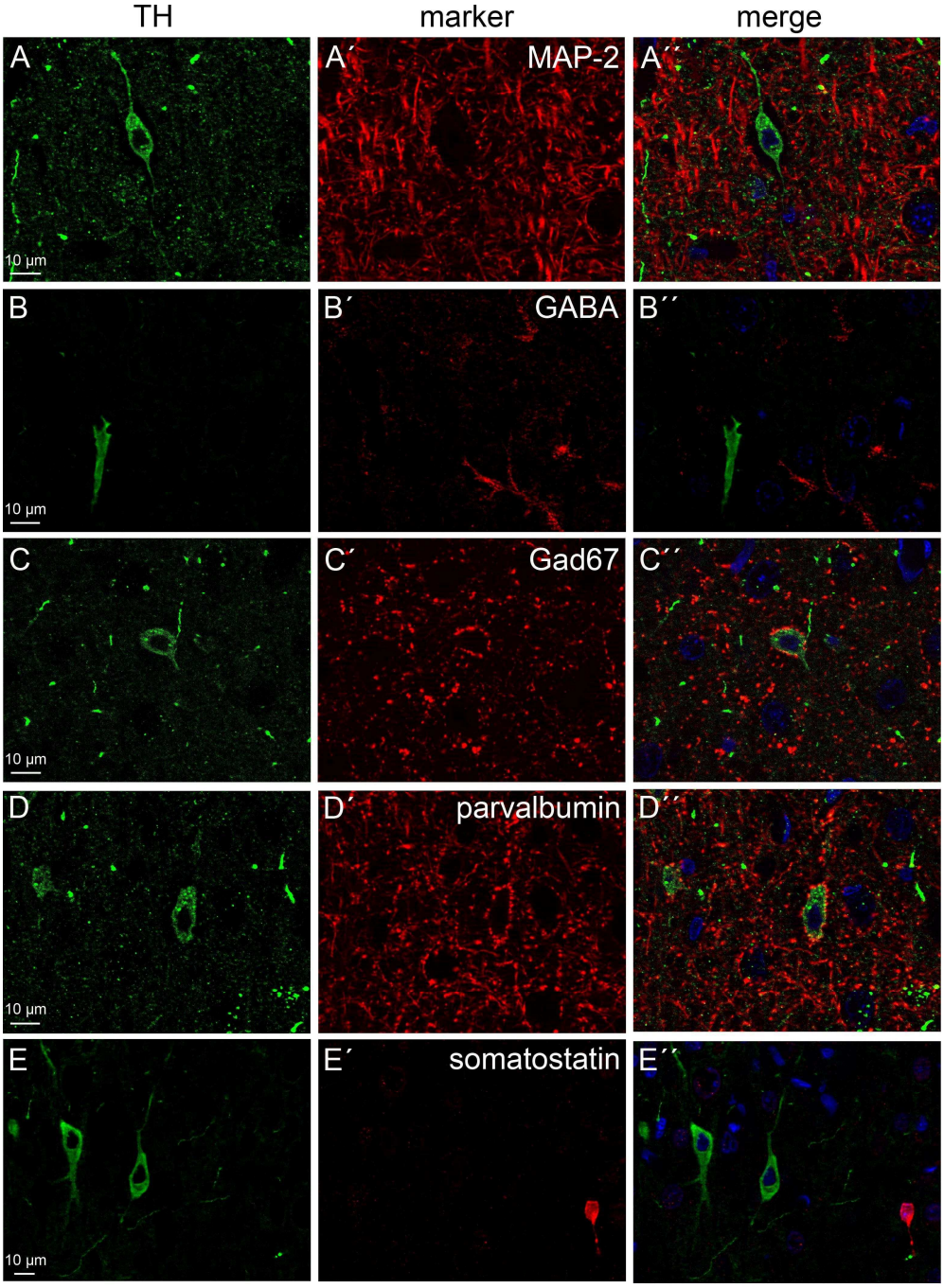

Figure 26 Double immunohistochemistry of tyrosin hydroxylase (TH) in the lateral cortex of 6-OHDA lesioned rats 4d post-lesion with diverse markers: microtubule associated protein 2 (MAP-2) (**A**), γ-amino butyric acid (GABA) (**B**), glutamic acid decarboxylase 67 (GAD67) (**C**), parvalbumin (**D**), somatostatin (**E).** Cell nuclei are depicted in blue.

We detected no co-staining of the TH^+ cells with GABA (Fig. 26B) or Gad67 (Fig. 26C), however we observed co-expression of TH with c-Fos (Fig. 27A) and calretinin (Fig. 27B). Double immunohistochemistry of TH with parvalbumin (Fig. 26D) or somatostatin (Fig. 26E) did not reveal co-expression of these markers with TH but showed that TH^+ cell somata are contacted by $Gad67^+$ (Fig. 26C) and $parvalbumin^+$ cell processes (Fig. 26D). Co-staining of TH with either calbindin, Pax6, or neuropeptide Y was likewise negative (data not shown).

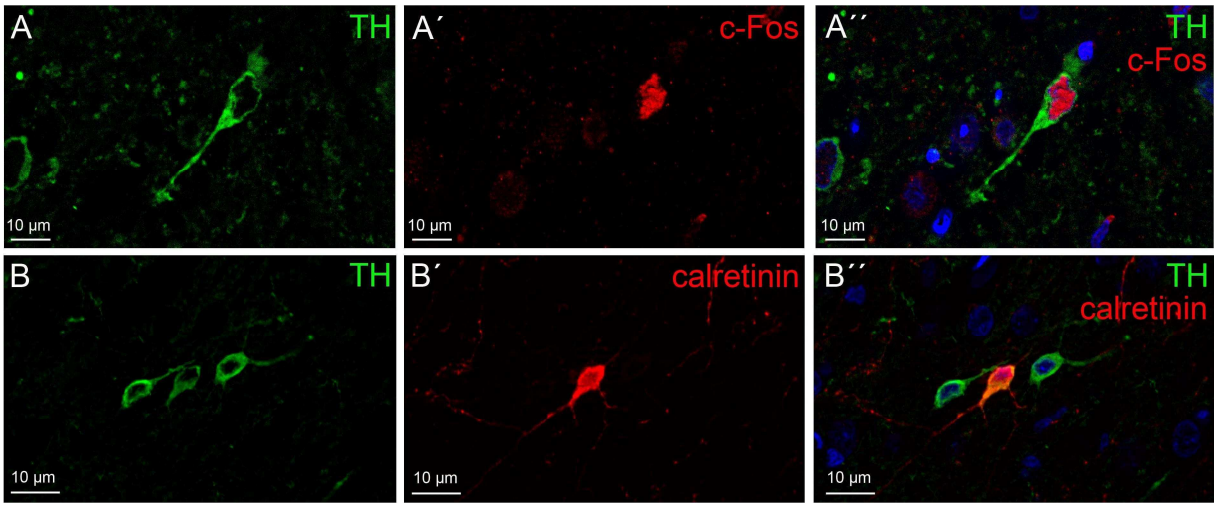

Figure 27 Positive double immunohistochemistry of tyrosin hydroxylase (TH) in the lateral cortex of 6-OHDA lesioned rats 4d post-lesion with c-Fos (**A**) and calretinin (**B**).

Darstellung des Eigenanteils bei Gemeinschaftsarbeiten (Publikationen) nach §9 (2):

Folgende Abbildungen wurden bereits veröffentlicht im Journal: European Journal of Neurosciene (Küppers *et. al.,* 2008): Fig. 8 B-C; Fig. 9 A-C, E; Fig.10 A-F.
Diese Daten stammen aus einer Gemeinschaftsarbeit mit Eva Küppers, Corinna Gleiser, Veronika Brito, T. Pauly, Bernhard Hirt und Stephan Grissmer. Für die Erzeugung der in dieser Dissertation gezeigten Abbildungen waren verantwortlich: Eva Küppers, Stephan Grissmer, Veronika Brito, Corinna Gleiser, Bernhard Hirt und ich. Zusammen mit Veronika Brito und Eva Küppers war ich beteiligt beim Anlegen der striatal Astrozytenkulturen, deren „Pflege", sowie die Behandlung der Zellen mit Dopamin und den Dopamin Antagonisten. Die PCRs wurden von mir und Eva Küppers durchgeführt, die Prolferationsassays von Eva Küppers und Stephan Grissmer, der Apoptoseassay von Veronika Brito und der Western Blot von Eva Küppers und Corinna Gleiser. Die siRNA Transfizierung wurde von Eva Küppers etabliert und durchgeführt. Die siRNA Kontrollexperimente wurden von Corinna Gleiser gemacht, die dazugehörigen Abbildungen stammen von Bernhard Hirt.

Folgende Abbildungen wurden bereits veröffentlicht im Journal: Cell and Tissue Resarch (Wachter *et al.,* 2010): Fig. 14 A-C, E-F; Fig. 15; Fig. 18 A-D, G-J, M; Fig. 20 A, C-F; Fig. 21 A, C; Fig. 22 B-C;Fig. 23 B-C, E; Fig. 24 B. Diese Daten stammen aus einer Gemeinschaftsarbeit mit Sonja Schürger, Jens Rolinger, Andreas von Ameln-Mayerhofer, Daniela Berg, H-J Wagner und Eva Küppers. Für die Erzeugung der in dieser Disseration gezeigten Daten waren verantwortlich: Sonja Schürger, Jens Rolinger und ich. Sonja Schürger und Jens Rolinger waren zuständig für die Betreuung der Ratten, die Durchführung der 6-OHDA Läsionen sowie für die Perfusionen. Herstellung der Kryoschnitte wurde von Sonja Schürger und mir ausgeführt. Die kompletten Immunhistochemischen Studien wurden von mir durchgeführt.

Alle anderen gezeigten Daten/Abbildungen in dieser Dissertation wurden von mir hergestellt. Ausnahme: Die Proliferationsassays in Kooperation mit Eva Küppers und die Betreuung der Ratten für die Molekularbiologie, die Durchführung der 6-OHDA Läsionen sowie die Perfusionen zusammen mit Rüdiger Sadler.

4. Discussion

4.1 Does dopamine has an effect on the proliferation of striatal astrocytes *in vitro*?

Dopamine is likely to modulate the function of striatal astrocytes

In this study we investigated if DA affects the proliferation of astrocytes in the rodent brain. The neurotransmitter DA is well known for its diverse modulating effects on neurons during development [98,106,107] and in adulthood [98]. The striatum is highly innervated by dopaminergic neurons under physiological conditions [94] and both the DA transporter [110] and DA receptors are found *in vitro* [10,100,101,102,103] and *in vivo* [99] on striatal astrocytes. Although the latter highly indicates a functional aspect of DA on astrocytes, only few studies have investigated DA-induced effects on astrocytes. DA treatment increases cAMP in striatal rat astrocyte cultures [10,101]. This occurs at low concentrations of DA (10 µM) via D_1 receptors [101] and at higher concentrations (100 µM) additionally via β-adrenergic receptors [10,101]. Furthermore, DA treatment in striatal astrocyte cultures is shown to induce pCREB via the D_4 receptor (200 µM) [99,136], to trigger transient increase in intracellular calcium via D_1 receptor activation (10 µM) [136] and to decrease the expression of the glutamate transporter GLT1 also via D_1 receptor activation (100 µM) [137]. We now report that DA treatment (100 µM) of striatal mouse astrocyte cultures decreased proliferation and the expression of the water channel AQP4 and that these events may be linked in a subsequent order.

Dopamine decreased the cell number in striatal astrocyte cultures

We stimulated striatal astrocyte cultures derived from neonatal Balb/C mice with 100 µM DA for 72h. Reports on physiological concentrations of DA in the CNS vary to a great extent. Some authors report concentrations of 6 nM DA in the extracellular space and 200 nM at the synapse and perisynaptic region [138], while others report concentrations of 10 µM in the extracellular space and suggest higher concentrations at the synapse [139]. The DA concentration within the neuronal terminal in a dopaminergic neuron may reach up to 10 mM [93], indicating that following neuronal activity the DA concentration at the synapse and varicosities may transiently be very high. We therefore assume that a concentration of 100 µM of DA is comparable to what astrocytes are transiently exposed with in the CNS.

In our culture model, treatment with 100 µM DA for 72h decreased the number of DAPI stained cell nuclei by approximately 20 %. This decrease in cell number could be due to reduced proliferation, cell death, or detachment of the cells from the glass plates. Since we did not detect loose cells in the culture medium (data not shown), we assumed they did not detach from the glass plate surface following treatment. We also excluded increased cell death either by apoptosis or necrosis by FACS analysis. Although DA is known to exert cytotoxic effects, especially in cell culture [111,113], and leads to apoptotic cell death in both neuronal and non-neuronal cells [93,111,113], we assume that the supplementation of the DA solution we used with ascorbic acid [140,141] and glutathione [113] may have prevented DA-induced apoptosis.

DA is involved in the regulation of proliferation of progenitor cells in the CNS during development [108,109] and in the adult CNS in the neurogenic niches [142,143,144,145]. During development DA reduces the proliferation of progenitor cells in the embryonic neostriatum in the rodent [108,109] via D_1 receptors that impede the transition from G_1 to S phase during the cell cycle. However, it is also shown that activation of D_2 receptors promotes this transition [108], although in different areas of the developing CNS and in distinct progenitor cells [109]. In the adult rodent CNS, reports on DA-induced changes in cell proliferation are contradictory. In some studies DA was shown to promote proliferation in the SVZ via D_2 or D_3 receptor activation [142,143,144], while other studies demonstrate an inhibitory effect of DA on the proliferation of

neural stem cells [145]. We showed that DA treatment resulted in a cell density dependent decrease of proliferation in striatal astrocyte cultures. The density dependent effect of DA may have several causes. Firstly, it is well established that astrocytes *in vitro* stop proliferation due to contact inhibition. Cultures grown in higher densities hence express a lower proliferation *per se* and the effect of DA on proliferation might therefore only be moderate. Secondly, gap junctions might influence the sensitivity of astrocytes to DA *in vitro* [136]. Down-regulation of gap junctions results in an upregulation of the D_1 receptor and an increased sensitivity of the astrocytes to DA [136]. Cells grown at lower densities exhibit less gap junctional coupling and therefore presumably more D_1 receptors than cells grown at higher densities.
In summary, data concerning modulation of proliferation of astrocytes *in vitro* by DA have not been published and hence we are the first to report that DA decreased proliferation in a cell density dependent manner in striatal mouse astrocyte cultures. This observation implies that in the striatum *in vivo* where DA is constantly present, DA might tonically inhibit astrocyte proliferation.

Dopamine decreased the expression of the water channel AQP4
In the CNS the water channel AQP4 is primarily expressed in astrocytes [59]. The function of AQP4 is dynamically regulated via several mechanisms such as phosphorylation or dephosphorylation, protein-protein interactions, subcellular distribution, and channel gating [68]. Zelenina *et al*. showed that a short DA treatment (3 min, 10 µM) results in protein kinase C (PKC) dependent phosphorylation of Ser180 of AQP4, which decreases the single channel water permeability in kidney cells [117]. Activation of PKC may also regulate AQP4 expression as a long term effect [68], however it has not been shown if DA treatment modulates the expression of AQP4 in striatal astrocytes. We demonstrated that treatment with 100 µM DA for 72h led to a significant decrease of ~50 % in the expression of both AQP4 mRNA and protein. AQP4 has six known isoforms in the rat brain [86] and three isoforms in the mouse brain [85] with AQP4 M1 and the shorter AQP4 M23 being the main isoforms in the adult rodent CNS [74,85,86]. In our study we demonstrated that only AQP4 M23 mRNA and protein expression is significantly decreased by about 30 % following DA treatment, while AQP4 M1 mRNA and protein expression was unaffected. Thus DA treatment with 100 µM for 72h reduced the expression of AQP4 M23, the most abundant isoform in the CNS [84]. Differential regulation of the AQP4 isoforms has been observed [146,147,148,149] although the consequences have not yet been determined. Conflicting data exist about the water permeability of M1 and M23 [84,89,149] so one can not argue (yet) that specific down-regulation of AQP4 M23 changes the water permeability. It is however understood that M1 and M23 contribute differently to the formation of OAPs. While M23 gives rise to large square arrays, M1 can not form square arrays on its own but assembles with M23 leading to smaller OAP formation than with M23 alone [88]. One could speculate that in our study OAP formation is affected by the DA treatment. To clarify this, freeze fracture studies would be necessary. Nevertheless the functional significance of OAPs is still unknown. The DA-induced decrease of AQP4 mRNA was ~ 50 %, while the reduction of AQP4 M23 mRNA was 30 %. This discrepancy suggests that another AQP4 isoform besides M23 or M1 might be affected by DA. In the mouse, three sequences of AQP4 isoforms are known, M1, M23 and M23x. AQP4 M23 and AQP4 M23x are developmentally regulated, but seem both to encode a functional AQP4 M23 protein [85]. It might be that all three AQP4 isoforms are expressed in neonatal astrocyte cultures and that AQP4 M23x is also affected by DA treatment or that a not yet determined AQP4 isoform is affected.
In summary, we showed that in striatal mouse astrocytes DA treatment exerts a regulatory effect on the expression of the water channel AQP4. DA treatment specifically decreased the AQP4 isoform M23 both on mRNA and protein level.

A noradrenergic receptor mediated the dopamine induced change in AQP4 expression
We were interested in the DA receptor that transmits the effect on AQP4 expression. DA interacts primarily with its five receptors (D_1-D_5), which are classified into two families, the D_1 receptor family (D_1, D_5) and the D_2 receptor family (D_2, D_3, D_4) [96]. DA receptors are G-protein coupled receptors. Each family induces distinct intracellular signalling cascades [96]. Our studies showed that the DA-induced decrease in AQP4 mRNA expression was however transmitted via an α_2-adrenergic receptor. Astrocytes express receptors of other catecholamines such as adrenergic receptors and all basic subtypes of adrenergic receptors (α_1, α_2, β_1, β_2) are expressed on astrocytes [10]. Crosstalk of DA with these receptors has also been reported in other studies [101,118,119,120].
In summary, although we did not completely examine the DA-induced signalling cascade that results in the decrease of AQP4 mRNA expression, we showed that it is mediated via an α_2-adrenergic receptor. This receptor type is known to induce a signalling cascade that leads to the activation of PKC [150], which has been shown in other studies to decrease AQP4 mRNA [68,150]. Further studies are required to identify the complete signalling cascade.

In our studies, we revealed that DA treatment (100 µM, 72h) exerted an inhibitory effect on proliferation of striatal mouse astrocyte cultures and down-regulated the expression of the water channel AQP4, especially the M23 isoform via an α_2-adrenergic receptor.

4.2 Does AQP4 influence proliferation?

Following the results of our first studies, we hypothesized that the DA-induced decrease of the water channel AQP4 and the observed decrease of proliferation may be linked. Proliferation is a complex process that is controlled by many different parameters. It is suggested that cell proliferation is phenomenologically correlated to cell volume [151]. Cell size including cell volume is connected to cell division and hence proliferation because cells need to increase their size before they divide [151]. Changes in cell volume can be quickly obtained via water influx through water channels such as AQP4. Water channels might therefore play a modulating role in proliferation and the DA-induced decrease of AQP4 could therefore be the reason for the observed decrease in cell proliferation. An involvement in proliferation is shown for AQP3 [152,153,154,155], AQP5 [156] and suggested for AQP1 [157] although data for AQP1 are contradictory [158].

AQP4 knock-down or pharmacological inhibition decreased proliferation in striatal astrocyte cultures
We investigated the putative involvement of AQP4 in proliferation of striatal mouse astrocytes by pharmacologically blocking the water channel by TEA and by a siRNA induced knock-down of AQP4. siRNA is shown to effectively knock-down AQP4 in mouse, rat and human astrocytes [121,159], while the use of TEA as a channel blocker for AQP4 is highly disputed [68,122,160,161,162,163]. TEA is a small organic cation that is approximately the same size as a hydrated potassium ion [164] and functions as a pore blocking agent for potassium channels [164,165]. The sensitivity of potassium channels to TEA is variable. Most channels can be grouped as either sensitive [166,167] or relatively insensitive [168]. TEA concentrations shown to efficiently block potassium channels range from 1 mM [165] to 300 mM [167] depending on the channel type. Brooks *et al.* tested TEA as an inhibitor of AQP1 in *Xenopus laevis* oocytes and found that incubation with 100 mM TEA for 15 min result in a decreased water permeability of about 20-40 %. The effect was dose-dependent (0.01-10 mM) and reversible [163]. Subsequently, Demeter *et al.* published data confirming the earlier study and extended the results to other AQPs. They showed that besides AQP1, AQP2 and AQP4 are also successfully blocked,

the latter with an efficiency of ~50 % and an IC_{50} value of ~9.8 µM [122]. The observation that concentrations below 20 µM are as effective on AQP4 as high concentrations above 100 mM revealed the possibility to pharmacologically block water channels with TEA without inflicting on potassium channels. However, several studies question the pharmacological blocking of AQPs by TEA [160,161,162].
In our study, both proliferation induced by bFGF and basal proliferation of the striatal astrocyte cultures were drastically reduced by AQP4 knock-down or pharmacologically blocking of AQP4 with TEA. This gives strong indication of the involvement of AQP4 in proliferation. Nicchia *et al*. described a likewise reduction in cell proliferation of ~68 % following AQP4 siRNA treatment in rat astrocyte cultures [121], which is similar to the observed decrease in basal proliferation by ~50 % following AQP4 knock-down in our mouse striatal astrocyte cultures. Though, since a microarray analysis revealed that the AQP4 knock-down in the rat leads to a changed expression of other genes (GLT1, hexokinase, metallothionein-I and c-Fos) [121] and a study in mouse astrocytes demonstrated a down-regulation of connexin43 following AQP4 siRNA transfection [121], it was suggested that the observed decrease in proliferation following transfection with AQP4 siRNA might not be directly modulated by AQP4 [68]. Especially since connexin43 is shown to be involved in the proliferation of astrocytes [169,170]. However, given that we could in addition show a decrease in proliferation when AQP4 was pharmacologically blocked by TEA, we suggest that AQP4 does in fact play a role in striatal astrocyte proliferation. Reports about proliferation in AQP4 null mice are contradictory and depend on the used knock-out mouse [171,172,173]. The lab of Allan Verkman stated no impaired proliferation in $AQP4^{-/-}$ astrocytes *in vitro*, although the proliferation was slightly decreased at all examined time points in direct comparison to wild type astrocytes cultures [171]. Furthermore, these $AQP4^{-/-}$ astrocyte cultures were treated after 2 weeks *in vitro* with the anti-proliferating agent cytosine arabinoside and subsequently with dibutyryl cAMP to induce differentiation [171]. The lab of Gang Hu demonstrated in their AQP4 knock-out mouse decreased proliferation in astrocytes [172] and in adult neural stem cells [173] *in vitro*, though their AQP4 knock-out mouse was openly questioned by the Verkman lab [174].
In summary, we showed that AQP4 knock-down by siRNA or pharmacologically blocking the water channel with TEA significantly decreased proliferation of the striatal mouse astrocytes cultures, indicating an involvement of AQP4 in proliferation.

AQP4 is also involved in the proliferation in the pancreatic cancer cell lines BxPC3 and PANC1
To further clarify an involvement of AQP4 in proliferation, we investigated a different cell culture model. Cancer cells often express AQP4 [175] and some studies indicate that highly proliferating cancer cells such as glioma cells [176,177,178] exhibit increased AQP4 expression. We investigated three different human pancreatic cancer cell lines, namely BxPC3, PANC1, and MIA PaCa-2 for their AQP4 expression. Immunocytochemical staining of AQP4 resulted in AQP4 immunoreactivity in BxPC3 and PANC1 cells, while the immunocytochemical staining in MIA PaCa-2 was questionable. Expression analysis on mRNA level confirmed AQP4 mRNA expression in BxPC3 cell cultures and in PANC1, but not MIA PaCa-2 at three days *in vitro*. Since we aimed to investigate the role of AQP4 in proliferation we only continued with the cell lines that expressed AQP4. Proliferation studies in BxPC3 and PANC1 cell cultures demonstrated that AQP4 knock-down with both 1 nM and 5 nM of AQP4 siRNA resulted in a decreased proliferation. The observed decrease correlated with the efficiency of the AQP4 knock-down by means of siRNA. AQP4 knock-down in BxPC3 cells proved to be more efficient at both concentrations used (- 15 % and - 45 % on mRNA level) than in PANC1 (- 8 % and – 18 %), which might explain why we observed a higher decrease in proliferation in BxPC3 cells (-32 % and -39 %) than in PANC1 (-6 % and – 20 %).

In summary, the reduction of AQP4 expression by siRNA (1 nM and 5 nM) in the human pancreatic cancer cell lines BxPC3 and PANC1 led to a significant decrease in proliferation. These data further indicate a modulating impact of AQP4 on proliferation.

4.3 Do astrocytes in the dopamine-depleted striatum *in vivo* increase in proliferation and in their expression of AQP4 ?

Diverse studies assume that neurodegenerative diseases may be linked to changes in the proliferation of astrocytes. Our observations of a down-regulation of proliferation of astrocytes by DA *in vitro* confirm and extend these assumptions at least for those neurodegenerative diseases correlated with perturbations of the dopaminergic transmission such as Parkinson's disease (PD). We hypothesized that under physiological conditions in the CNS the dopaminergic innervation of the striatum might tonically inhibit AQP4 expression, or AQP4 M23 expression, respectively. This thereby may prevent astrocyte proliferation. In PD the loss of DA in the striatum, due to cell death of the dopaminergic neurons comprising the nigrostriatal pathway [104], would abolish this inhibition and an increased expression of AQP4, AQP4 M23, as well as an increased proliferation should be observed. To investigate this hypothesis, we examined proliferation and AQP4 expression in a toxin-induced PD model in the adult rat.

The 6-OHDA lesion model

6-OHDA is a potent toxin for catecholaminergic neurons. Since 6-OHDA is taken up via the monoamine transporters, addition of a noradrenergic uptake inhibitor such as nortryptilin prevents the uptake of the neurotoxin into noradrenergic neurons and therefore results in selective dopaminergic cell death [104,114]. 6-OHDA does not permeate the BBB and has to be administered directly into the brain tissue [104]. Frequently used injection sites (uni- or bilaterally) are the striatum, the medial forebrain bundle (MFB) or the substantia nigra (SN) targeting dopaminergic nerve terminals, axons or somata, respectively [104,114]. Since we aimed to investigate astrocyte responses to DA depletion in the striatum, intrastriatal injection would have been favorable. However, direct injection into the striatum leads to reactive astrocytes due to mechanical injury by the needle, making it difficult to investigate the astrocyte response to the 6-OHDA lesion itself, especially since cell proliferation and upregulation of AQP4 have been observed in reactive gliosis [7,179,180]. We therefore decided to use an alternative 6-OHDA lesion model. In the early 70s Zigmond and Stricker showed that intraventricular injection of 6-OHDA in adult rats results in a long lasting depletion of DA in the striatum [181]. Measured at 7d post-lesion the striatal DA is reduced by 62-88 % following intraventricular injection [181,182], which is comparable to the DA depletion following intrastriatal injection with > 80 % [183,184,185] measured between 3d and 5 weeks post-lesion. The distribution pathway of the neurotoxin following injection into the lateral ventricles into the brain tissue is not known. Earlier studies performed with injection of radioactive labeled DA into the lateral ventricles showed that DA is rapidly taken up into the brain tissue adjacent to the ventricles [186] and that the distribution within the tissue is dose dependent, with increasing doses of DA resulting in a distribution further away from the ventricles [187]. Since 6-OHDA is akin to DA, a similar distribution can be assumed.

In 2000, Rodriguez *et al*. provided a detailed study about the cell-loss pattern of dopaminergic neurons in the midbrain following intraventricular 6-OHDA lesion [115]. Intraventricular injection result in a progressive degeneration of dopaminergic cells within the first week, similar to the intrastriatal model [188], but without the additional mechanical injury to the nigrostriatal system due to the needle injection [115] Bilateral intraventricular injections of 50 µg 6-OHDA cause only subtle changes, while the maximal response is reached with 300 µg 6-OHDA [115]. Therefore, the 105 µg of 6-OHDA used in our experiments can be regarded as a modest lesion.

In our study, successful lesions were determined by the disappearance of TH, the rate limiting enzyme in the DA synthesis that is present in all catecholaminergic neurons [95]. TH expression was investigated in the striatum of all animals used for experiments. Animals with a decrease of less than 10 % in either TH immunoreactivity, TH protein or TH mRNA expression were excluded from the experiments. In total, only one animal was excluded, which indicates a high efficiency of our lesion model. By RT-PCR and Western blot analysis, we observed that the TH protein and mRNA expression were decreased to nearly 50 % already at 1d post-lesion and afterwards fluctuated slightly around this value. These data match with the examined TH mRNA and protein expression following intrastriatal injection [189,190]. By immunohistochemistry at 4d post-lesion we also observed a drastic reduction of TH^+ fibres in the lateral cortex, indicating that this region may also be affected by the intraventricular 6-OHDA lesion induced dopaminergic cell death. No statements of dopaminergic de-afferentiation in the cortex are made in the classical injection site models of 6-OHDA.
In summary, we demonstrated that following intraventricular injection of the neurotoxin 6-OHDA, TH expression in the striatum diminished permanently from the first day post-lesion. These data imply the loss of dopaminergic fibers in the striatum is presumably due to the cell death of dopaminergic neurons. Although we have not determined the exact decrease of the DA concentration in the striatum by e.g. HPLC, we assume based on the data from several other groups that DA is progressively depleted in the striatum following the intraventricular 6-OHDA lesion.

Proliferating cells were detected in the striatum and the lateral cortex following 6-OHDA lesion
By performing immunohistochemistry using an antibody against the Ki-67 protein we determined proliferating cells in sham and 6-OHDA lesioned rats at 4d post-lesion. Ki-67 is a protein that is expressed in all active phases of the cell cycle (late G_1, S, G_2 and M), but not in resting or quiescent cells in G_0 [123]. Astonishingly, despite its discovery nearly 30 years ago, the function of Ki-67 remains an enigma [123]. As expected $Ki\text{-}67^+$ proliferating cells were observed in the SVZ, one of the two neurogenic niches in the adult brain [2] in both sham and 6-OHDA lesioned animals. Contradictory results are published concerning proliferation in the SVZ following 6-OHDA lesion. While both a decrease [142,143] and an increase in proliferation are described [188], we detected no changes in proliferation in the SVZ. A decreased proliferation in the SVZ is described at 28 days [143] and 6 weeks post-lesion [142], respectively. Therefore it might be too early to detect in our model at 4d post-lesion a decreased proliferation. Aponso *et* al. described an increase in proliferation at 3d post-lesion [188], which may be due to a different injection site.
We detected a striking increase in proliferation in the striatum and interestingly also in the lateral cortex at 4d post-lesion in 6-OHDA lesioned rats. These regions are the two areas where we observed a marked decrease in TH immunoreactivity following 6-OHDA lesion. The appearance of proliferating cells in the striatum following DA depletion is described in a study using intrastriatal injection of 6-OHDA in the rat [188] and in a study using the dopaminergic neurotoxin MPTP in mice [191], while an increased proliferation in the cortex following 6-OHDA lesion has not yet been reported. A recently published study performed microarray analysis in the striatum of 6-OHDA lesioned rats and showed that 3d post-lesion 111 genes are altered in their expression. Many of these genes are involved in cell cycle pathways, indicating a re-entry of cells into the cell cycle following 6-OHDA lesion [185]. It is not known, if this proliferation promoting effect is induced directly by the toxin, by the DA depletion or by neuronal cell death. Reports on proliferating cells in e.g. the striatum of human PD patients post-mortem are rare [192]. This might indicate that the observed proliferation in our 6-OHDA model in the rat is either toxin-induced, conditional upon the species or it may depend on the progress of the disease if one assumes that proliferation might only occur in very early stages of PD.

In summary, we showed that 4d following intraventricular injection of 6-OHDA, cells in the striatum and the lateral cortex were proliferating. According to our hypothesis that DA might tonically inhibit astrocyte proliferation and hence loss of DA would diminish this inhibition, we suggest that the increase in proliferation is a result of the 6-OHDA induced DA depletion in the striatum and the lateral cortex. In addition we confirmed that the proliferating cells were $GFAP^+$ astrocytes (see discussion below).

Changes of AQP4 expression following 6-OHDA lesions

Upon the discovery of an increased cell proliferation in the striatum following 6-OHDA lesion we investigated the expression of the water channel AQP4. Vizuette *et al*. published the only study so far where they investigated AQP4 expression in the CNS following 6-OHDA lesion. In their study, injection of 6-OHDA into the MFB increased AQP4 mRNA expression in the SN, although this is suggested to be independent of dopaminergic cell death but rather be due to BBB disruption [179]. Fan *et al*. examined the MPTP model in the mouse and detected a decreased AQP4 mRNA expression in the striatum and the SN at 7d following MPTP-lesion [172]. MPTP is a neurotoxin, which results in a similar destruction of dopaminergic neurons and hence DA depletion as it is shown in rats for 6-OHDA [111]. In our study we observed a significant increase in AQP4 mRNA in both sham and 6-OHDA lesion animals in the striatum on the first day post-surgery, indicating that this might be a surgery related effect. A rapid increase of AQP4 expression is known to occur in reactive astrocytes in cases of impaired BBB [179,193]. We do not assume that the 6-OHDA lesion alters the BBB integrity, however it is suggested that the anesthetic isoflurane used in our study may affect the BBB [194] and hence could be responsible for the increased AQP4 mRNA shortly after the surgery. The increase in AQP4 mRNA expression was far more pronounced in sham animals than in 6-OHDA lesioned rats, suggesting that the toxin inhibits the AQP4 mRNA upregulation. In contrast to the sham animals, AQP4 mRNA sustained an increased level in 6-OHDA lesioned rats, which corroborates our hypothesis that following 6-OHDA induced DA-depletion AQP4 expression increases *in vivo*.

In our *in vitro* studies in striatal mouse astrocytes we showed that DA specifically decreased AQP4 M23 mRNA, while M1 mRNA was not affected. A comparable differential effect on the AQP4 isoforms was observed in the 6-OHDA lesion model *in vivo*. At 4d post-lesion AQP4 M23 mRNA was significantly increased in the striatum of 6-OHDA lesioned rats, while no change occurred in the expression of AQP4 M1 mRNA. In addition, we showed that AQP4 z mRNA expression resembled that of M23 following the 6-OHDA lesion. After M1 and M23, AQP4 z (AQP4e) is the third functional AQP4 isoform expressed in the rat brain [86]. AQP4 z was recently described to be present at low levels in the rat, but not detected at all in human or mouse CNS [195]. Due to its low expression level it is suggested that AQP4 z may have no functional impact [195].

Investigation of AQP4 protein expression in the striatum by means of Western blot displayed several bands representing the distinct isoforms M23 (~32 kDa), M1 (~34 kDa) and z (~39 kDa) [86]. Contrary to the mRNA expression differences, no change in AQP4 M23 protein expression at 4d post-lesion was detected, while AQP4 M1 protein expression was significantly decreased in 6-OHDA lesioned animals. Immunostaining of AQP4 in our study resulted in a diffuse staining pattern of the neuropil and a clear labelling along blood vessels, similar to descriptions made by other groups [196]. Measurement of the AQP4 immunoreactivity did likewise not differ between sham and 6-OHDA lesioned rats, indicating no change in AQP4 protein expression following 6-OHDA lesion. Discrepancies between AQP4 mRNA and protein expression in the CNS under pathological conditions have not been reported. The observed differences probably reflect normally occurring discrepancies between mRNA and protein expression due to different mRNA and protein stability and turnover [197,198]. Moe *et al*., showed in the adult physiological rat brain discrepancies between AQP4 mRNA and protein expression of several

isoforms and suggested posttranscriptional regulation of *AQP4* gene expression [86]. However, they observed mainly a higher AQP4 M23 protein expression than what would have been expected by the examined AQP4 M23 mRNA expression [86].
In summary, at 4d post-lesion AQP4 M23 mRNA expression was significantly increased in 6-OHDA lesioned rats, while no change was observed for AQP4 M1 mRNA. Contrary to the observed mRNA expression AQP4 M23 protein was not increased in 6-OHDA lesioned animals and AQP4 M1 protein expression was decreased at 4d post-lesion.

4.4 Which cells are susceptible for dopamine treatment in striatal astrocytes *in vitro?*

Based on the results of the first experiments two questions arose. Firstly, since astrocytes are heterogeneous [4] we wanted to investigate whether we could deduce a certain phenotype in our mouse striatal culture system that is susceptible for DA. Secondly, we aimed to determine the phenotype and the origin of the proliferating cells in the DA depleted rat model *in vivo*.

Astrocytes in culture are heterogeneous
When working with astrocyte cultures one has to perform control stainings for neurons, oligodendrocytes, and microglia and morphologically examine the cultures for ependymal cells and fibroblasts, since astrocyte cultures are never 100 % pure [199]. The striatal astrocyte cultures were prepared from neonatal mice (P1-P4), a time point when astrogenesis peaks, which is assumed to yield the highest possible purity of astrocytes in culture [199]. The only noticeable contamination we could observe comprised microglia (estimated < 1 %) and a few oligodendrocytes as described in other studies [199,200]. We assume that this low amount of contamination is not responsible for any of the observed effects.
Immunocytochemical staining with an antibody against the astrocyte marker GFAP revealed that in untreated astrocytes cultures ~52 % of all cells at ~2 weeks in culture were $GFAP^+$, which corresponds well with observations made by other groups in mouse astrocyte cultures [200,201]. The GFAP immunostaining exhibited the expected typical dense IF network within the cell. As previously observed [201], we showed that ~80 % of all cells at ~2 weeks in culture were $nestin^+$ and the staining pattern of nestin was very similar to that of GFAP matching the IF network, as expected. The IF protein and progenitor marker nestin is expressed by astrocytes *in vitro* [40], although the reason for this expression is unclear. Astrocytes *in vitro* may be reactive [202] or that the cultural environment may hinder their full differentiation [203]. In our untreated striatal astrocytes cultures, ~66 % of all cells expressed AQP4. AQP4 immunoreactivity was diffusely dispersed with occasional clear membrane associated staining, which matches to the observed staining pattern of AQP4 made by other groups working with mouse astrocyte cultures [146,159]. Since the used AQP4 antibody used in our study, recognizes the C-terminus of AQP4, no differentiation could be made between AQP4 isoforms, which differ in their N-terminus but not their C-terminus [74].
Sergent-Tanguy *et al*. described a selective decrease in the number of $nestin^+/GFAP^-$ cells as well as an increase in the number of $nestin^+/GFAP^+$ cells in rat astrocyte cultures following cell cycle inhibition [201]. Since we observed proliferating cells that stained positive for AQP4, GFAP and nestin, respectively, we tried to evaluate if one of these cell populations was affected by the DA-induced decrease in proliferation. However, quantification analysis revealed no changes in the total number of $AQP4^+$, $GFAP^+$ or $nestin^+$ cells, respectively and no changes in the number of $AQP4^+/GFAP^+$, $AQP4^+/nestin^+$ and $GFAP^+/nestin^+$ cells following DA treatment. These findings differ from our initial observation, that DA decreased the expression of AQP4 mRNA and protein in striatal astrocyte cultures. It might be due to the fact that immunocytochemistry is not a real quantitative method, since a down-regulation of the AQP4 mRNA and even protein in a single cell will not be reflected in a decrease in number of AQP^+

cells. Even if AQP4 expression is decreased the cells may still express AQP4 protein to which the antibody can bind resulting in a positive staining in the immunocytochemistry.
In summary, by performing immunocytochemistry we could not identify a distinct phenotype in the striatal astrocyte cultures that was specifically decreased. One therefore might consider a different strategy to elucidate the DA susceptible phenotype. Co-staining with a proliferation marker might help to identify the proliferating cells and their respective phenotype in untreated control cultures and based on these observations striatal astrocyte cultures might be examined following DA treatment.

4.5 What is the origin and the phenotype of the proliferating cells following 6-OHDA lesion?

Intraventricular injection of 6-OHDA in adult rats resulted in an increase of proliferating cells in the striatum and the lateral cortex at 4d post-lesion. In the physiological adult brain proliferating cells are usually only detected in the two neurogenic niches, the SVZ and the dentate gyrus where stem and progenitor cells persist during adulthood [2]. However, in case of severe insults to the CNS, proliferation is described to occur in the adult brain outside of these niches in conjunction with reactive gliosis [7,55,58,188,191,204,205,206].

Reactive gliosis following 6-OHDA lesion
Following basically any insult to the brain astrocytes become reactive [7]. Hallmarks of reactive gliosis are upregulation of IF proteins such as GFAP, nestin and vimentin, hypertrophy of cellular processes, and proliferation [7]. Reactive gliosis is described in some cases in the brain of human PD patients [192,207] and basically in every 6-OHDA-induced PD model in the rodent at least around the injection site. In the animal model one therefore has to discriminate between reactive gliosis due to the surgery *per se* and reactive gliosis due to the 6-OHDA lesion.
To identify surgery related effects in our study the mRNA data were normalized to the sham values obtained 24d post-lesion, which represent most likely a value that is not biased by the surgery. By doing this we revealed that in the striatum no significant increase of GFAP, nestin or vimentin on mRNA level occurred in sham animals, indicating no effect of the intraventricular injection *per se* on the striatum. In the lateral cortex however, we observed a significant increase of GFAP mRNA at the first day post-lesion and a significant increase of nestin mRNA at 1d and 4d post-lesion in sham animals, indicating reactive gliosis due to the surgery in that brain region. This reaction may be explained by the needle puncture in the dorsal cortex during the intraventricular injection procedure. The mechanical lesion to the brain tissue resulted in reactive gliosis with clearly visible upregulation of GFAP and nestin immunoreactivity including scar formation demarcating the needle puncture (data not shown). Several studies report a "spreading" of reactive gliosis to areas away from the direct site of mechanical lesion [38,40], which might explain the observations made in the lateral cortex of the sham animals. In summary, we assume no reactive gliosis due to the surgery *per se* in the striatum but a slight reaction of astrocytes within the first 4d post-lesion in the lateral cortex.
Reactive gliosis in the striatum defined by an upregulation of GFAP was described following 6-OHDA injection into the striatum [190,208,209], the MFB [190,210], and the SN [202,211] but not for the intraventricular 6-OHDA lesion model. In our study we showed that intraventricular application of 6-OHDA resulted in an increased expression of GFAP mRNA and higher immunoreactivity in the striatum in the first days after the lesion. In the cortex, increased GFAP expression was observed only in two studies following 6-OHDA injection into the striatum [212] or into the SN [202]. We report a more intense GFAP immunoreactivity at 4d post-lesion and a drastic increase of GFAP mRNA during the first week post-lesion, indicating reactive gliosis in

the lateral cortex of 6-OHDA lesioned rats. Furthermore, the GFAP immunostaining revealed hypertrophic cells in the lateral cortex and the striatum.
Reactive astrocytes are known to re-induce the progenitor marker nestin [40,41]. Nevertheless, no data about an increase of nestin expression in the striatum following 6-OHDA lesion were found in literature and only one study reported increased nestin expression in the cortex following intrastriatal 6-OHDA lesion [212]. We demonstrated in our study the appearance of stellated nestin^{+} cells following 6-OHDA lesion in both the striatum and the lateral cortex at 4d post-lesion and confirmed this increase of nestin on molecular level in the first week post-lesion. Additionally we provide data that demonstrate an increased expression of vimentin, which is also described to be expressed in reactive astrocytes [29], in the striatum and the lateral cortex in 6-OHDA lesioned animals at 4d post-lesion.
In summary, our data show that following intraventricular injection of 6-OHDA reactive gliosis occurs defined by an upregulation of GFAP, nestin and vimentin expression and cellular hypertrophy in the striatum and the lateral cortex. Although we determined that the reactive gliosis in the lateral cortex in the first days post-lesion might be partially induced by the surgery itself, the data otherwise suggested that following 6-OHDA lesion reactive astrocytes occur in the striatum and the lateral cortex, which both represent target regions for dopaminergic fibres and are therefore associated with dopaminergic cell death following 6-OHDA lesion. These are also the areas were we observed proliferating cells following 6-OHDA lesion.

Determination of the origin and phenotype of the proliferating cells following 6-OHDA lesion
Proliferating cells observed under pathological conditions can be (I) microglia, which become activated in case of brain insults [55], (II) progenitor cells from e.g. the SVZ that migrate into the particular area [124,213,214], (III) NG2 glia [204,205,206,215] or (IV) reactive astrocytes that originate from resident mature astrocyte that de-differentiate and regain proliferation capacity [58].
Microglia are not involved in the proliferative response in the striatum and the lateral cortex
Microglia are resident CNS immune cells that become rapidly activated in response to brain insults. In the activated state microglia proliferate and migrate to the site of injury were they release both neurotrophic and neurotoxic substances and remove cellular debris [55]. Microglia were investigated in this study by using the ionized calcium binding adaptor molecule 1 (Iba-1), which is a known microglia marker [216]. Activated proliferating microglia were observed in the vicinity of the needle puncture in the dorsal cortex as has been described by others [185,217,218,219]. Activation of microglia was also described in 6-OHDA lesions in areas exhibiting dopaminergic cell loss [219], although no assessment of microglia proliferation was made. In our study, we did not find proliferating microglia in either the striatum or the lateral cortex, although from morphological assessment the microglia appeared activated. Resting microglia normally exhibit small cell bodies with subtle branched processes [55,216], however we observed a rather bloated morphology with thick short processes. Henry *et al*., suggested activation of microglia in 6-OHDA lesions as a secondary phenomenon to the neuronal cell death to remove cellular debris [219].
In summary, we excluded microglia as the source of the proliferating cells observed at 4d post-lesion in the striatum and the lateral cortex of 6-OHDA lesioned rats.

SVZ-derived progenitors did not migrate towards the striatum or the lateral cortex
Progenitor cells in the SVZ are capable of proliferation [2]. Several studies report that proliferating progenitor cells from the SVZ have the potential to migrate in case of a brain insult to the injured area and differentiate [124,213,214]. In our 6-OHDA lesion model we observed proliferating cells ubiquitously distributed in the striatum and the lateral cortex, which argues against a migration from the SVZ, in which case a gradient of proliferating cells would be

expected [124]. Furthermore, we often observed cells in pairs or cells actively progressing through mitosis suggesting that at least some resident cells did divide. Nevertheless, we used the migration marker doublecortin (Dcx) [220] to investigate for migrating progenitor cells. The microtubule-associated protein Dcx is required in neuronal migration during development [125] and in the adult CNS its expression remains within the neurogenic niches, where it is transiently expressed in proliferating progenitor cells [220]. As expected, we observed Dcx in the SVZ in both proliferating and non-proliferating cells. Dcx^+ cells in the area of the needle puncture just dorsal of the lateral ventricle. This indicates that progenitor cells indeed migrate to injured areas, although it might be that these Dcx^+ cells also belong to the rostral migratory stream [220]. However, in the striatum or the lateral cortex of 6-OHDA lesioned animals, no Dcx staining was observed. Therefore, we concluded that the proliferating cells following 6-OHDA lesion are derived from resident cells in the respective areas and do not migrate from the SVZ into the areas of dopaminergic cell loss.

NG2 glia comprise a small fraction of the proliferating cells in the striatum

The NG2 glia are a resident cell population in the adult CNS parenchyma with the potential to proliferate both under physiological and pathological conditions [5,56]. These glia cells (5-8 % of the total glia number), that express chondroitin sulphate proteoglycan were initially believed to be merely oligodendrocyte precursors during development and postnatally [5,56]. However, it soon became clear that NG2 cells in the developing CNS not only differentiate into oligodendrocytes but into neurons and astrocytes [5,56]. Due to their persistent and ubiquitous appearance in the adult brain they were recently suggested to be a fifth class of non-neuronal cells in the CNS [56]. The functional aspect of NG2 glia in the physiological and pathological adult CNS are currently investigated by several groups. NG2 glia express functional receptors for e.g. glutamate or GABA and interact with neurons [5,56,221]. Following brain injury, several studies showed that NG2 cells respond to brain injury with hypertrophy, upregulation of chondroitin sulphate proteoglycan and an increase in cell number [56] at the site of injury, which indicates a role for NG2 glia during brain injury [56]. Following cryoinjury [205], needlestick injury [206], mechanical lesions [204], and systemic inflammation models [204] in the cortex, NG2 glia were shown to generate new $GFAP^+$ astrocytes that may belong to the pool of reactive astrocytes. Quantification of the number of $NG2^+$ cells per mm^2 in our study revealed an increase of $NG2^+$ cells in the striatum but not in the lateral cortex following 6-OHDA lesion, indicating proliferation of NG2 cells in the striatum. However, in relation to the total fraction of proliferating cells in the striatum the $NG2^+$ cells comprised only 5 %. We assume that increased proliferation of NG2 glia may depend on the kind of lesion or injury and, that intraventricular 6-OHDA lesions do not induce increased proliferation of NG2 glia in the lateral cortex and only to a small amount in the striatum.

$GFAP^+$ astrocytes proliferate in response to the 6-OHDA lesion

In our study, we found that following 6-OHDA lesions ~86 % of the proliferating cells in the striatum and ~78 % in the lateral cortex were $GFAP^+$, indicating that they are astrocytes. This finding corresponds well with the two studies that also found proliferating cells in the striatum following either 6-OHDA [188] or MPTP [191] lesion. Since we could exclude that progenitor cells from the SVZ migrated towards the striatum and the lateral cortex (see above) we assume that the proliferating $GFAP^+$ cells may be derived from resident cells such as NG2 glia or de-differentiated resident astrocytes. NG2 glia cells, which comprised 5 % of the proliferating cells in the striatum are described to yield $GFAP^+$ progeny [204,205,206,215], although this finding is recently under question [58,222,223]. Nevertheless, in our study we found that a minor fraction of the proliferating $GFAP^+$ cells in the striatum may be derived from NG2 cells. However, the largest part of the proliferating cells must have been derived from a different origin.

De-differentiation of a subpopulation of resident astrocytes following 6-OHDA lesion

In 2008 Buffo *et al.* described that mature resident astrocytes in the cortex have the potential to de-differentiate and regain proliferation capacity in response to a stab wound lesion [58]. We hypothesized that in our study following intraventricular 6-OHDA lesion and hence DA depletion in the striatum and the lateral cortex, a subpopulation of resident mature astrocytes de-differentiated and regained proliferation capacity. Several observations supported this hypothesis.

1) In our 6-OHDA lesion model we observed the appearance of stellated nestin$^+$ cells both in the striatum and the lateral cortex at 4d post-lesion of which nearly 100 % co-stained with GFAP. The progenitor marker nestin is expressed in neuroepithelial cells and radial glia during development [32,50] and is re-induced in reactive astrocytes [40,41]. This change in cytoskeleton in response to brain injuries is often suggested as a step towards a more immature phenotype of the reactive astrocytes, which may somehow help them cope with a changed environment, although the exact function of the upregulation of nestin remains speculative. We showed that following 6-OHDA lesion the nestin$^+$ cells expressed Ki-67, which indicates proliferation. Since we detected more nestin$^+$ cells than proliferating cells per mm^2, we conclude that not all nestin$^+$ cells were proliferative, however, we assume that most proliferating cells were GFAP$^+$/nestin$^+$.

2) We detected a clear increase in stellated vimentin$^+$ cells in the striatum and the lateral cortex 4d post-lesion in our rat model. As expected, immunostainings revealed co-expression of vimentin in GFAP$^+$ and nestin$^+$ cells. Vimentin is another IF protein, which is highly expressed during development in radial glia [50], but is mostly downregulated to a nearly undetectable level in the adult CNS [19].

3) Roughly 83 % of all proliferating cells in the striatum and ~80 % in the lateral cortex were Pax6$^+$. The transcription factor Pax6 is known to be expressed in subsets of radial glia cells and plays a crucial role during development [224]. During development Pax6 controls proliferation through a direct control of cell cycle regulators [126,224], although it needs to be emphasized that Pax6 functions in a highly context dependent manner [224]. In the adult brain, Pax6 remains primarily in the neurogenic niches [224], but it was recently shown to be expressed in astrocytes [126,127,128]. In our study, Pax6$^+$ cells were present in the striatum and the lateral cortex and quantification revealed a significant increase of Pax6$^+$ cells in the striatum and the lateral. Pax6$^+$ cells were further shown to coexpress GFAP, nestin and vimentin. In the lateral cortex, we observed a higher number of Pax6$^+$ cells in 6-OHDA-lesioned animals although we did not detect an increased Pax6 mRNA expression. This may be due to the fact, that we only took cells into account that exhibited a clear nuclear Pax6 expression, although we observed cells that exhibited a faint Pax6 staining in their soma. In the zebrafish, Pax6 is capable of intercellular transfer and may be secreted to the cell surface where it functions as a signalling molecule [225]. If this mechanism also is the same in the rodent, Pax6 protein already present within the cell could translocate to the cell nucleus yielding more Pax6$^+$ cells in our analysis without prior gene transcription.

In summary, the proliferating GFAP$^+$ cells in the striatum and the lateral cortex following 6-OHDA lesion in the adult rat were shown to co-expresse markers such as nestin, vimentin and Pax6, which are all known to be expressed in radial glia cells [50], the precursors of most astrocytes. We suggest that following 6-OHDA lesion a subpopulation of astrocytes in the striatum and the lateral cortex has the capacity to de-differentiate and regain proliferation capacity. This would confirm previous studies that reported de-differentiation of mature astrocytes in the adult mouse cerebral cortex following stab-wound lesion [58] and de-differentiation of Müller glia in the retina of adult mice following intraocular NMDA (N-methyl-D-aspartic acid) injection [226]. Furthermore, *in vitro* studies suggest that purified astrocytes de-differentiate into radial glia like cells following scratch wound assay [129] and cyroinjury [130].

The progeny of the proliferating de-differentiated cells is of astrocytic nature although Karl *et al.* reported the generation of few new neurons in the retina [226]. Recently, the presumably immense regenerative potential of astrocytes was revealed [16,58,227,228,229]. De-differentiated proliferating cortical astrocytes exhibit stem cell potential when taken into cell culture [58,227,229] and postnatal mouse astrocytes *in vitro* generate functional neurons [227] following forced expression of certain transcription factors such as e.g. Pax6 [228,229]. Therefore resident parenchymal astrocytes may represent a source for cell regeneration following brain insults and might even be able to generate neurons given an appropriate environment.

4.6 Observations of tyrosine hydroxylase immunoreactive cells following 6-OHDA lesion

An unexpected observation in our 6-OHDA lesion model concerned the occurrence of bi- and multipolar TH^+ cell somata in the lateral cortex at 4d post-lesion. Since degenerating, swollen dopaminergic axons exhibit a similar morphology as bipolar cell bodies [135], we verified the cellular nature of the TH^+ cells using the nuclear stain DAPI thereby revealing clearly labelled TH^+ cells with a DAPI stained cell nucleus. Closer investigation of TH immunoreactivity in the lateral cortex of sham animals likewise revealed few TH^+ cells, although we detected significantly more TH^+ cells following 6-OHDA lesion. Reports on TH^+ cells outside the classical location of dopaminergic neurons exist for rodents and primates and describe TH^+ cells during development and in the adult brain in areas such as e.g. cortex [131,132,133,134], striatum, globus pallidus, hypothalamus or cerebellum [230]. In the rat, TH^+ cells in the cortex are mainly observed during development and decrease immensely in their number after puberty [133,230], which is suggested to result from a down-regulation of the TH expression to a non detectable level [133]. The presumable reappearance of TH^+ cells in the cortex following 6-OHDA lesion has not been reported yet.
TH^+ cells are found through all cortical layers with a tendency to occur in layer II-III [131,132], which matches with our estimations of the localization of the TH^+ cells. In general it is assumed that these cortical TH^+ cells are neurons [131,132,133]. However, in our study, staining with the neuronal marker MAP-2 did not reveal a clear neuronal identity of the TH^+ cells. MAP-2 stains predominantly dendrites and hence a different neuronal maker such as NeuN needs to be tested in order to reliably determine or exclude a neuronal identity. Nevertheless, we assume a neuronal origin of TH^+ cells based upon morphology and the fact that they did not co-stain with glial marker, but with c-Fos, which is a transcription factor of the immediate early gene family that is often used as a marker of neuronal activity.
Cortical TH^+ neurons exhibit oval or round somata with a length of 10-20 µm across their long axis [131,132,230] and their morphology mainly indicates that they are non-pyramidal cells [131,132,230]. These descriptions match to our observations of the TH^+ cells in the lateral cortex following 6-OHDA lesion. According to literature most cortical TH^+ neurons express the inhibitory neurotransmitter GABA or/and its synthesizing enzyme glutamic acid decarboxylase (Gad), indicating that they are cortical interneurons [131,132,134]. Interneurons constitute around ¼ of the total number of neurons in the mammalian cortex and comprise a heterogeneous group differing in morphology, physiological properties and in the expression of neurotransmitters, peptides and molecules [132]. GABAergic cortical interneurons can be roughly divided into three subgroups containing either parvalbumin, calretinin or somatostatin. In our study we did not detect co-localization of TH with GABA or Gad67, but clearly with calretinin in several cells. This matches to the study conducted by Asmussen *et al.,* where they demonstrated that TH^+ interneurons in the adult rat cortex belong to the calretinin expressing group of cortical interneurons [133].
The appearance of cells expressing the rate-limiting enzyme in the DA synthesis pathways in an area where DA was presumably depleted by 6-OHDA might indicate a compensatory effect for

the loss of DA in our model. According to the literature, cortical TH^+ interneurons express only TH and no other enzymes involved in the synthesis of catecholamines [230]. However, another neuronal cell type that is often observed close by expresses aromatic amino acid decarboxylase (AADC), the enzyme necessary to convert L-DOPA into DA [132,230]. It is suggested that these two cell populations may function in a cooperative synthesis to produce DA [230].
In summary we observed a significant increase of TH^+ cells in the lateral cortex following 6-OHDA lesions. The TH^+ cells coexpressed c-Fos and calretinin, which indicates that they are cortical interneurons. Further studies are required in our 6-OHDA lesion model to reveal the exact phenotype, origin and function of the TH^+ cells, which may suggest a compensatory mechanism for the DA-loss in the lateral cortex.

5. Conclusion

DA affected the proliferation of striatal mouse astrocytes and the expression of the water channel AQP4, or AQP4 M23 *in vitro*. In the DA-depleted striatum in a 6-OHDA lesion model in the rat *in vivo* we also observed changes in astrocyte proliferation and the expression of AQP4 M23 mRNA, thus confirming our assumption that DA affects striatal astrocyte proliferation, probably via modulation of AQP4 expression. These data imply a so far undetermined influence of DA on astrocytes in the adult mammalian striatum and cortex, suggesting that in neurodegenerative diseases that are correlated with perturbations of the dopaminergic transmission such as PD, astrocytes may also be affected. Furthermore, pharmacological modulation of the expression of AQP4 could be used to influence astrocyte proliferation, thus representing a therapeutical tool for treatment of reactive gliosis.

The observed increase in proliferation following 6-OHDA lesion seemed to be due to de-differentiation of resident mature astrocytes that regained proliferation capacity. Taken together with the occurrence of TH^+ cells after the 6-OHDA lesion, these data point to a de-differentiation process followed by a presumable re-programming of cells. This bears new prospects for cell therapy in PD and presumably other neurodegenerative diseases, in which resident astrocytes could be used as an endogenous source for new cells. This implies the necessity to better understand the mechanisms of de-differentiation of astrocytes. It needs to be corroborated that the proliferating cells are derived from resident astrocytes by genetic fate mapping analysis and factors that determine the outcome of the newly generated cells need to be indentified and characterized. Since recent *in vitro* data showed that astrocytes can be reprogrammed by forced expression of certain transcription factors to generate functional neurons, astrocytes might present a valuable tool in designing new approaches to cell therapy and might be able to give rise to neurons which could compensate for the loss of neuronal cells. Therefore, it will also be quite exciting to examine if the observed TH^+ cells might be derived from the de-differentiated astrocytes.

6. Materials and Methods

6.1 Materials

6.1.1 Equipment

Cell culture	
24-well plates, flat bottom, 1.9 cm^2	Corning
96-well plates, flat bottom, 34 mm^2	Greiner Bio-One
Cell culture flask, 75 cm^2	Corning
Cell strainer, 70 µm, nylon	BD Falcon
Culture dishes, 94x16 mm, 58 cm^2	Greiner Bio-One
Glass plates, Ø 12 mm	R. Langenbrinck
Neubauer Counting chamber ´improved´	Bioanalytic GmbH
6-OHDA lesion	
Bone wax	Johnson&Johnson
Dental drill, HM1 007	Meisinger
Hamilton Syringe, 10 µl	Hamilton
Stereotactic device	Stoelting
Surgical tools	Roth
Yarn	Johnson&Johnson
Histology	
Coverslips, 24x32 mm	R. Langenbrinck
Cryostat, M560	Micron
Dako Cytomation Pen	Dako
Microscope slides, SuperFrost R Plus, 75x25 mm	R. Langenbrinck
Microscope slides, 76x25 mm	R. Langenbrinck
Microtome, DSC2	Leica
Steamer, Multi Gourmet	Braun
Zeiss Axioplan2 fluorescent microscope	Zeiss
Zeiss confocal laser scanning microscope 510	Zeiss
Zeiss Imager.M2 Apoptome	Zeiss
Molecular Biology	
Gel documentation, Quantum ST4	Vilber Lourmat
Grinder	IKA
Hyperfilm ECL	Amersham
Potter Elvehjem Tissue Grinder with Teflon Pestle	Sigma
Sonifier, Cell Disruptor BD15	Branson
Spectrometer, GeneQuant 1300	GE Healthcare
Thermal Cycler, DNA 480	Perklin Elmer
Thermal Cycler, MyCyler™	Bio-Rad
Thermomixer, 5436	Eppendorf
Ultra-centrifuge, Optima™	Beckman

6.1.2 Chemicals and Substances

Most chemicals were purchased from Sigma-Aldrich, chemicals listed below were obtained from the following distributors.

5x RT-PCR reaction buffer	Promega
6x Orange DNA Loading Dye	Fermentas
6x DNA Loading Dye	Fermentas

10x CoralLoad PCR buffer	Quiagen
10x Hexanucleotide mix	Roche
10x *Taq* Reaction buffer	Invitrogen
50 mM $MgCl_2$	Invitrogen
Acetic acid	Merck
Aceton	Merck
Acidic Haemalaun according to Mayer	Chroma
Acrylamide, 40 %	Serva
Agarose	Lonza
Ampuwa	Fresenius Kabi
Antibiotic powder, Nebacetin	Sandoz GmbH
Bepanthen eye and nose salve	Bayer Vital
$C_6H_5Na_3O_7$ x 2 H_2O	Merck
Chloral hydrate	Merck
Chloroform	Merck
DAB (diamino-benzidine)	Serva
DePeX	Serva
dNTPs (deoxyribo-nucleotides)	Amersham
DTT (dithiothreitol)	Roth
EDTA (ethylene diamine tetraacetic acid)	Serva
EGTA (ethylene glycol tetraacetic acid)	Serva
Erythrosin	Merck
Ethanol	AppliChem
FCS (fetal calf serum)	Biochrome AG
Fentanyl	Ratiopharm
FluorSave™ Reagent	Calbiochem
FZ (fungizone)	Gibco
GelGreen	Biotium
Glycerol	Serva
Glycine	Roth
HCl, 1N	Merck
Heparin Na 25000	Medac
HEPES	Serva
H_2O_2 (30 %)	Merck
INTERFERin™	Polyplus Transfection
Iodine, Braunol	B.Braun
Isofluran	Abbot GmbH
Isopropanol	AppliChem
KCl	AppliChem, Merck
KH_2PO_4	Fluka, Merck
KH_2PO_4 x $_2H_2O$	Merck
NaCl	Merck, AppliChem
NaCl liquid (0.9 %)	Fresenius Kabi
NaH_2PO_4 x H_2O	Merck
Na_2HPO_4	AppliChem, Merck
Na_2HPO_4 x $2H_2O$	Merck
Narcorene	Merial
NH_4Cl	Merck
Normal goat serum	Dako
Normal donkey serum	Dako

Methanol	VWR
2-Methylbutan	AppliChem
Milk powder, non-fat	Sucofin
$MgCl_2$	Merck
Pefabloc SC-Protease Inhibitor	Roth
PFA (paraformaldehyde)	Merck
Ponceau Red	Chroma
Procain hydrochloride	Merck
P/S (penicilin-streptomycin solution)	Gibco
RNase Exitus-Plus™	AppliChem
RNase free water (DEPC-treated)	Roth
SCH 23390	Tocris
SDS (sodium dodecyl sulphate)	AppliChem
Sucrose	AppliChem
Sulpiride	Tocris
Staurosporine	Tocris
Sytox60	Molecular Probes
Sytox green	Molecular Probes
TEA (tetra-ethyl-ammonium chloride)	Fluka
Tissue Tek® Compound	Sakura
Tris	Roth
Tris, ultra pure	Paesel
Urea	Merck
X-Ray developer	Tetenal
X-Rax fixation	Tetenal
Xylol	Merck

6.1.3 Kits

Annexin V conjugate	Molecular Probes
BCA Protein Assay Kit	Pierce
Biotinylated tyramide, Amplification Kit	Molecular Probes
CyQUANT® NF Cell Proliferation Assay Kit	Molecular Probes
ECL™ Western Blotting Detection Reagents	Amersham
One Step Western Blot Kit	Gene Script Corp.
PeqGOLD RNApure	Peqlab
Vectastain ABC-Kit	Vector Linaris

6.1.4 Enzymes

Deoxyribonuclease I Amplification Kit	Sigma
M-MLV reverse transcriptase	Promega
Taq DNA polymerase	Invitrogen
Trypsin	Gibco

6.1.5 Size standards

Mass Ruler™ Low Range DNA Ladder	Fermentas
O´GeneRuler™ 50 bp DNA Ladder	Fermentas
O'GeneRuler™ 100 bp DNA Ladder	Fermentas
Precision Plus Protein™ Standards, all blue	Bio-Rad

6.1.6 Media

DMEM (Dulbeccos´s modified Eagle´s medium) Gibco
MEM (minimal essential medium) Earle (1x) mod. Biochrome AG

6.1.7 Buffers and Solutions

cell culture
Chloral hydrate solution
NaCl liquid (0.9 %), 9.5 µM chloral hydrate

Dissection buffer, pH 7.4
NaCl liquid (0.9 %), 4 mM KCl, 10 mM HEPES, 12.5 mM glucose, 0.1 % bovine serum albumin

DMEM 10 % FCS
DMEM, 10 % FCS, 5 µl/ml P/S, 1 µl/ml FZ

MEM 10 % FCS / 20 % FCS
MEM Earle (1x) mod., 10 or 20 % FCS, 5 µl/ml P/S, 1 µl/ml FZ

5x PBS/EDTA, pH 7.4
$H_2O_{dist.}$, 13.5 mM KCl, 7.5 mM KH_2PO_4, 0.7 M NaCl, 21 mM Na_2HPO_4 x 2 H_2O, 2.7 mM EDTA
0.1 % Trypsin solution
PBS/EDTA, 0.1 % Trypsin

6-OHDA lesion
6-OHDA-solution
Ampuwa, 0.1 % ascorbic acid, 105 µg/10 µl 6-OHDA hydrochloride

Perfusion solution, pH 7.4
0.125 M phosphate buffer, 2 % PFA

Pre-solution
NaCl liquid (0.9 %), 500 IE/dl Heparin NA 2500, 0.5 g/dl Procain hydrochloride

Histology
Antibody dilution buffer (abdb)
PBS, 5 % normal goat or donkey serum, 0.5 % Triton X-100

Ammonium chloride, 50 mM
PBS, 50 mM NH_4Cl

Blocking solution
PBS II , 0.1 % ovalbumin, 0.5 % fish gelatine

Citrate buffer, 10 mM, pH 6.0
$H_2O_{dist.}$, solution X: 0.1 M $C_6H_8O_7$ x 2 H_2O, solution Y: 0.1 M $C_6H_5Na_3O_7$ x $2H_2O$
500 ml $H_2O_{dist.}$, 9 ml solution X , 41 ml solution Y

Goat serum dilution buffer (GSDB)
PBS, 16 % normal goat serum, 0.3 % Triton X-100/bovine serum albumin, 0.3 M NaCl

PBS, 10 mM, pH 7.4
$H_2O_{dist.}$, 0.12 M NaCl, 20 mM Na_2HPO_4, 3 mM KH_2PO_4, 3 mM KH_2PO_4

PBS^{++}
PBS, 0.3 % Triton X-100

PBS II, pH 7.4
$H_2O_{dist.}$, 137 mM NaCl, 3 mM KCl, 8 mM Na_2HPO_4, 2 mM KH_2PO_4 x $2H_2O$

PFA, 2 % or 4 %
PBS, 2 % or 4 % PFA

Pre-incubation buffer
PBS, 5 % normal goat or donkey serum, 0.5 % Triton X-100, 1 % bovine serum albumin

Pre-incubation buffer for ABC/DAB-staining
$H_2O_{dist.}$, 4 % normal goat serum, 0.25 % Triton X-100

Tris-HCL buffer, 0.1 M, pH 7.5
PBS, 0.2 M tris amino-methan, 0.1 N HCl

Triton X-100/bovine serum albumin
PBS, 3 % Triton X-100, 0.1 % bovine serum albumin

Molecular Biology
10 % ammonium persulfate (APS)
$H_2O_{dist.}$, 10 % APS

10x Electrophorese buffer, pH 8.3
$H_2O_{dist.}$, 25 mM Tris, 190 mM glycine, 0.1 % SDS

Glycine, 100mM, pH 2.5
$H_2O_{dist.}$, 100 mM glycine

6x Laemmli buffer
$H_2O_{dist.}$, 375 mM Trizma Base, 60 % glycerol, 12 % SDS, 0.012 % bromophenol blue, add 10 % β-Mercaptoethanol just before use

PBS-Tween, pH 7.4
$H_2O_{dist.}$, 81 mM Na_2HPO_4, 19 mM NaH_2PO_4 xH_2O, 0.1 M NaCl, 0.1 % Tween 20

Phosphate buffer I according to Sörensen, 0.1 M, pH 7.4
$H_2O_{dist.}$, solution X: 0.2 M Na_2HPO_4 x 2 H_2O, Solution Y: 0.2 M NaH_2PO_4 x H_2O
100 ml $H_2O_{dist.}$, 40.5 ml solution X , 9.5 ml solution Y

10 % SDS, pH 7.2
$H_2O_{dist.}$, 10 % SDS

SDS-PAGE sample buffer, pH 6.8, according to [84]
$H_2O_{dist.}$, 10 mM Trizma Base, 3 % SDS, 6 % glycerol, 0.01 % bromophenol blue, 0.1 M DTT

5 % Skim milk
PBS-Tween, 5 % milk powder, non-fat

Solubilization buffer, pH 8.0, according to [84]
$H_2O_{dist.}$, 20 mM Trizma Base, 5 % SDS, 5 mM EDTA

10x TAE, pH 8.5
$H_2O_{dist.,}$ 0.4 M Trizma-Base, 0.2 M acetic acid, 2 % 0.5 M EDTA, pH 8.0

Tissue homogenization buffer, pH 7.4, according to [231]
0.01 M phosphate buffer, pH 7.4, 1 % SDS, 150 mM NaCl, 5 mM EDTA

Tissue homogenization buffer, pH 7.0, according to [84]
$H_2O_{dist.,}$ 7.5 mM sodium phosphate, 0.25 M sucrose, 5 mM EDTA, 5 mM EGTA

Transfer buffer, pH 8.3**,** (Towbin buffer with 1 % SDS)
$H_2O_{dist.}$, 25 mM Trizma Base, 192 glycine, 1 % SDS, 20 % methanol

Tris-HCl, 1.5 M, pH 8.8
$H_2O_{dist.}$, 1.5 M Trizma Base

Tris-HCl, 0.5 M, pH 6.8
$H_2O_{dist.}$, 0.5 M Trizma Base

6.1.8 Master Mixes

Table 2 Master Mix for cDNA synthesis

compounds	amount
RNase free water	2.5 µl
5x RT-PCR reaction buffer	5 µl
dNTPs (10 pmole/µl)	1 µl
Hexanucleotides (10 pmole/µl)	1.5 µl
M-MLV reverse transcriptase	1 µl

Table 3 Master Mix for RT-PCR

compounds	amount
RNase free water	17.6 µl
10x *Taq* Reaction buffer or 10 x CoralLoad PCR buffer	2.5 µl
Primer forward (10 pmole/µl)	0.5 µl
Primer reverse (10 pmole/µl)	0.5 µl
$MgCl_2$ (50 mM)	0.75 µl
dNTPs (10 pmole/µl)	0.5 µl
Taq DNA polymerase	0.15 µl

6.1.9 Gels

Table 4 SDS-PAGE Gels

compounds stacking gel	5 %	compounds running gel	7 %	12 %	15 %
H_2O	6.15 ml	H_2O	5.65 ml	4.27 ml	3.65 ml
2 M Urea*	1.2 g	4 M Urea*	-	2.4 g	-
0.5 M Tris HCl pH 6.8	2.5 ml	1.5 M Tris HCl pH 8.8	2.5 ml	2.5 ml	2.5 ml
10 % SDS	100 µl	10 % SDS	100 µl	100 µl	100 µl
40 % Acrylamide	1.25 ml	40 % Acrylamide	1.75 ml	3.15 ml	3.75 ml
10 % APS	30 µl	10 % APS	30 µl	30 µl	30 µl
TEMED	15 µl	TEMED	15 µl	15 µl	15 µl

* addition of urea is required in AQP4 Western blotting

Table 5 Agarose Gels

compounds	small gel	middle gel	big gel
TAE buffer 1x	100 ml	200 ml	300 ml
Agarose	1.5 g	3 g	4.5 g
GelGreen	8 µl	16 µl	24 µl

6.1.10 Antibodies

Antibodies used in immunochemistry (Tab. 6) were tested in control tissues for specificity and appropriate dilution. To exclude unspecific staining of the secondary antibodies (Tab. 8), controls were made applying only secondary antibodies. Antibodies used in Western Blot (WB) (Tab. 6) were tested in control tissues or cell lines known to express the respective protein.

Table 6 Primary antibodies for immunochemistry and Western blotting

Primary antibody	host		dilution (immuno)	dilution (WB)	Company
anti-AQP4	rabbit	polyclonal	1:500	1:500	Chemicon
anti-AQP4 (H-80)	rabbit	polyclonal	1:200	1:400	Santa Cruz
c-Fos	rabbit	polyclonal	1:500		Santa Cruz
anti-calbindin	mouse	monoclonal	1:200		SWant
anti-calretinin	rabbit	polyclonal	1:2000		Millipore
anti-Dcx	goat	polyclonal	1:500		Santa Cruz
anti-GABA	rabbit	polyclonal	1:100		Chemicon
anti-Gad67	mouse	monoclonal	1:1000		Chemicon
anti-GAPDH				1:1000	Santa Cruz
anti-GFAP	rabbit	polyclonal	1:400		Dako
anti-GFAP	mouse	monoclonal	1:400	1:1000	Millipore
anti-Iba-1	rabbit	polyclonal	1:1000		Wako
anti-Ki-67	mouse	monoclonal	1:50		Dako
anti-MAP2	mouse	monoclonal	1:500		Sigma
anti-nestin	mouse	monoclonal	1:100	1:200	Millipore
anti-NG2	rabbit	polyclonal	1:500		Millipore
anti-parvalbumin	mouse	monoclonal	1:1000		Sigma
anti-Pax6	rabbit	polyclonal	1:800		MBL
anti-TH	mouse	monoclonal	1:1000		Immunostar
anti-TH	rabbit	polyclonal	1:1000	1:1000	Abcam
anti-somatostatin	rabbit	polyclonal	1:1000		Immunostar
anti-vimentin	mouse	monoclonal	1:100	1:1000	Santa Cruz

Table 7 Fab conjugated and unconjugated antibodies

Antibody	host		dilution (immuno)	Company
anti-rabbit IgG Fab coupled to Cy3 (580nm)	goat	polyclonal	1:200	Dianova
anti-rabbit IgG Fab coupled to Cy2 (520nm)	goat	polyclonal	1:100	Dianova
anti-rabbit IgG Fab unconjugated	goat	polyclonal	1:65	Dianova
anti-mouse IgG Fab unconjugated	rabbit	polyclonal	20 µg/ml	Dianova

Table 8 Secondary antibodies for immunochemistry and Western Blotting

Secondary antibodies	host	dilution (immuno)	dilution (WB)	Company
anti-rabbit Alexa Fluor 488 nm	goat	1:400		Molecular Probes
anti-rabbit Alexa Fluor 546 nm	goat	1:400		Molecular Probes
anti-mouse Alexa Fluor 488 nm	goat	1:400		Molecular Probes
anti-mouse Alexa Fluor 546 nm	goat	1:400		Molecular Probes
anti-goat Alexa Fluor 488 nm	donkey	1:400		Molecular Probes
anti-mouse Alexa Fluor 555 nm	donkey	1:400		Molecular Probes
anti-mouse HRP conjugate			1:1000	Amersham
anti-rabbit HRP conjugate			1:1000	Amersham

6.1.11 Primer

Primer sequences (Tab. 9) were either taken from the stated reference or were designed using the open source program Primer3 [232]. Primers were designed to be specific to the respective mRNA sequence of the gene of interest. mRNA sequences were obtained from the database of the National Center for Biotechnology Information (NCBI) (http://www.ncbi.nlm.nih.gov/). Primers were designed with a length of 18-30 nucleotides, a G/C content between 40-60 % and a melting temperature that allowed annealing between 55-65 °C. Primer3 automatically checks for internal secondary structures and self-complementarity. The size of the end-products was defined between 160 and 500 bp. The NCBI blast program was used to check for sequence homology with other mRNAs. Primer sequences were purchased either from Eurofins MWG Operon, Germany or from Biomers, Germany.

6.1.12 si-RNA

19 or 21 nucleotide long RNA duplexes, identical to a sequence of the human or mouse AQP4 RNA, respectively were chemically synthesized by Eurofins MWG Operon, Germany.

AQP4 human si-RNA: 5′ - CGG ACU GAU GUC ACU GGC U – 3′
human si-RNA control: 5′ - CCC GAC AGU UCC AUG UAU A – 3′
AQP4 mouse si-RNA: 5′ - UCA AUU AUA CUG GAG CCA GUU – 3′ [159]
mouse si-RNA control made of AQP4 siRNA scrambled sequences [159]

Table 9 Primer pairs used in RT-PCR

primer	used in	5´-3´	T (°C)	PCR cycles	product	reference
β-actin	rat	TGT CAC CAA CTG GGA CGA TA TCT CAG CTG TGG TGG TGA AG	60	25	392	
β-actin	human	TGC CAT CCT AAA AGC CAC C ACC AAA AGC CTT CAT ACA TCT C	59	25	227	
AQP4	human	GGA ATT TCT GGC CAT GCT TA AGA CTT GGC GAT GCT GAT CT	59	32	225	
AQP4 M1	mouse	ATG AGT GAC GGA GCT GCA GCG A ACC ATG GTA GCA ATG CTG AGT CC	62	34	253	
AQP4 M1	mouse	CTC CCA GTG TAC TGG AGC CCG TGG TGA CTC CCA ATC CTC CAA C	62	34	510	[146]
AQP4 M23	mouse	GGA AGG CTA GGT TGG TGA CTT CTG ATG TGG CCA AAG CAC TGC AC	62	34	288	
AQP4 M23	mouse	GGA AGG CTA GGT TGG TGA CTT C TGG TGA CTC CCA ATC CTC CA C	62	34	460	[146]
AQP4 F16	rat	CCT GCA GCA GAG AGA GCA TC (+16) CCA ATT GCT AAA GCA ACG GA (+530)	62	34	535	[86]
AQP4 M1	rat	AGG GAA GGC ATG AGT GAC GG (M1_pr) CCA ATT GCT AAA GCA ACG GA (+530)	62	28	590	[86]
AQP4 M23	rat	CCC AGA AGA CAG CAC CTG TG (yAQP4_41) CCA ATT GCT AAA GCA ACG GA (+530)	62	34	615	[86]
AQP4 z	rat	AAC CGC CCT GTG TCT ATA GT (zAQP4_10) CCA ATT GCT AAA GCA ACG GA (+530)	62	34	600	[86]
GAPDH	rat	AGA CAG CCG CAT CTT CTT GT TAC TCA GCA CCA GCA TCA C	60	25	323	
GFAP	rat	TTG TTT GCT AGG CCC AAT TC CCT CGG GAT CTT TTC CTT TC	58	25	356	
GFAP	mouse	CAC GAA CGA GTC CCT AGA GC ATG GTG ATG CGG TTT CTT C	60	32	234	
HPRT	rat	GCT TTT CCC GCG AGC CGA CCG CT AGG GCC ACA ATG TGA TGG CCT C	60	25	222	
HPRT	mouse	GCT GGT GAA AAG GAC CTC T GCA GGT GTT CTA GTC CTG TG	60	28	249	
nestin	rat/mouse	CCA GAG CTG GAC TGG AAC TC ACC TGC CTC TTT TGG TTC CT	61	30	161	
NG2	rat	AGA CCT AGA GGC AGG CAA CA GGT CAG GTC CTC CAC TGT GT	58	30	424	
Pax6	rat/mouse	AAC AAC CTG CCT ATG CAA CC ACT TGG ACG GGA ACT GAC AC	58	30	206	
TH	rat	GCT ACC GAG AGG ACA GCA TC GCA CCA TAA GCC TTC AGC TC	61	30	382	
vimentin	rat/mouse	ATG CTT CTC TGG CAC GTC TT CAC CTG TCT CCG GTA TTC GT	60	25	335	

6.1.13 Animals

Pregnant Balb/c mice were purchased from Harlan-Winkelmann GmbH, Germany and were kept in an in-house animal facility until parturition. Adult Sprague-Dawley rats (n = 74) were purchased from Charles River, Germany. The animals were kept at 20-22°C, in 50-60 % air humidity, in a standard dark-light rhythm. Animal housing was in standard cages, gritted with

sawdust, where the animals had access to standard rodent fodder and water *ad libitum*. All experiments were carried out in accordance with the European Communities Council Directive (86/608/EEC) regarding the care and use of animals for experimental procedures and were approved by the Regierunspräsidium Tübingen (ZP2/09). Adequate efforts were made to minimize discomfort and pain of the animals.

6.1.14 Cell Lines

The human pancreatic cancer cell lines BxPC3, MIA PaCa-2 and PANC1 as well as human embryonic kidney cells (HEK) stably transfected with the water channel aquaporin 4 were kindly provided by Prof. Grissmer (Dep. of Applied Physiology, Ulm University, Germany).

6.1.15 Software

The following softwares have been used in the process of data acquisition, image processing, data analysis and statistical analysis: Adobe Photoshop, Microsoft Office Excel 2003, ImageJ [233], Quantum Capt ST4 (Vilber Lourmat), SigmaStat, Zeiss AxioVision LE 4.8.1, Zeiss LSM Image Brower 3.2.0.07.

6.2 Methods

Cell Culture

6.2.1 Primary astrocyte cultures

Newly born Balb/c mice were taken to establish primary striatal astrocyte cell cultures at postnatal day (P) one to four. While the mother mouse was killed with an overdose of chloral hydrate (ip), the pups were decapitated and the striatum was excised and transferred to chilled dissection buffer. Tissues from at least five animals were used to establish one cell culture line. The tissues were dissociated enzymatically for 15 min at RT in a 0.1 % trypsin-solution until the dissociation was stopped with the same volume of pre-warmed MEM 20 % FCS. The tissues were further dissociated mechanically with a 10- and 5 ml pipette and passed through a cell-strainer. The obtained cell solution was centrifuged at 1400 rpm for four minutes at 21°C and the pellet was resuspended in 10 ml prewarmed MEM 20 % FCS. The cells were seeded into a poly-DL-ornithine coated culture dish (58 cm^2) and incubated at 37°C in 5 % CO_2 in an air ventilated humidified incubator. The medium was changed daily upon reaching confluency, then the cells were split at a ratio of 1:3 (first passage) into poly-DL-ornithine coated culture dishes (58 cm^2) in MEM 10 % FCS. Thereafter the medium was changed every second day and after reaching confluency the cells were split again (second passage) and used to setup experiments.

6.2.2 Immortalized human cell lines

HEK cells and the human pancreatic cancer cell lines BxPC3, MIA PaCa-2 and PANC1 were cultured in cell culture flasks (75 cm^2) in DMEM 10 % at 37°C in 5 % CO_2 in an air-ventilated humidified incubator. The medium was changed twice a week upon the cells reached confluency and were used to setup experiments. For continuous culturing cells were split at a ratio of 1:30 (BxPC3) or 1:20 (HEK, MIA PaCa-2, PANC1) in new cell culture flasks or frozen for future experiments [234].

6.2.3 Coating

Culture dishes and plates used in experiments of primary astrocyte cultures were coated with 0.1 mg/ml poly-DL-ornithine in Ampuwa. The solution was added to the dishes/plates to completely cover the growth area. Following 60 min incubation at RT, the solution was removed, the dishes/plates were washed twice with Ampuwa and allowed to air-dry.

6.2.4 Changing the medium

The old medium was aspirated and the cells were washed once with PBS/EDTA. Then prewarmed fresh medium was added to the cells and they were incubated again.

6.2.5 Splitting

Once cells reached confluency, the medium was aspirated and the cells were washed once with PBS/EDTA. To detach the cells, they were incubated with 0.1 % trypsin solution for several minutes at RT. BxPC3 cells require an incubation time of at least 10 min at 37°C. The detached cells were transferred to prewarmed medium and were centrifuged at 1400 rpm for four minutes at 21°C. The pellet was resuspended in 1 ml medium and the cells were either plated at the appropriate ratio for further culturing or they were counted and used to setup experiments. To be counted, cells were resuspended in 4 ml medium. 20 µl of this solution was mixed with 160 µl medium and 20 µl trypan blue solution and transferrred into a Neubauer counting chamber. Viable cells in the four big squares in the upper and lower compartment of the chamber were counted and the determined average number of cells per square was used to calculate the total amount of medium the cells needed to be diluted with to obtain the desired number of cells/well after plating:

$$\frac{(\text{cell number [cells]} * 100\,000) * \text{well volume [ml/well]}}{\text{density [cells/well]}}$$

The 4 ml cell solution was made up with medium to the determined final volume and mixed well before the cells were seeded and incubated at 37°C.

6.2.6 Treatment of cells

One day after seeding the cells into the appropriate plates or dishes the respective treatment was initiated. Treatments occurred daily and lasted for 72h unless stated otherwise. Cells were treated with 100 µM dopamine (DA) complemented with 1 µM L-ascorbic acid and 1 mM glutathione to slow down oxidation of DA in the medium [140] and to protect against DA-induced cytotoxcity [113,141], respectively. To reveal the DA receptor family mediating the observed DA-induced effects, cells were treated simultaneously with 100 µM DA and a receptor antagonist. D_1-like receptors were blocked by 1 µM SCH 23390 and D_2-like receptors by 1 µM sulpiride. Furthermore, cells were treated simultaneously with 100 µM DA and with 1 µM of the α_2-adrenergic receptor antagonist yohimbine. Proliferation was stimulated by treating cells with 10 µg/ml bFGF. Pharmacological blocking of the water channel AQP4 was performed using 10-100 µM TEA. The K^+-channel blocker TEA [164,165] was shown to reversibly block AQP4 already at minor concentrations, which showed no effect on K^+-channels [122]. To induce apoptosis, cells were incubated with 300 nM staurosporine, a microbial alcaloid antibiotic, for 24h. In all experiments controls were incubated in normal medium. Following the treatment, cells were assessed by histological or molecular methods.

6.2.7 AQP4 knock-down using siRNAs

One day after the cells were seeded into the appropriate plates or dishes for the experiment, the transfection of AQP4 siRNA was performed using INTERFERin™ according to the manufacturer´s instructions. In brief, cells were transfected with either 1 nM or 5 nM AQP4 siRNA for 72h. For control purpose the cells were treated with serum-free medium only (C_0), transfection reagent only (C_1) and with transfection reagent plus scrambled control RNA (C_2). Specific silencing was validated by RT-PCR and Western blot analysis. Following the 72h treatment, cells were assessed by histological or molecular methods.

6.2.8 Proliferation Assay

Primary striatal astrocytes were cultured in 96-well plates at a density of 1250, 2500, 5000 and 10 000 cells/well. Immortalized human cells were plated in uncoated 96-well plates at a density of 600 cells/well. Following cell treatment proliferation was measured using the CyQUANT® Cell Proliferation Assay Kit according to manufacturer´s instructions. The bacteriophage λ DNA, provided with the kit was used to create a standard curve to calibrate the assay for future experiments.

6.2.9 Apoptosis Assay

Cells were seeded at a density of 50 000 cells/well in 24-well plates. Following cell treatment apoptotic cells were counted using the annexin V conjugate assay according to manufacturer´s instructions. Deviating from the instructions only 2.5 µl of the annexin V conjugate was added to each 100 µl cell suspension and the incubation time was decreased to 10 min at RT. The number of annexin-positive cells was analyzed using a fluorescent-activated cell sorting scan flow cytometer (FACS) and expressed as the number of cells shifted after fluorescence labeling from the polygonal gate R1 to the polygonal gate R2. To distinguish necrotic cells propidium iodide was used as a marker of dead cells and the polygonal gate R3 was defined for this population of cells.

6-OHDA lesions

6.2.10 Stereotactic 6-OHDA lesion

Experiments were performed on adult Sprague-Dawley rats weighing 240-310 g. Twenty minutes before surgery, the rats received 30 mg nortryptilin/kg bodyweight by ip injection, a noradrenergic uptake inhibitor to prevent the loss of noradrenergic neurons. Rats were initially anesthetized with 2 % isoflurane and the head was placed in a stereotactic device. For continuous isoflurane inhalation anesthesia (1.5 %) a mask was placed above the animals´ nose. To prevent the eyes from drying out, they were covered with eye salve and to maintain the body temperature of the animal, a heating pad was placed underneath it. The coordinates for the bilateral intraventricular 6-OHDA lesion were AP: -0.7; L: +/- 1.3 and DV: -3.6 according to [235]. A hole was carefully drilled into the skull at the appropriate position using a dental drill. Injection of a single dose of either 105 µg 6-OHDA dissolved in 10 µl 0.1 % ascorbic acid solution into the lateral ventricle was made using a Hamilton syringe at a rate of 2.5 µl/min. After injection the needle was kept in the lateral ventricle for several minutes to prevent diffusion of 6-OHDA into the brain tissue, before it was slowly withdrawn. The same procedure was performed for the other lateral ventricle. Sham-operated animals received only a single dose of 10 µl 0.1 % ascorbic solution into the lateral ventricles. After surgery the rats received 5 µg fentanyl/kg bodyweight by ip ijection to prevent post-operative pain. Keeping in mind that bilateral 6-OHDA lesions can lead to apahgia and adipsia [181,236], the animals were strictly observed for weight loss over the following days. This monitoring revealed that 6-OHDA lesioned animals exhibited, to a certain degree, a decreased food intake and drinking behaviour. If necessary, pap was carefully given manually using a pipette.

The animals were divided into the following experimental groups: immunohistochemistry (n=10), PCR (n=32) (Tab. 10) and WB (n=32) (Tab. 10). Immunohistochemistry was performed 4d post-lesion only, while PCR and WB were performed at 1d, 4d, 7d and 24d post-lesion.

Table 10 Number of animals (n) per investigated group in molecular biology

	1d		4d		7d		24d	
n =	**sham**	**6-OHDA**	**sham**	**6-OHDA**	**sham**	**6-OHDA**	**sham**	**6-OHDA**
PCR	4	4	2	4	3	4	3	4
WB	4	3	3	4	3	3	3	4

Half of the animals in each group received 6-OHDA lesions, while the other half received sham-operations. 9 animals died in total, 5 animals during the operation, mostly short times after anesthesia and 4 animals in the first two days following the operation, resulting in often only 3 animals per investigated group (Tab. 10). At first glance, a total of three animals seems to be very low, possibly limiting the validity of our results. However, due to our animal welfare policies we did not pursue to investigate more animals.

6.2.11 Tissue preparation for immunohistochemistry

4d post-lesion the animals were terminally anesthetized by ip administration of 65 mg narcorene solution/kg bodyweight. The animals were transcardially perfused with pre-solution for five minutes followed by 250 ml of the perfusion solution. The brains were removed and post-fixed in the perfusion solution at 4°C for two hours and subsequently immersed for two hours in PBS at 4°C. For cryosectioning, brains were cryoprotected in 30 % sucrose in PBS over night and embedded and frozen in Tissue Tek® compound. Coronal sections of the striatum at the level of the comissura anterior (Bregma – 0.92 up to 1.0) were created using a cryostat set at 20 µm and were transferred onto Superfrost microscope slides. One brain was used for paraffin sections, which were prepared at the Institute of neuropathology (University of Tübingen, Germany). Coronal sections of the striatum were made using a microtome set at 6 µm and were transferred onto a microscope slides.

6.2.12 Tissue preparation for PCR and WB

1d, 4d, 7d and 24d post-lesion animals were anesthetized using CO_2 and decapitated with a guillotine. The brains were removed, placed onto an ice-cold metal plate and the following sections of the brain were removed (Fig. 28) and placed on ice: the cerebellum, the striatum, the lateral cortex and the brain stem. For control purposes, tissue samples were also taken from liver, kidney and muscle. Tissues for WB were placed in a 2 ml Eppendorf tube and quickly frozen in liquid N_2. Tissues for PCR were placed in 2 ml Eppendorf tubes containing 1 ml PeqGOLD RNA pure and stored on ice.

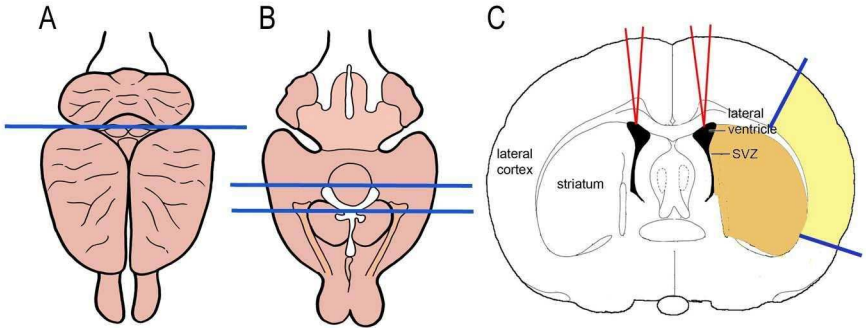

Figure 28 Schematic overviews of the adult rat brain indicating the cutting pattern. **A** Dorsal view of the adult rat brain. The blue line indicates the first cut to remove the cerebellum and brain stem. **B** Ventral view of the adult rat brain. The two blue lines indicate the incisions that were made to obtain the desired section of the brain. **C** Coronal view of the brain section removed in **B**, the blue lines indicate the incisions to remove the desired cortical (yellow) and striatal parts (orange). The red lines indicate the injection puncture.

Histology

6.2.13 Hematoxylin and Eosin (HE) staining

To get a rough overview of the morphology of the cells, they were stained with HE. Hematoxylin solutions stain cell nuclei purple, while eosin stains the cytoplasm pink. Cells were seeded at a density of at least 20 000 cells/well on glass cover slips (Ø 12 mm) in 24-well plates The cells were washed twice with ice-cold PBS and fixed for 30 min in 4 % paraformaldehyde. After washing with Ampuwa, the fixed cells were covered with acidic haemalaun solution

according to Mayer for 15 min at RT and subsequently rinsed with tap water. The cells were washed with Ampuwa and covered with 0.1 % eosin for 10 min at RT before they were dehydrated in an ascending alcohol series (70 %, 80 %, 90 %, 96 %, 99 %, 99 %) and deparaffinized twice for 5 min in xylol. The glass cover slips were mounted in DePeX on microscope slides and stored at RT. The HE staining was investigated using a Zeiss Axioplan2 microscope.

6.2.14 ABC/DAB staining with tyramide signal amplification

Avidin-biotin peroxidase complex (ABC) detection by diaminobenzidin (DAB) was performed on frozen rat brain sections using the Vectastain ABC-kit. To enhance the signal, the biotinylated tyramide amplification kit was used in addition. The sections were air dried and encircled with a DAKO cytomation pen. Following 10 min incubation in PBS, the sections were incubated for 90 min in pre-incubation buffer for ABC/DAB-staining before the primary antibody was applied overnight at 4°C. A washing step consisting of a quick rinse with Ampuwa followed by three 15 min PBS^{++} washes, was performed before the sections were incubated with the biotinylated secondary antibody for 1h at RT. The sections were washed as described previously and incubated for 30 min at RT with the ABC reagent, prepared according to manufacturer´s instructions, followed by another washing step. To amplify the signal, the sections were incubated for 15 min at RT with biotinylated tyramid, prepared according to manufacturer´s instructions, washed again before incubating for 40 min at RT with the ABC reagent. The sections were washed twice in PBS^{++} and once in PBS for 10 min and the antibody was visualized with 0.3 mg/ml DAB in PBS supplemented with 5 µl/ml H_2O_2. Following the visualization process, the sections were washed three times for 5 min in PBS, processed in an ascending alcohol series with xylol and mounted in DePeX. The staining was investigated using a Zeiss Axioplan2 microscope.

6.2.15 Immunocytochemistry on primary astrocyte cultures

For immunocytochemistry primary striatal astrocytes were seeded on glass cover slips (Ø 12 mm) in 24-well plates. The cells were washed briefly in PBS and fixed for 20 min in 4 % PFA. Subsequently the cells were washed twice for 10 min in PBS and briefly in Ampuwa, before being quenched for 15 min in ammonium chloride. To permeabilize the cells, they were incubated for 5 min in Triton X-100/BSA. To prevent antibodies to bind non-specifically the cells were incubated for 30 min in GSDB, before the primary antibody diluted in GSDB was added and incubated overnight at 4°C. The cells were washed three times for 5 min, respectively in Triton X-100/BSA and incubated for 90 min at RT with the secondary antibody diluted in GSDB. After an additional wash with Triton X-100/BSA the cell nuclei were stained for 10 min with DAPI. The cells were washed twice for 10 min in Ampuwa and the glass cover slips were mounted onto microscope slides in FluorSave™ reagent.

For GFAP/AQP4 double staining a modified protocol was used due to the fact that we first did not possess a monoclonal GFAP antibody and hence had to work with two polyclonal antibodies derived from rabbit. In the modified protocol all steps up to the overnight incubation with the primary antibody (AQP4) were identical to the above described immunocytochemistry protocol. Following the overnight incubation of the first antibody the cells were washed three times for 5 min in PBS and incubated for 1h at RT with anti-rabbit IgG goat Fab coupled to Cy3 diluted in GSDB. The cells were washed in PBS and incubated for 1h at 37°C with anti-rabbit IgG goat Fab unconjugated diluted in GSDB, to completely saturate the binding sites of the first primary antibody. In a next step, cells were washed again, incubated with the second polyclonal primary antibody (GFAP) for 2h at 37°C , before being washed again in PBS and incubated with anti-rabbit IgG goat Fab coupled to Cy2 for 1h at RT. Following a last washing step in PBS the cell nuclei were stained with DAPI as described above and the glass cover slips were mounted onto

microscope slides in FluorSave™ reagent. Fluorescence was detected using a Zeiss Axioplan2 fluorescent microscope.

6.2.16 Immunocyotchemistry on immortalized cancer cells

For immunocytochemistry immortalized cells were seeded at a density of 20 000 cells/well on glass cover slips (Ø 12 mm) in 24-well plates. The cells were washed shortly in PBS II and were fixed in an ice-cold methanol/acetone solution (1:1) for 10 min at – 18°C. The solution was removed and the cells were allowed to air-dry for at least 15 min. The cells were washed for 5 min in PBS II and incubated for 20 min in PBS Tween 20, followed by 20 min in ammonium chloride. Following three 10 min washes in PBS II, the cells were incubated for 30 min with 0.3 % H_2O_2 in PBS II to block for endogenous peroxidases, washed again in PBS II and incubated for 30 min in blocking solution before the cells were incubated overnight at 4°C with primary antibody in blocking solution. The next day, cells were washed as described in PBS II as described previously, incubated with the secondary antibody in blocking solution for 90 min at RT and washed again. To stain the cell nuclei, the cells were incubated with DAPI for 10 min. The cells were washed twice for 10 min in Ampuwa and the glass cover slips were mounted onto microscope slides in FluorSAVE™ reagent. Fluorescence was detected using a Zeiss Imager.M2 Apoptome.

6.2.17 Immunohistochemistry on frozen sections

Frozen sections were post-fixed in an ice-cold chloroform-acetone solution (1:1) for 5 min at -18°C, air-dried in RT, encircled with a DAKO cytomation pen and washed in PBS for 5 min. The sections were incubated in pre-incubation buffer for 30 min at RT, before the primary antibody diluted in abdb was added and incubated overnight at 4°C. The next day sections were washed three times with PBS for 5 min, and incubated with the appropriate secondary antibody diluted in abdb for 90 min at RT. Subsequently the sections were washed in PBS and if a cell nucleus staining was required the sections were incubated for 15 min at RT in either Syto60 (1: 10 000 in 0.01 M Tris-HCl buffer, pH 7.5), Sytox green (1:5000 in PBS) or DAPI (36 µM in PBS). The sections were washed twice in Ampuwa for 10 min and were mounted in FluorSAVE™ reagent. Fluorescence was detected using a Zeiss confocal laser scaning microscope 510 (LSM).

6.2.18 Modifications of the immunohistochemistry protocol

For double stainings (monoclonal/polyclonal) half the concentration of antibodies was used and the antibodies were applied simultaneously. For some antibodies or combinations of antibodies modifications to the above described protocol were made to obtain a signal.

The Ki-67 and Pax6 antibodies required heat mediated antigen retrieval. Therefore, frozen sections were post-fixed in an ice-cold chloroform-acetone solution (1:1) for 5 min at -18°C and were allowed to air-dry at RT for at least 60 min. Citrate buffer was pre-heated in a Braun FS20 Multigourmet steamer for 20 min and the air-dried sections were placed into citrate buffer in the steamer for 5 min. The sections were washed three times for 5 min at RT in PBS and starting with incubation in the pre-incubation buffer the above described protocol was followed.

For double stainings with two monoclonal antibodies of the same species a modified protocol was used. In this modified protocol all steps up to the overnight incubation with the first primary antibody were identical to the above described immunohistochemistry protocol. Following the overnight incubation the sections were washed three times for 5 min in PBS and incubated for 1h at 37°C with anti-mouse IgG rabbit Fab unconjuated diluted in abdb, which masked the first primary monoclonal antibody as a polyclonal antibody. The sections were washed with PBS as described above and incubated for 90 min at RT with a secondary antibody appropriate for a polyclonal primary antibody. After a washing step with PBS, the second primary monoclonal

antibody diluted in abdb was added for 2h at 37°C, before being washed again with PBS and incubation with the appropriate secondary antibody for 90 at RT. The sections were washed again and cell nuclei were stained as described in the immunohistochemistry protocol above.
The above described protocol did not work for antibodies that required heat mediated antigen retrieval. In the case of the two monoclonal mouse antibodies Ki-67 and nestin co-staining was performed with the same secondary antibody. Ki-67 expression is restricted to the nucleus, while nestin stains the cytoskeletal intermediate filament network in the cytoplasm. This spatial difference allowed the discrimination between the two stainings.

Molecular Biology

6.2.19 RNA isolation
Primary striatal astrocytes were seeded at a density of 50 000 cells/well, the immortalized cell lines at a density of 20 000 cells/well in 24-well plates. Following treatment, the cells were scraped into PeqGOLD RNAPure™ and transferred into 2 ml Eppendorf tubes. Brain tissue was obtained as described in 2.12 and resuspended with PeqGOLD RNAPure™ in 2 ml Eppendorf tubes, respecitvely and homogenized using a potter. Total RNA was isolated according to manufacturer´s instructions. The obtained pellet was suspended in RNase free water and completely solved by incubation at 60°C for 10 min. RNA concentration and purity was determined by measuring the absorbance at 260 nm and 280 nm, respectively using a spectrophotometer.

6.2.20 DNase digestion and cDNA synthesis
1 µg of RNA was used for DNase digestion using the Deoxyribonuclease I amplification kit according to manufacturer´s instructions before being reverse transcribed to cDNA.
For reverse transcription the sample was adjusted to a volume of 14 µl with RNase free water, denatured for 5 min at 95°C and placed immediately on ice. 11 µl of RT MM was added to each tube before incubating at 37°C for 60 min. To inactivate the enzyme, the tubes were incubated at 95°C for 10 min.

6.2.21 RT-PCR
For conventional RT-PCR 1.5 µl cDNA was mixed with 23.5 µl PCR MM. Water was used as non template control in each run to check for possible DNA contamination. If the RT-PCR was performed with the thermal cycler DNA 480, one drop of mineral oil was added to the top of the samples. Conditions for the thermal cycler DNA 481 were as followed: initial denaturation at 95°C for 5 min, initial annealing at 62°C for 1 min and initial elongation at 72°C for 2 min (1x), denaturation at 95°C for 1 min, annealing according to table x for 1 min, elongation at 72°C for 2 min (PCR cylces see table x) and a final elongation at 72°C for 7 min. Conditions for the Thermal Cycler, MyCyler™ were as followed: initial denaturation at 94°C for 5 min, denaturation at 95°C for 30 sec, annealing according to table x for 30 sec, elongation 72°C for 30 sec (PCR cylces see table x) and a final elongation at 72°C for 7 min. The amplified RT-PCR products were visualized by GelGreen stained agarose gel electrophoresis and the size was estimated using a Mass Ruler.
The gels were scanned and evaluated using the QuantumCapt Software from Vilber Lourmat. Semi-quantitative relative analysis of the target genes was performed by determination of the ratios of the respective target gene and the internal standard.

6.2.22 Protein extraction
Primary striatal astrocytes were seeded in 24-well plates at a density of 50 000 cells/well, the immortalized cell lines at a density of 20 000 cells/well. Following treatment, the cells were

washed twice with ice-cold PBS and membrane proteins were extracted according to Neely *et* al., 1999. In brief, cells were scraped into homogenization buffer and centrifuged to yield the post-nuclear supernatant, which was then centrifuged in a Beckman ultra-centrifuge to obtain the crude membrane fraction in the pellet. The pellet was solubilised in solubilisation buffer and protein concentration was determined using a BCA Protein assay kit according to manufacturer´s instructions.
Isolated brain tissue was obtained as described in 6.2.12 and protein was extracted according to Sorbo *et al.,* [231]. The tissue was thoroughly homogenized in 500 µl ice-cold tissue homogenization buffer supplemented with Pefabloc SC protease inhibitor, using 4 strokes of a sonifier. Homogenates were centrifuged for 30 min at 12 000 rpm at 4°C and the supernatant was transferred into a new tube. Protein concentration was determined using a BCA Protein assay kit according to manufacturer´s instructions.

6.2.23 SDS – polyacrylamid gel electrophoresis (SDS-PAGE)
Cell culture samples underwent a methanol-chloroform precipitation according to Wessel and Flüge, 1983 and the resulting pellet was resuspended at a concentration of 2 µg/µl protein in SDS-PAGE sample buffer according to Neely *et al*., 1999. 20 µg of each sample was separated on a 12 % SDS polyacrylamide/4.0 M urea gel in electrophoresis buffer at 150 V. Urea was shown to result in a better resolution of AQP4 [84].
Brain tissue samples were prepared as followed: 20 µg of each brain tissue sample was diluted in 6x Laemmli buffer, boiled for 5 min at 95°C and separated on a 12 % SDS polyacrylamide gel (proteins < 150 kDa) or on a 7 % SDS polyacrylamide gel (proteins > 150 kDa) in electrophoresis buffer at 150 V for ~50 min. For the large nestin protein boiling resulted in disruption of the protein and was hence neglected. For investigation of AQP4 protein expression 20 µg of brain tissue samples were diluted in 6x Laemmli buffer and were, without boiling [231], separated on a 15 % SDS polyacrylamide/4.0 M urea gel in electrophoresis buffer at 150V for at least 120 min.

6.2.24 Semi-dry blot transfer
After electrophoresis proteins were transferred onto a nitrocellulose membrane. Therefore, the membrane and filter papers were soaked in freshly prepared transfer buffer and a sandwich of filter paper/gel/membrane/filter paper was placed on the semi-dry transfer system with the membrane closest to the anode. The transfer was run for at least ~ 45 min, depending on the protein size, at 15 V and 150 mA. To check for successful protein transfer from the gel to the membrane, the membranes were stained with Ponceau Red for ~ 5 min. Poncau Red stains proteins on nicrocellulose membranes with > 50 ng/band. To destain the membrane before immunoblotting, the membranes were washed with water several times until the staining disappeared.

6.2.25 Immunoblotting
Western blot detection for the cell culture samples was performed using the One Step Western Blot Kit according to manufacturer´s instructions. Brain tissue samples were processed using conventional immunoblotting. To prevent non-specific background binding of the antibodies, the membrane was blocked for 1h with 5 % skim milk. The membrane was briefly rinsed with PBS-Tween before the primary antibody was added in PBS-Tween with 1 % BSA overnight at 4°C. Following the overnight incubation, the membrane was washed three times for 15 min at RT in PBS-Tween before the peroxidase conjugated secondary antibody was added in PBS-Tween for 2h at RT. The membrane was washed again in PBS-Tween as previously and immunoreactive proteins were visualized by chemiluminescence detection using the Amersham ECL™ Western Blotting detection Kit according to manufacturer´s instructions and films were developed

manually in a bath application. The bands on the developed films were scanned and the optical density was measured using Image J software.

6.2.26 Data evaluation and statistical analysis

Proliferation assay
Proliferation was assayed in 3-6 independent experiments. The obtained data were calibrated to the bacteriophage λ standard curve for DNA content in each experiment. Calibration served to avoid variations in the assay outcome in experiments measured at different time points. Values of treated samples were normalized to untreated control samples. Statistical analysis was performed using Mann-Whitney rank-sum test or Student´s t-test if normality and variance tests were passed.

Apoptosis assay
In the apoptosis assay, annexin V^+ cells were counted and expressed as the number of cells shifted after fluorescence labelling from the polygonal gate R1 to the polygonal gate R2. To distinguish necrotic cells propidium iodide was used as a marker of dead cells and the polygonal gate R3 was defined for this population of cells. Statistical analysis for the three independent experiments was performed using Student´s t-test for paired data.

Relative quantification of mRNA expression
Relative quantification of mRNA expression of target genes was performed by determining the ratio of the target gene and a reference housekeeping gene. In the striatal mouse astrocyte cultures 4-10 independent culture experiments were performed. The PCR products were separated on agarose gels and their size was estimated using the O`GeneRuler ™ 50 bp ladder. Expression of the housekeeping gene hypoxanthine phophorilbosyl-treansferase (HPRT) was used as a reference. Furthermore the HPRT primers were designed in a way so they could be used to detect genomic contamination, indicated by the appearance of a band at 1100 bp. For the first data (Fig. 2) gels were scanned and the optical density was measured using ImageJ. For subsequent data gels were scanned using Quantum ST4 gel documentation ensuring that images were not overexposed. Using Quantum Capt the quantification threshold was adjusted and the intensities (grey values) of the individual bands were determined. In both methods values were normalized to a band of the ladder and the target/reference gene ratio was determined. Values of treated samples were calculated as percentage of the untreated control samples. Statistical analysis was performed using a Student´s t-test for unpaired data. Pancreatic cancer cell line samples were quantitated as described above using Quantum Capt, although β-actin was used as a reference. In the rat brain samples 2-4 animals were investigated per group. The PCR products were separated on agarose gels and their size was estimated using the Mass Ruler™ Low Range DNA Ladder. Gels were evaluated as described above using Quantum Capt. Three different housekeeping genes, namely β-actin, HPRT and glyceraldehyde-3-phosphate dehydrogenase (GAPDH) were tested for uniform mRNA expression in the 6-OHDA lesion model. HPRT mRNA levels were drastically reduced at 4d post-lesion in both sham and 6-OHDA lesioned animals, while β-actin and GAPDH mRNA expression was rather stable under both conditions and during all examined time points and resulted in similar results in the relative quantification of the target genes. The graphs display the relative quantification of the target genes to GAPDH. Values of 6-OHDA lesioned animals were normalized to the average sham 24d post-lesion value. The latter was done to detect any changes in gene expression that were directly surgery related. 24d post-lesion no surgery related changes in mRNA expression are expected to persist in sham animals. Statistical analysis was performed using Mann-Whitney rank-sum test or Student´s t-test if normality and variance tests were passed.

Relative quantification of protein expression
Protein levels were analysed in three independent experiments in astrocyte cell cultures and in rat brain samples with 3-4 animals per group. The size of the bands was estimated using the all blue Precision Plus Protein™ Standard. Bands were scanned and the optical density was determined using ImageJ software. For relative quantification of protein expression of a target gene the ratio of the OD of the target gene and the OD of the reference housekeeping gene HPRT or GAPDH was determined. Values were calculated as percentage of the untreated or sham values. Statistical analysis was conducted using Student´s t-test.

Quantification of cell numbers
For the quantifications in the striatal mouse astrocyte cultures 3-7 independent experiments were performed in duplicate for each condition. 20 random images were taken from each coverslip at a magnification of 40x. Fluorescently stained or immuno-positive cells were manually counted in a blind manner. For quantification of DAPI stained cell nuclei the values were normalized to an area of 1 mm^2 before statistical analysis was performed. In case of the immunopositive cells, values were calculated either as percentage of the total number of counted cells or as percentage of the respective immunopositive cell population. Statistical analysis was performed using Mann-Whitney rank-sum test or Student´s t-test if normality and variance tests were passed.
For the quantification of Ki-67^+, nestin$^+$, NG2^+, Pax6^+ and TH^+ cells in the rat brain sections 4-15 random images comprising an area of at least 146.2 µm x 146.2 µm in the area of interest or tile scans were taken. Immunopositive cells were counted manually in a blind manner and the counted values were normalized to an area of 1 mm^2 before statistical analysis except in the case of TH, where the entire area of the lateral cortex was counted. For the quantification of double positive cells, Ki-67^+ cells were observed for double staining with a particular marker under high magnification (63x/1.4 oil immersion objective). For each area of interest at least 10 images were taken and cells were counted manually. The same procedure was used for examination of nestin double stainings.

Immunoreactivity intensity measurement
For intensity measurements, images were taken immediately after the immunostaining was performed to avoid any loss of immunofluorescence due to bleaching. All images were taken in the same microscopy session to avoid differences due to fluctuations of the LSM performance. A section of a random sham-operated rat was used to set the parameters at the LSM and subsequently all stained slides were examined using strictly the same parameters. Four images were taken in the striatal neurophil in all animals using a high magnification (63x/1.4 oil immersion objective). Intensity of the immunoreactivity was determined using ImageJ. For TH the complete image was analysed, while in case of AQP4 six ROIs of the same size were set in areas that were free of blood vessels and only contained neuropils. In all cases a background correction was performed. Values of 6-OHDA lesioned sections were calculated as percentage of the values obtained in sham animals. Statistical analysis was conducted using Student´s t-test.

7. References

1. Iwatsuki H, Suda M (2010) Seven kinds of intermediate filament networks in the cytoplasm of polarized cells: structure and function. Acta Histochem Cytochem 43: 19-31.
2. Kriegstein A, Alvarez-Buylla A (2009) The glial nature of embryonic and adult neural stem cells. Annu Rev Neurosci 32: 149-184.
3. Nedergaard M, Ransom B, Goldman SA (2003) New roles for astrocytes: redefining the functional architecture of the brain. Trends Neurosci 26: 523-530.
4. Hewett JA (2009) Determinants of regional and local diversity within the astroglial lineage of the normal central nervous system. Journal of Neurochemistry 110: 1717-1736.
5. Nishiyama A, Komitova M, Suzuki R, Zhu X (2009) Polydendrocytes (NG2 cells): multifunctional cells with lineage plasticity. Nat Rev Neurosci 10: 9-22.
6. Peters J, Palay S, Webster H (1976) The Fine Structure of the Nervous System: the Neurons and Supporting Cells. Philadelphia, London, Toronto: W. B. Saunders Company.
7. Sofroniew MV, Vinters HV (2010) Astrocytes: biology and pathology. Acta Neuropathol 119: 7-35.
8. Robel S, Berninger B, Gotz M (2011) The stem cell potential of glia: lessons from reactive gliosis. Nat Rev Neurosci 12: 88-104.
9. De Keyser J, Mostert JP, Koch MW (2008) Dysfunctional astrocytes as key players in the pathogenesis of central nervous system disorders. J Neurol Sci 267: 3-16.
10. Hansson E, Rönnbäck L (2003) Astrocytic receptors and second messenger systems. Advances in Molecular and Cell Biology 31: 475-501.
11. Wolburg H, Noell S, Mack A, Wolburg-Buchholz K, Fallier-Becker P (2009) Brain endothelial cells and the glio-vascular complex. Cell Tissue Res 335: 75-96.
12. Maragakis NJ, Rothstein JD (2006) Mechanisms of Disease: astrocytes in neurodegenerative disease. Nat Clin Pract Neurol 2: 679-689.
13. Wolburg H, Wolburg-Buchholz K, Fallier-Becker P, Noell S, Mack AF (2011) Structure and functions of aquaporin-4-based orthogonal arrays of particles. Int Rev Cell Mol Biol 287: 1-41.
14. Haydon PG, Carmignoto G (2006) Astrocyte control of synaptic transmission and neurovascular coupling. Physiol Rev 86: 1009-1031.
15. Kielian T (2008) Glial connexins and gap junctions in CNS inflammation and disease. J Neurochem 106: 1000-1016.
16. Costa MR, Gotz M, Berninger B (2010) What determines neurogenic competence in glia? Brain Res Rev.
17. Walz W (2000) Controversy surrounding the existence of discrete functional classes of astrocytes in adult gray matter. Glia 31: 95-103.
18. Pekny M, Wilhelmsson U, Bogestal YR, Pekna M (2007) The role of astrocytes and complement system in neural plasticity. Int Rev Neurobiol 82: 95-111.
19. Middeldorp J, Hol EM (2011) GFAP in health and disease. Prog Neurobiol 93: 421-443.
20. Liem RK, Messing A (2009) Dysfunctions of neuronal and glial intermediate filaments in disease. J Clin Invest 119: 1814-1824.
21. Eriksson JE, Dechat T, Grin B, Helfand B, Mendez M, et al. (2009) Introducing intermediate filaments: from discovery to disease. J Clin Invest 119: 1763-1771.
22. Minin AA, Moldaver MV (2008) Intermediate vimentin filaments and their role in intracellular organelle distribution. Biochemistry (Mosc) 73: 1453-1466.
23. Guerette D, Khan PA, Savard PE, Vincent M (2007) Molecular evolution of type VI intermediate filament proteins. BMC Evol Biol 7: 164.
24. Goldman RD, Grin B, Mendez MG, Kuczmarski ER (2008) Intermediate filaments: versatile building blocks of cell structure. Curr Opin Cell Biol 20: 28-34.
25. Eng LF, Ghirnikar RS, Lee YL (2000) Glial fibrillary acidic protein: GFAP-thirty-one years (1969-2000). Neurochem Res 25: 1439-1451.
26. Gomes FC, Paulin D, Moura Neto V (1999) Glial fibrillary acidic protein (GFAP): modulation by growth factors and its implication in astrocyte differentiation. Braz J Med Biol Res 32: 619-631.
27. Ralton JE, Lu X, Hutcheson AM, Quinlan RA (1994) Identification of two N-terminal non-alpha-helical domain motifs important in the assembly of glial fibrillary acidic protein. J Cell Sci 107 (Pt 7): 1935-1948.
28. Eliasson C, Sahlgren C, Berthold CH, Stakeberg J, Celis JE, et al. (1999) Intermediate filament protein partnership in astrocytes. J Biol Chem 274: 23996-24006.
29. Pekny M, Pekna M (2004) Astrocyte intermediate filaments in CNS pathologies and regeneration. J Pathol 204: 428-437.
30. Gomi H, Yokoyama T, Fujimoto K, Ikeda T, Katoh A, et al. (1995) Mice devoid of the glial fibrillary acidic protein develop normally and are susceptible to scrapie prions. Neuron 14: 29-41.

31. Pekny M, Leveen P, Pekna M, Eliasson C, Berthold CH, et al. (1995) Mice lacking glial fibrillary acidic protein display astrocytes devoid of intermediate filaments but develop and reproduce normally. Embo J 14: 1590-1598.
32. Hockfield S, McKay RD (1985) Identification of major cell classes in the developing mammalian nervous system. J Neurosci 5: 3310-3328.
33. Lendahl U, Zimmerman LB, McKay RDG (1990) CNS stem cells express a new class of intermediate filament protein. Cell 60: 585-595.
34. Gilyarov AV (2008) Nestin in central nervous system cells. Neurosci Behav Physiol 38: 165-169.
35. Frederiksen K, McKay RD (1988) Proliferation and differentiation of rat neuroepithelial precursor cells in vivo. J Neurosci 8: 1144-1151.
36. Kalman M, Ajtai BM (2001) A comparison of intermediate filament markers for presumptive astroglia in the developing rat neocortex: immunostaining against nestin reveals more detail, than GFAP or vimentin. Int J Dev Neurosci 19: 101-108.
37. Duggal N, Schmidt-Kastner R, Hakim AM (1997) Nestin expression in reactive astrocytes following focal cerebral ischemia in rats. Brain Res 768: 1-9.
38. Holmin S, Almqvist P, Lendahl U, Mathiesen T (1997) Adult nestin-expressing subependymal cells differentiate to astrocytes in response to brain injury. Eur J Neurosci 9: 65-75.
39. Dahlstrand J, Zimmerman LB, McKay RD, Lendahl U (1992) Characterization of the human nestin gene reveals a close evolutionary relationship to neurofilaments. J Cell Sci 103 (Pt 2): 589-597.
40. Frisen J, Johansson CB, Torok C, Risling M, Lendahl U (1995) Rapid, widespread, and longlasting induction of nestin contributes to the generation of glial scar tissue after CNS injury. J Cell Biol 131: 453-464.
41. Lin RC, Matesic DF, Marvin M, McKay RD, Brustle O (1995) Re-expression of the intermediate filament nestin in reactive astrocytes. Neurobiol Dis 2: 79-85.
42. Gallo V, Armstrong RC (1995) Developmental and growth factor-induced regulation of nestin in oligodendrocyte lineage cells. J Neurosci 15: 394-406.
43. Wislet-Gendebien S, Wautier F, Leprince P, Rogister B (2005) Astrocytic and neuronal fate of mesenchymal stem cells expressing nestin. Brain Res Bull 68: 95-102.
44. Steinert PM, Chou YH, Prahlad V, Parry DA, Marekov LN, et al. (1999) A high molecular weight intermediate filament-associated protein in BHK-21 cells is nestin, a type VI intermediate filament protein. Limited co-assembly in vitro to form heteropolymers with type III vimentin and type IV alpha-internexin. J Biol Chem 274: 9881-9890.
45. Park D, Xiang AP, Mao FF, Zhang L, Di CG, et al. (2010) Nestin is required for the proper self-renewal of neural stem cells. Stem Cells 28: 2162-2171.
46. Yang J, Dominguez B, de Winter F, Gould TW, Eriksson JE, et al. (2011) Nestin negatively regulates postsynaptic differentiation of the neuromuscular synapse. Nat Neurosci 14: 324-330.
47. Sahlgren CM, Pallari HM, He T, Chou YH, Goldman RD, et al. (2006) A nestin scaffold links Cdk5/p35 signaling to oxidant-induced cell death. Embo J 25: 4808-4819.
48. Miller FD, Gauthier AS (2007) Timing is everything: making neurons versus glia in the developing cortex. Neuron 54: 357-369.
49. Rowitch DH, Kriegstein AR (2010) Developmental genetics of vertebrate glial-cell specification. Nature 468: 214-222.
50. Malatesta P, Appolloni I, Calzolari F (2008) Radial glia and neural stem cells. Cell Tissue Res 331: 165-178.
51. Dahlstrand J, Lardelli M, Lendahl U (1995) Nestin mRNA expression correlates with the central nervous system progenitor cell state in many, but not all, regions of developing central nervous system. Brain Res Dev Brain Res 84: 109-129.
52. Pekny M (2001) Astrocytic intermediate filaments: lessons from GFAP and vimentin knock-out mice. Prog Brain Res 132: 23-30.
53. Eddleston M, Mucke L (1993) Molecular profile of reactive astrocytes--implications for their role in neurologic disease. Neuroscience 54: 15-36.
54. Privat A (2003) Astrocytes as support for axonal regeneration in the central nervous system of mammals. Glia 43: 91-93.
55. Garden GA, Moller T (2006) Microglia biology in health and disease. J Neuroimmune Pharmacol 1: 127-137.
56. Wang A, He BP (2009) Characteristics and functions of NG2 cells in normal brain and neuropathology. Neurol Res 31: 144-150.
57. Buttitta LA, Edgar BA (2007) Mechanisms controlling cell cycle exit upon terminal differentiation. Curr Opin Cell Biol 19: 697-704.
58. Buffo A, Rite I, Tripathi P, Lepier A, Colak D, et al. (2008) Origin and progeny of reactive gliosis: A source of multipotent cells in the injured brain. Proc Natl Acad Sci U S A 105: 3581-3586.

59. Nielsen S, Nagelhus EA, Amiry-Moghaddam M, Bourque C, Agre P, et al. (1997) Specialized membrane domains for water transport in glial cells: high-resolution immunogold cytochemistry of aquaporin-4 in rat brain. J Neurosci 17: 171-180.
60. Papadopoulos MC, Saadoun S, Verkman AS (2008) Aquaporins and cell migration. Pflugers Arch 456: 693-700.
61. Chrispeels MJ, Agre P (1994) Aquaporins: water channel proteins of plant and animal cells. Trends Biochem Sci 19: 421-425.
62. Abe K, Saito H (1998) Adenosine stimulates stellation of cultured rat cortical astrocytes. Brain Res 804: 63-71.
63. Badaut J, Lasbennes F, Magistretti PJ, Regli L (2002) Aquaporins in brain: distribution, physiology, and pathophysiology. J Cereb Blood Flow Metab 22: 367-378.
64. Verkman AS (2011) Aquaporins at a glance. Journal of Cell Science 124: 2107-2112.
65. Kozono D, Yasui M, King LS, Agre P (2002) Aquaporin water channels: atomic structure molecular dynamics meet clinical medicine. J Clin Invest 109: 1395-1399.
66. Nozaki K, Ishii D, Ishibashi K (2008) Intracellular aquaporins: clues for intracellular water transport? Pflugers Arch 456: 701-707.
67. Agre P, King LS, Yasui M, Guggino WB, Ottersen OP, et al. (2002) Aquaporin water channels--from atomic structure to clinical medicine. J Physiol 542: 3-16.
68. Zelenina M (2010) Regulation of brain aquaporins. Neurochem Int 57: 468-488.
69. Verkman AS, Mitra AK (2000) Structure and function of aquaporin water channels. Am J Physiol Renal Physiol 278: F13-28.
70. Tani K, Mitsuma T, Hiroaki Y, Kamegawa A, Nishikawa K, et al. (2009) Mechanism of aquaporin-4's fast and highly selective water conduction and proton exclusion. J Mol Biol 389: 694-706.
71. Yool AJ (2007) Aquaporins: multiple roles in the central nervous system. Neuroscientist 13: 470-485.
72. Verkman AS (2008) Mammalian aquaporins: diverse physiological roles and potential clinical significance. Expert Rev Mol Med 10: e13.
73. Tait MJ, Saadoun S, Bell BA, Papadopoulos MC (2008) Water movements in the brain: role of aquaporins. Trends Neurosci 31: 37-43.
74. Jung JS, Bhat RV, Preston GM, Guggino WB, Baraban JM, et al. (1994) Molecular characterization of an aquaporin cDNA from brain: candidate osmoreceptor and regulator of water balance. Proc Natl Acad Sci U S A 91: 13052-13056.
75. Yang B, Brown D, Verkman AS (1996) The mercurial insensitive water channel (AQP-4) forms orthogonal arrays in stably transfected Chinese hamster ovary cells. J Biol Chem 271: 4577-4580.
76. Papadopoulos MC, Verkman AS (2007) Aquaporin-4 and brain edema. Pediatr Nephrol 22: 778-784.
77. Venero JL, Vizuete ML, Ilundain AA, Machado A, Echevarria M, et al. (1999) Detailed localization of aquaporin-4 messenger RNA in the CNS: preferential expression in periventricular organs. Neuroscience 94: 239-250.
78. Amiry-Moghaddam M, Xue R, Haug FM, Neely JD, Bhardwaj A, et al. (2004) Alpha-syntrophin deletion removes the perivascular but not endothelial pool of aquaporin-4 at the blood-brain barrier and delays the development of brain edema in an experimental model of acute hyponatremia. Faseb J 18: 542-544.
79. Wen H, Nagelhus EA, Amiry-Moghaddam M, Agre P, Ottersen OP, et al. (1999) Ontogeny of water transport in rat brain: postnatal expression of the aquaporin-4 water channel. Eur J Neurosci 11: 935-945.
80. Cavazzin C, Ferrari D, Facchetti F, Russignan A, Vescovi AL, et al. (2006) Unique expression and localization of aquaporin-4 and aquaporin-9 in murine and human neural stem cells and in their glial progeny. Glia 53: 167-181.
81. Tomas-Camardiel M, Venero JL, de Pablos RM, Rite I, Machado A, et al. (2004) In vivo expression of aquaporin-4 by reactive microglia. J Neurochem 91: 891-899.
82. Saadoun S, Papadopoulos MC (2010) Aquaporin-4 in brain and spinal cord oedema. Neuroscience 168: 1036-1046.
83. Amiry-Moghaddam M, Frydenlund DS, Ottersen OP (2004) Anchoring of aquaporin-4 in brain: molecular mechanisms and implications for the physiology and pathophysiology of water transport. Neuroscience 129: 999-1010.
84. Neely JD, Christensen BM, Nielsen S, Agre P (1999) Heterotetrameric composition of aquaporin-4 water channels. Biochemistry 38: 11156-11163.
85. Zelenin S, Gunnarson E, Alikina T, Bondar A, Aperia A (2000) Identification of a new form of AQP4 mRNA that is developmentally expressed in mouse brain. Pediatr Res 48: 335-339.
86. Moe SE, Sorbo JG, Sogaard R, Zeuthen T, Petter Ottersen O, et al. (2008) New isoforms of rat Aquaporin-4. Genomics.
87. Rossi A, Pisani F, Nicchia GP, Svelto M, Frigeri A (2010) Evidences for a leaky scanning mechanism for the synthesis of the shorter M23 protein isoform of aquaporin-4: implication in orthogonal array formation and neuromyelitis optica antibody interaction. J Biol Chem 285: 4562-4569.

88. Furman CS, Gorelick-Feldman DA, Davidson KG, Yasumura T, Neely JD, et al. (2003) Aquaporin-4 square array assembly: opposing actions of M1 and M23 isoforms. Proc Natl Acad Sci U S A 100: 13609-13614.
89. Silberstein C, Bouley R, Huang Y, Fang P, Pastor-Soler N, et al. (2004) Membrane organization and function of M1 and M23 isoforms of aquaporin-4 in epithelial cells. Am J Physiol Renal Physiol 287: F501-511.
90. Badaut J, Verbavatz JM, Freund-Mercier MJ, Lasbennes F (2000) Presence of aquaporin-4 and muscarinic receptors in astrocytes and ependymal cells in rat brain: a clue to a common function? Neurosci Lett 292: 75-78.
91. Nagelhus EA, Mathiisen TM, Ottersen OP (2004) Aquaporin-4 in the central nervous system: cellular and subcellular distribution and coexpression with KIR4.1. Neuroscience 129: 905-913.
92. Strohschein S, Hüttmann K, Gabriel S, Binder DK, Heinemann U, et al. (2011) Impact of aquaporin-4 channels on K+ buffering and gap junction coupling in the hippocampus. Glia 59: 973-980.
93. Ziv I, Shirvan A, Offen D, Barzilai A, Melamed E (2001) Molecular biology of dopamine-induced apoptosis : possible implications for Parkinson's disease. Methods Mol Med 62: 73-87.
94. Zeiss CJ (2005) Neuroanatomical phenotyping in the mouse: the dopaminergic system. Vet Pathol 42: 753-773.
95. Siegel G, Agranoff B, Albers W, Fisher S, Uhler J (2006) Basic Neurochemistry. Philadelphia: Lippincott-Raven.
96. Missale C, Nash SR, Robinson SW, Jaber M, Caron MG (1998) Dopamine receptors: from structure to function. Physiol Rev 78: 189-225.
97. Goto Y, Grace AA (2007) The dopamine system and the pathophysiology of schizophrenia: a basic science perspective. Int Rev Neurobiol 78: 41-68.
98. Smythies J (2005) Section II. The dopamine system. Int Rev Neurobiol 64: 123-172.
99. Miyazaki I, Asanuma M, Diaz-Corrales FJ, Miyoshi K, Ogawa N (2004) Direct evidence for expression of dopamine receptors in astrocytes from basal ganglia. Brain Res 1029: 120-123.
100. Bal A, Bachelot T, Savasta M, Manier M, Verna JM, et al. (1994) Evidence for dopamine D2 receptor mRNA expression by striatal astrocytes in culture: in situ hybridization and polymerase chain reaction studies. Brain Res Mol Brain Res 23: 204-212.
101. Zanassi P, Paolillo M, Montecucco A, Avvedimento EV, Schinelli S (1999) Pharmacological and molecular evidence for dopamine D(1) receptor expression by striatal astrocytes in culture. J Neurosci Res 58: 544-552.
102. Brito V, Beyer C, Kuppers E (2004) BDNF-dependent stimulation of dopamine D5 receptor expression in developing striatal astrocytes involves PI3-kinase signaling. Glia 46: 284-295.
103. Hosli E, Hosli L (1997) Autoradiographic studies on the uptake of 3H-dopamine by neurons and astrocytes in explant and primary cultures of rat CNS: effects of uptake inhibitors. Int J Dev Neurosci 15: 45-53.
104. Schober A (2004) Classic toxin-induced animal models of Parkinson's disease: 6-OHDA and MPTP. Cell Tissue Res 318: 215-224.
105. Guillin O, Abi-Dargham A, Laruelle M (2007) Neurobiology of dopamine in schizophrenia. Int Rev Neurobiol 78: 1-39.
106. Kuppers E, Beyer C (2001) Dopamine regulates brain-derived neurotrophic factor (BDNF) expression in cultured embryonic mouse striatal cells. Neuroreport 12: 1175-1179.
107. Kuppers E, Sabolek M, Anders U, Pilgrim C, Beyer C (2000) Developmental regulation of glutamic acid decarboxylase mRNA expression and splicing in the rat striatum by dopamine. Brain Res Mol Brain Res 81: 19-28.
108. Ohtani N, Goto T, Waeber C, Bhide PG (2003) Dopamine modulates cell cycle in the lateral ganglionic eminence. J Neurosci 23: 2840-2850.
109. Popolo M, McCarthy DM, Bhide PG (2004) Influence of dopamine on precursor cell proliferation and differentiation in the embryonic mouse telencephalon. Dev Neurosci 26: 229-244.
110. Karakaya S, Kipp M, Beyer C (2007) Oestrogen Regulates the Expression and Function of Dopamine Transporters in Astrocytes of the Nigrostriatal System. Journal of Neuroendocrinology 19: 682-690.
111. Blum D, Torch S, Lambeng N, Nissou M, Benabid AL, et al. (2001) Molecular pathways involved in the neurotoxicity of 6-OHDA, dopamine and MPTP: contribution to the apoptotic theory in Parkinson's disease. Prog Neurobiol 65: 135-172.
112. Luo Y, Roth GS (2000) The roles of dopamine oxidative stress and dopamine receptor signaling in aging and age-related neurodegeneration. Antioxid Redox Signal 2: 449-460.
113. Clement MV, Long LH, Ramalingam J, Halliwell B (2002) The cytotoxicity of dopamine may be an artefact of cell culture. J Neurochem 81: 414-421.
114. Lane E, Dunnett S (2008) Animal models of Parkinson's disease and L-dopa induced dyskinesia: how close are we to the clinic? Psychopharmacology (Berl) 199: 303-312.
115. Rodriguez M, Barroso-Chinea P, Abdala P, Obeso J, Gonzalez-Hernandez T (2001) Dopamine cell degeneration induced by intraventricular administration of 6-hydroxydopamine in the rat: similarities with cell loss in parkinson's disease. Exp Neurol 169: 163-181.

116. Schumacher A, Arnhold S, Addicks K, Doerfler W (2003) Staurosporine is a potent activator of neuronal, glial, and "CNS stem cell-like" neurosphere differentiation in murine embryonic stem cells. Mol Cell Neurosci 23: 669-680.
117. Zelenina M, Zelenin S, Bondar AA, Brismar H, Aperia A (2002) Water permeability of aquaporin-4 is decreased by protein kinase C and dopamine. Am J Physiol Renal Physiol 283: F309-318.
118. Hansson E, Ronnback L, Lowenthal A, Noppe M (1985) Primary cultures from defined brain areas; effects of seeding time on cell growth, astroglial content and protein synthesis. Brain Res 353: 175-185.
119. Cornil CA, Balthazart J, Motte P, Massotte L, Seutin V (2002) Dopamine activates noradrenergic receptors in the preoptic area. J Neurosci 22: 9320-9330.
120. Cornil CA, Castelino CB, Ball GF (2008) Dopamine binds to alpha(2)-adrenergic receptors in the song control system of zebra finches (Taeniopygia guttata). J Chem Neuroanat 35: 202-215.
121. Nicchia GP, Frigeri A, Liuzzi GM, Svelto M (2003) Inhibition of aquaporin-4 expression in astrocytes by RNAi determines alteration in cell morphology, growth, and water transport and induces changes in ischemia-related genes. Faseb J 17: 1508-1510.
122. Detmers FJ, de Groot BL, Muller EM, Hinton A, Konings IB, et al. (2006) Quaternary ammonium compounds as water channel blockers. Specificity, potency, and site of action. J Biol Chem 281: 14207-14214.
123. Scholzen T, Gerdes J (2000) The Ki-67 protein: From the known and the unknown. Journal of Cellular Physiology 182: 311-322.
124. Zhu H, Dahlstrom A (2007) Glial fibrillary acidic protein-expressing cells in the neurogenic regions in normal and injured adult brains. J Neurosci Res 85: 2783-2792.
125. Gleeson JG, Lin PT, Flanagan LA, Walsh CA (1999) Doublecortin is a microtubule-associated protein and is expressed widely by migrating neurons. Neuron 23: 257-271.
126. Callaerts P, Halder G, Gehring WJ (1997) PAX-6 IN DEVELOPMENT AND EVOLUTION. Annual Review of Neuroscience 20: 483-532.
127. Sakurai K, Osumi N (2008) The Neurogenesis-Controlling Factor, Pax6, Inhibits Proliferation and Promotes Maturation in Murine Astrocytes. J Neurosci 28: 4604-4612.
128. Nacher J, Varea E, Blasco-Ibañez JM, Castillo-Gomez E, Crespo C, et al. (2005) Expression of the transcription factor Pax6 in the adult rat dentate gyrus. Journal of Neuroscience Research 81: 753-761.
129. Yang H, Cheng XP, Li JW, Yao Q, Ju G (2009) De-differentiation response of cultured astrocytes to injury induced by scratch or conditioned culture medium of scratch-insulted astrocytes. Cell Mol Neurobiol 29: 455-473.
130. Yu T, Cao G, Feng L (2006) Low temperature induced de-differentiation of astrocytes. J Cell Biochem 99: 1096-1107.
131. Kosaka T, Hama K, Nagatsu I (1987) Tyrosine hydroxylase-immunoreactive intrinsic neurons in the rat cerebral cortex. Exp Brain Res 68: 393-405.
132. Benavides-Piccione R, DeFelipe J (2007) Distribution of neurons expressing tyrosine hydroxylase in the human cerebral cortex. Journal of Anatomy 211: 212-222.
133. Asmus SE, Anderson EK, Ball MW, Barnes BA, Bohnen AM, et al. (2008) Neurochemical characterization of tyrosine hydroxylase-immunoreactive interneurons in the developing rat cerebral cortex. Brain Research 1222: 95-105.
134. Kosaka T, Kosaka K, Hataguchi Y, Nagatsu I, Wu JY, et al. (1987) Catecholaminergic neurons containing GABA-like and/or glutamic acid decarboxylase-like immunoreactivities in various brain regions of the rat. Exp Brain Res 66: 191-210.
135. Tande D, Hoglinger G, Debeir T, Freundlieb N, Hirsch EC, et al. (2006) New striatal dopamine neurons in MPTP-treated macaques result from a phenotypic shift and not neurogenesis. Brain 129: 1194-1200.
136. Reuss B, Leung DSY, Ohlemeyer C, Kettenmann H, Unsicker K (2000) Regionally Distinct Regulation of Astroglial Neurotransmitter Receptors by Fibroblast Growth Factor-2. Molecular and Cellular Neuroscience 16: 42-58.
137. Brito VI, Rozanski VE, Beyer C, Kuppers E (2009) Dopamine regulates the expression of the glutamate transporter GLT1 but not GLAST in developing striatal astrocytes. J Mol Neurosci 39: 372-379.
138. Kawagoe KT, Garris PA, Wiedemann DJ, Wightman RM (1992) Regulation of transient dopamine concentration gradients in the microenvironment surrounding nerve terminals in the rat striatum. Neuroscience 51: 55-64.
139. Jobe PC, Laird Ii HE, Ko KH, Ray T, Dailey JW (1982) Abnormalities in Monoamine Levels in the Central Nervous System of the Genetically Epilepsy-Prone Rat. Epilepsia 23: 359-366.
140. Pardo B, Mena MA, Casarejos MJ, Paíno CL, De Yébenes JG (1995) Toxic effects of L-DOPA on mesencephalic cell cultures: protection with antioxidants. Brain Research 682: 133-143.
141. Werner P, Cohen G (1993) Glutathione Disulfide (GSSG) as a Marker of Oxidative Injury to Brain Mitochondriaa. Annals of the New York Academy of Sciences 679: 364-369.

142. Hoglinger GU, Rizk P, Muriel MP, Duyckaerts C, Oertel WH, et al. (2004) Dopamine depletion impairs precursor cell proliferation in Parkinson disease. Nat Neurosci 7: 726-735.
143. Baker SA, Baker KA, Hagg T (2004) Dopaminergic nigrostriatal projections regulate neural precursor proliferation in the adult mouse subventricular zone. Eur J Neurosci 20: 575-579.
144. Van Kampen JM, Hagg T, Robertson HA (2004) Induction of neurogenesis in the adult rat subventricular zone and neostriatum following dopamine D3 receptor stimulation. European Journal of Neuroscience 19: 2377-2387.
145. Kippin TE, Kapur S, van der Kooy D (2005) Dopamine specifically inhibits forebrain neural stem cell proliferation, suggesting a novel effect of antipsychotic drugs. J Neurosci 25: 5815-5823.
146. Noell S, Fallier-Becker P, Beyer C, Kroger S, Mack AF, et al. (2007) Effects of agrin on the expression and distribution of the water channel protein aquaporin-4 and volume regulation in cultured astrocytes. Eur J Neurosci 26: 2109-2118.
147. Hirt L, Ternon B, Price M, Mastour N, Brunet JF, et al. (2009) Protective role of early aquaporin 4 induction against postischemic edema formation. J Cereb Blood Flow Metab 29: 423-433.
148. Van Hoek AN, Bouley R, Lu Y, Silberstein C, Brown D, et al. (2009) Vasopressin-induced differential stimulation of AQP4 splice variants regulates the in-membrane assembly of orthogonal arrays. Am J Physiol Renal Physiol 296: F1396-1404.
149. Fenton RA, Moeller HB, Zelenina M, Snaebjornsson MT, Holen T, et al. (2010) Differential water permeability and regulation of three aquaporin 4 isoforms. Cell Mol Life Sci 67: 829-840.
150. Lodish H, Berk A, Zipursky S (2000) Molecular Cell Biology. New York: W. H. Freeman.
151. Dubois JM, Rouzaire-Dubois B (2004) The influence of cell volume changes on tumour cell proliferation. Eur Biophys J 33: 227-232.
152. Thiagarajah JR, Zhao D, Verkman AS (2007) Impaired enterocyte proliferation in aquaporin-3 deficiency in mouse models of colitis. Gut 56: 1529-1535.
153. Hara-Chikuma M, Verkman AS (2008) Prevention of skin tumorigenesis and impairment of epidermal cell proliferation by targeted aquaporin-3 gene disruption. Mol Cell Biol 28: 326-332.
154. Levin MH, Verkman AS (2006) Aquaporin-3-Dependent Cell Migration and Proliferation during Corneal Re-epithelialization. Investigative Ophthalmology & Visual Science 47: 4365-4372.
155. Nakahigashi K, Kabashima K, Ikoma A, Verkman AS, Miyachi Y, et al. (2011) Upregulation of Aquaporin-3 Is Involved in Keratinocyte Proliferation and Epidermal Hyperplasia. J Invest Dermatol 131: 865-873.
156. Zhang Z, Chen Z, Song Y, Zhang P, Hu J, et al. (2010) Expression of aquaporin 5 increases proliferation and metastasis potential of lung cancer. The Journal of Pathology 221: 210-220.
157. Hoque MO, Soria J-C, Woo J, Lee T, Lee J, et al. (2006) Aquaporin 1 Is Overexpressed in Lung Cancer and Stimulates NIH-3T3 Cell Proliferation and Anchorage-Independent Growth. Am J Pathol 168: 1345-1353.
158. Ruiz-Ederra J, Verkman AS (2007) Aquaporin-1–Independent Microvessel Proliferation in a Neonatal Mouse Model of Oxygen-Induced Retinopathy. Investigative Ophthalmology & Visual Science 48: 4802-4810.
159. Nicchia GP, Srinivas M, Li W, Brosnan CF, Frigeri A, et al. (2005) New possible roles for aquaporin-4 in astrocytes: cell cytoskeleton and functional relationship with connexin43. Faseb J 19: 1674-1676.
160. Yang B, Kim JK, Verkman AS (2006) Comparative efficacy of HgCl2 with candidate aquaporin-1 inhibitors DMSO, gold, TEA+ and acetazolamide. FEBS Lett 580: 6679-6684.
161. Søgaard R, Zeuthen T (2008) Test of blockers of AQP1 water permeability by a high-resolution method: no effects of tetraethylammonium ions or acetazolamide. Pflügers Archiv European Journal of Physiology 456: 285-292.
162. Ho JD, Yeh R, Sandstrom A, Chorny I, Harries WEC, et al. (2009) Crystal structure of human aquaporin 4 at 1.8 Å and its mechanism of conductance. Proceedings of the National Academy of Sciences 106: 7437-7442.
163. Brooks HL, Regan JW, Yool AJ (2000) Inhibition of aquaporin-1 water permeability by tetraethylammonium: involvement of the loop E pore region. Mol Pharmacol 57: 1021-1026.
164. Khodakhah K, Melishchuk A, Armstrong CM (1997) Killing K channels with TEA+. Proc Natl Acad Sci U S A 94: 13335-13338.
165. Heginbotham L, MacKinnon R (1992) The aromatic binding site for tetraethylammonium ion on potassium channels. Neuron 8: 483-491.
166. Hille B (1967) The selective inhibition of delayed potassium currents in nerve by tetraethylammonium ion. J Gen Physiol 50: 1287-1302.
167. Tang Q-Y, Zhang Z, Xia X-M, Lingle CJ (2010) Block of mouse Slo1 and Slo3 K⁺ channels by CTX, IbTX, TEA, 4-AP and quinidine. Channels 4: 22-41.
168. Armstrong CM, Binstock L (1965) Anomalous Rectification in the Squid Giant Axon Injected with Tetraethylammonium Chloride. J Gen Physiol 48: 859-872.
169. Homkajorn B, Sims NR, Muyderman H (2010) Connexin 43 regulates astrocytic migration and proliferation in response to injury. Neuroscience Letters 486: 197-201.

170. Herrero-González S, Valle-Casuso JC, Sánchez-Alvarez R, Giaume C, Medina JM, et al. (2009) Connexin43 is involved in the effect of endothelin-1 on astrocyte proliferation and glucose uptake. Glia 57: 222-233.
171. Saadoun S, Papadopoulos MC, Watanabe H, Yan D, Manley GT, et al. (2005) Involvement of aquaporin-4 in astroglial cell migration and glial scar formation. J Cell Sci 118: 5691-5698.
172. Fan Y, Kong H, Shi X, Sun X, Ding J, et al. (2008) Hypersensitivity of aquaporin 4-deficient mice to 1-methyl-4-phenyl-1,2,3,6-tetrahydropyrindine and astrocytic modulation. Neurobiol Aging 29: 1226-1236.
173. Kong H, Fan Y, Xie J, Ding J, Sha L, et al. (2008) AQP4 knockout impairs proliferation, migration and neuronal differentiation of adult neural stem cells. J Cell Sci 121: 4029-4036.
174. Saadoun S, Tait MJ, Reza A, Davies DC, Bell BA, et al. (2009) AQP4 gene deletion in mice does not alter blood-brain barrier integrity or brain morphology. Neuroscience 161: 764-772.
175. Verkman AS, Hara-Chikuma M, Papadopoulos MC (2008) Aquaporins--new players in cancer biology. J Mol Med 86: 523-529.
176. Warth A, Kröger S, Wolburg H (2004) Redistribution of aquaporin-4 in human glioblastoma correlates with loss of agrin immunoreactivity from brain capillary basal laminae. Acta Neuropathologica 107: 311-318.
177. Warth A, Simon P, Capper D, Goeppert B, Tabatabai G, et al. (2007) Expression pattern of the water channel aquaporin-4 in human gliomas is associated with blood–brain barrier disturbance but not with patient survival. Journal of Neuroscience Research 85: 1336-1346.
178. McCoy E, Sontheimer H (2007) Expression and function of water channels (aquaporins) in migrating malignant astrocytes. Glia 55: 1034-1043.
179. Vizuete ML, Venero JL, Vargas C, Ilundain AA, Echevarria M, et al. (1999) Differential upregulation of aquaporin-4 mRNA expression in reactive astrocytes after brain injury: potential role in brain edema. Neurobiol Dis 6: 245-258.
180. Saadoun S, Papadopoulos MC, Davies DC, Krishna S, Bell BA (2002) Aquaporin-4 expression is increased in oedematous human brain tumours. J Neurol Neurosurg Psychiatry 72: 262-265.
181. Zigmond MJ, Stricker EM (1972) Deficits in feeding behavior after intraventricular injection of 6-hydroxydopamine in rats. Science 177: 1211-1214.
182. Hu XT, Wachtel SR, Galloway MP, White FJ (1990) Lesions of the nigrostriatal dopamine projection increase the inhibitory effects of D1 and D2 dopamine agonists on caudate-putamen neurons and relieve D2 receptors from the necessity of D1 receptor stimulation. J Neurosci 10: 2318-2329.
183. Cunningham LA, Su C (2002) Astrocyte Delivery of Glial Cell Line-Derived Neurotrophic Factor in a Mouse Model of Parkinson's Disease. Experimental Neurology 174: 230-242.
184. Alvarez-Fischer D, Henze C, Strenzke C, Westrich J, Ferger B, et al. (2008) Characterization of the striatal 6-OHDA model of Parkinson's disease in wild type and alpha-synuclein-deleted mice. Exp Neurol 210: 182-193.
185. Na SJ, DiLella AG, Lis EV, Jones K, Levine DM, et al. (2010) Molecular profiling of a 6-hydroxydopamine model of Parkinson's disease. Neurochem Res 35: 761-772.
186. Scott DE, Dudley GK, Knigge KM (1974) The ventricular system in neuroendocrine mechanisms. II. In vivo Monoamine transport by ependyma of the median eminence. Cell Tissue Res 154: 1-16.
187. Fuxe K, Ungerstedt U (1968) Histochemical studies on the distribution of catecholamines and 5-hydroxytryptamine after intraventricular injections. Histochemie 13: 16-28.
188. Aponso PM, Faull RLM, Connor B (2008) Increased progenitor cell proliferation and astrogenesis in the partial progressive 6-hydroxydopamine model of Parkinson's disease. Neuroscience 151: 1142-1153.
189. Iwata S, Nomoto M, Morioka H, Miyata A (2004) Gene expression profiling in the midbrain of striatal 6-hydroxydopamine-injected mice. Synapse 51: 279-286.
190. Walsh S, Finn DP, Dowd E (2011) Time-course of nigrostriatal neurodegeneration and neuroinflammation in the 6-hydroxydopamine-induced axonal and terminal lesion models of Parkinson's disease in the rat. Neuroscience 175: 251-261.
191. Mao L, Lau Y-S, Petroske E, Wang JQ (2001) Profound astrogenesis in the striatum of adult mice following nigrostriatal dopaminergic lesion by repeated MPTP administration. Developmental Brain Research 131: 57-65.
192. Mythri R, Venkateshappa C, Harish G, Mahadevan A, Muthane U, et al. (2011) Evaluation of Markers of Oxidative Stress, Antioxidant Function and Astrocytic Proliferation in the Striatum and Frontal Cortex of Parkinson's Disease Brains. Neurochemical Research: 1-12.
193. Saadoun S, Papadopoulos MC, Davies DC, Bell BA, Krishna S (2002) Increased aquaporin 1 water channel expression in human brain tumours. Br J Cancer 87: 621-623.
194. Noda A, Takamatsu H, Minoshima S, Tsukada H, Nishimura S (2003) Determination of Kinetic Rate Constants for 2-[lsqb]18F[rsqb]fluoro-2-deoxy-d-glucose and Partition Coefficient of Water in Conscious Macaques and Alterations in Aging or Anesthesia Examined on Parametric Images With an Anatomic Standardization Technique. J Cereb Blood Flow Metab 23: 1441-1447.

195. Rossi A, Crane JM, Verkman AS (2011) Aquaporin-4 Mz isoform: Brain expression, supramolecular assembly and neuromyelitis optica antibody binding. Glia 59: 1056-1063.
196. Noell S, Wolburg-Buchholz K, Mack AF, Beedle AM, Satz JS, et al. (2011) Evidence for a role of dystroglycan regulating the membrane architecture of astroglial endfeet. European Journal of Neuroscience 33: 2179-2186.
197. Fu N, Drinnenberg I, Kelso J, Wu JR, Paabo S, et al. (2007) Comparison of protein and mRNA expression evolution in humans and chimpanzees. PLoS One 2: e216.
198. Tian Q, Stepaniants SB, Mao M, Weng L, Feetham MC, et al. (2004) Integrated Genomic and Proteomic Analyses of Gene Expression in Mammalian Cells. Molecular & Cellular Proteomics 3: 960-969.
199. Saura J (2007) Microglial cells in astroglial cultures: a cautionary note. J Neuroinflammation 4: 26.
200. Puschmann TB, Dixon KJ, Turnley AM (2010) Species differences in reactivity of mouse and rat astrocytes in vitro. Neurosignals 18: 152-163.
201. Sergent-Tanguy S, Michel DC, Neveu I, Naveilhan P (2006) Long-lasting coexpression of nestin and glial fibrillary acidic protein in primary cultures of astroglial cells with a major participation of nestin(+)/GFAP(-) cells in cell proliferation. J Neurosci Res 83: 1515-1524.
202. Wu VW, Schwartz JP (1998) Cell culture models for reactive gliosis: new perspectives. J Neurosci Res 51: 675-681.
203. Schmidt-Kastner R, Humpel C (2002) Nestin expression persists in astrocytes of organotypic slice cultures from rat cortex. Int J Dev Neurosci 20: 29-38.
204. Zhao J-W, Raha-Chowdhury R, Fawcett JW, Watts C (2009) Astrocytes and oligodendrocytes can be generated from NG2+ progenitors after acute brain injury: intracellular localization of oligodendrocyte transcription factor 2 is associated with their fate choice. European Journal of Neuroscience 29: 1853-1869.
205. Tatsumi K, Takebayashi H, Manabe T, Tanaka KF, Makinodan M, et al. (2008) Genetic fate mapping of Olig2 progenitors in the injured adult cerebral cortex reveals preferential differentiation into astrocytes. Journal of Neuroscience Research 86: 3494-3502.
206. Burns KA, Murphy B, Danzer SC, Kuan C-Y (2009) Developmental and post-injury cortical gliogenesis: A Genetic fate-mapping study with Nestin-CreER mice. Glia 57: 1115-1129.
207. Miklossy J, Doudet DD, Schwab C, Yu S, McGeer EG, et al. (2006) Role of ICAM-1 in persisting inflammation in Parkinson disease and MPTP monkeys. Exp Neurol 197: 275-283.
208. Stromberg I, Bjorklund H, Dahl D, Jonsson G, Sundstrom E, et al. (1986) Astrocyte responses to dopaminergic denervations by 6-hydroxydopamine and 1-methyl-4-phenyl-1,2,3,6-tetrahydropyridine as evidenced by glial fibrillary acidic protein immunohistochemistry. Brain Res Bull 17: 225-236.
209. Gomide V, Bibancos T, Chadi G (2005) Dopamine cell morphology and glial cell hypertrophy and process branching in the nigrostriatal system after striatal 6-OHDA analyzed by specific sterological tools. Int J Neurosci 115: 557-582.
210. Chung EK, Chen LW, Chan YS, Yung KK (2008) Downregulation of glial glutamate transporters after dopamine denervation in the striatum of 6-hydroxydopamine-lesioned rats. J Comp Neurol 511: 421-437.
211. Nomura T, Yabe T, Rosenthal ES, Krzan M, Schwartz JP (2000) PSA-NCAM distinguishes reactive astrocytes in 6-OHDA-lesioned substantia nigra from those in the striatal terminal fields. Journal of Neuroscience Research 61: 588-596.
212. Yoo YM, Lee U, Kim YJ (2005) Apoptosis and nestin expression in the cortex and cultured astrocytes following 6-OHDA administration. Neuroscience Letters 382: 88-92.
213. Gordon RJ, McGregor AL, Connor B (2009) Chemokines direct neural progenitor cell migration following striatal cell loss. Mol Cell Neurosci 41: 219-232.
214. Yan Y-P, Lang BT, Vemuganti R, Dempsey RJ (2009) Persistent migration of neuroblasts from the subventricular zone to the injured striatum mediated by osteopontin following intracerebral hemorrhage. Journal of Neurochemistry 109: 1624-1635.
215. Dimou L, Simon C, Kirchhoff F, Takebayashi H, Gotz M (2008) Progeny of Olig2-Expressing Progenitors in the Gray and White Matter of the Adult Mouse Cerebral Cortex. J Neurosci 28: 10434-10442.
216. Ito D, Imai Y, Ohsawa K, Nakajima K, Fukuuchi Y, et al. (1998) Microglia-specific localisation of a novel calcium binding protein, Iba1. Molecular Brain Research 57: 1-9.
217. Amat JA, Ishiguro H, Nakamura K, Norton WT (1996) Phenotypic diversity and kinetics of proliferating microglia and astrocytes following cortical stab wounds. Glia 16: 368-382.
218. Norton WT (1999) Cell reactions following acute brain injury: a review. Neurochem Res 24: 213-218.
219. Henry V, Paille V, Lelan F, Brachet P, Damier P (2009) Kinetics of microglial activation and degeneration of dopamine-containing neurons in a rat model of Parkinson disease induced by 6-hydroxydopamine. J Neuropathol Exp Neurol 68: 1092-1102.
220. Brown JP, Couillard-Després S, Cooper-Kuhn CM, Winkler J, Aigner L, et al. (2003) Transient expression of doublecortin during adult neurogenesis. The Journal of Comparative Neurology 467: 1-10.

221. Hamilton N, Vayro S, Wigley R, Butt AM (2010) Axons and astrocytes release ATP and glutamate to evoke calcium signals in NG2-glia. Glia 58: 66-79.
222. Tripathi RB, Rivers LE, Young KM, Jamen F, Richardson WD (2010) NG2 glia generate new oligodendrocytes but few astrocytes in a murine experimental autoimmune encephalomyelitis model of demyelinating disease. J Neurosci 30: 16383-16390.
223. Komitova M, Serwanski DR, Lu QR, Nishiyama A (2011) NG2 cells are not a major source of reactive astrocytes after neocortical stab wound injury. Glia 59: 800-809.
224. Osumi N, Shinohara H, Numayama-Tsuruta K, Maekawa M (2008) Concise Review: Pax6 Transcription Factor Contributes to both Embryonic and Adult Neurogenesis as a Multifunctional Regulator. Stem Cells 26: 1663-1672.
225. Lesaffre B, Joliot A, Prochiantz A, Volovitch M (2007) Direct non-cell autonomous Pax6 activity regulates eye development in the zebrafish. Neural Dev 2: 2.
226. Karl MO, Hayes S, Nelson BR, Tan K, Buckingham B, et al. (2008) Stimulation of neural regeneration in the mouse retina. Proceedings of the National Academy of Sciences 105: 19508-19513.
227. Heinrich C, Blum R, Gascon S, Masserdotti G, Tripathi P, et al. (2010) Directing astroglia from the cerebral cortex into subtype specific functional neurons. PLoS Biol 8: e1000373.
228. Heins N, Malatesta P, Cecconi F, Nakafuku M, Tucker KL, et al. (2002) Glial cells generate neurons: the role of the transcription factor Pax6. Nat Neurosci 5: 308-315.
229. Berninger B, Costa MR, Koch U, Schroeder T, Sutor B, et al. (2007) Functional properties of neurons derived from in vitro reprogrammed postnatal astroglia. J Neurosci 27: 8654-8664.
230. Ugrumov MV (2009) Non-dopaminergic neurons partly expressing dopaminergic phenotype: distribution in the brain, development and functional significance. J Chem Neuroanat 38: 241-256.
231. Sørbø JG, Moe SE, Holen T (2007) Early upregulation in nasal epithelium and strong expression in olfactory bulb glomeruli suggest a role for Aquaporin-4 in olfaction. FEBS Letters 581: 4884-4890.
232. Rozen S, Skaletsky H (2000) Primer3 on the WWW for general users and for biologist programmers. Methods Mol Biol 132: 365-386.
233. Rasband WS (1997-2009) ImageJ.
234. Lindl T, Bauer J (1987) Zell und Gewebekultur. Stuttgart: Gustav Fischer Verlag.
235. Paxinos G, Watson C (1986) The Rat Brain in Stereotaxic Coordinates. The Rat Brain in Stereotaxic Coordinates: Academic Press.
236. Zigmond MJ, Stricker EM (1973) Recovery of feeding and drinking by rats after intraventricular 6-hydroxydopamine or lateral hypothalamic lesions. Science 182: 717-720.

8. Acknowledgements

A very warm “thank you” goes to my boss Eva Küppers who offered me the possibility to keep working with aquaporins. The decision to come to Tübingen and work in her lab was really easy! I couldn’t imagine finding such a supportive, stimulating and motivating boss anywhere else. I’ve learnt a lot from you in these past three years. I would also like to thank Prof. Wagner for the financial support, without it this thesis would not have been possible. A very big hug and “thank you” goes to Elke Maier, who taught me a lot of her immense technical knowledge and supported me in every possible way in the lab. The same applies to Uli Mattheus who always had an open ear for my technical questions. I had so much fun with you guys in the Histology lab! I also want to thank: Nils for bearing with my constant chatting in the PhD office, for all the nice coffee breaks and for becoming a good friend; Corinna for her support with my AQP4 questions; the people from the coffee/lunch breaks that always cheered up my day and all the members of the Wagner group. A special thanks also to Mihnea Nicolescu who gave me a lot of support with the image processing and transferred some of my sketches into the beautiful pictures also shown in the thesis. I would also like to thank my co-operation partners, especially Andreas von Ameln-Mayerhofer and the other people from his lab, for the good times during the months of rat surgery. Special thanks to Rüdiger for his unique music taste and Sonja for adorable company.
I would also like to thank Tanja and especially Jess for correcting my thesis for proper English, Ulla for all the phone calls discussing the life-as-a-PhD-student, Jan for his incredible patience with me during the writing phase and all the good food he cooked for me and finally my parents for helping me become what I am.